

Aus dem Institut für Stammzellforschung und Regenerative Medizin (ISRM) der Heinrich-Heine-Universität Düsseldorf

Direktor: Univ.-Prof. Dr. James Adjaye

Hepatic differentiation of human induced pluripotent stem cells with different CYP2D6 variants

Dissertation

Zur Erlangung des Grades eines Doktors der Medizin der Medizinischen Fakultät der Heinrich-Heine-Universität Düsseldorf

vorgelegt von

Kevin Bielec

2021

Als Inauguraldissertation gedruckt mit der Genehmigung der
Medizinischen Fakultät der Heinrich-Heine-Universität Düsseldorf

Gez.:

Dekan: Prof. Dr. med. Nikolaj Klöcker

Erstgutachter/in: Prof. Dr. James Adjaye

Zweitgutachter/in: Prof. Dr. Patrick Küry

„Man kann niemanden überholen, wenn man in seine/ihre Fußstapfen tritt“

Francois Truffaut

Auflistung eigener Publikationen

Zusammenfassung

Das polymorph exprimierte Enzym Zytochrom P450 2D6 (CYP2D6) spielt eine zentrale Rolle bei der hepatischen Metabolisierung von 20-25% aller klinisch eingesetzten Medikamente, darunter >160 verschiedene Arzneimittel der wichtigsten Wirkstoffklassen wie z.B. trizyklische Antidepressiva, Opioide, Antiarrhythmika und β -Blocker. Seine genetische Variabilität führt jedoch zu erheblichen interindividuellen Unterschieden hinsichtlich erreichter wirksamer Blutspiegel eines Arzneimittels und somit seiner Sicherheit und Wirksamkeit. Da medikamenteninduzierte Leberschädigung (DILI) der häufigste Grund für den Rückzug von Arzneimitteln vom Markt ist, besitzt die Entwicklung eines zellbasierten *In-vitro*-Testsystems, das die Metabolisierung von Arzneimitteln und die hepatotoxischen Wirkungen von Kandidaten für neue Prüfpräparate (IND) angemessen widerspiegelt, enormes wissenschaftliches und wirtschaftliches Potenzial. Hiermit könnten unerwünschte Arzneimittelwirkungen (UAW) in frühen Stadien der Arzneimittelentwicklung aufgedeckt, die Notwendigkeit von Tierversuchen reduziert und letztlich die Sicherheit neuer Medikamente vor klinischer Applikation erhöht werden.

In dieser Studie wurden zwei induziert pluripotente Stammzelllinien (hiPSC) mit unterschiedlichen *CYP2D6*-Varianten unter Verwendung dreier verschiedener Matrix / Medium-Kombinationen in Hepatozyten-ähnliche Zellen (HLCs) differenziert. Nach dem dreistufigen Differenzierungsprotokoll, das eine physiologische Hepatogenese nachahmt, wurden die abgeleiteten HLCs auf ihre molekulare und biochemische Konstitution untersucht. Besonderes Augenmerk wurde auf die Expression von *CYP2D6* gelegt.

Die mittels quantitativer Echtzeit-PCR (qRT-PCR) gemessene Hochregulierung der Hepatozyten-assoziierten Genexpression (*HNF4A*, *ALB*, *AFP*, *CYP3A4*, *CYP2D6*) und Herunterregulierung des Pluripotenzmarkers *OCT4* spiegelten die morphologischen Veränderungen wider, die während des Differenzierungsprozesses von hiPSC in HLCs beobachtet wurden. Die Expression hepatozytärer Biomarker wurde durch Immunfluoreszenzfärbung (*HNF4a*, E-Cadherin, *AFP*, *ALB*) und Durchflusszytometrie (*HNF4A*, *AFP*) auf Proteinlevel bestätigt. Metabolische Aktivität wurde durch Aufnahme und Freisetzung von Indozyaninrot (ICG) innerhalb von 24 Stunden nach der Anwendung, Durchführung einer PAS-Färbung zum Nachweis von Glykogenspeicherung, Nachweis der Harnstoffsekretion in Differenzierungsmedien und Messung der *CYP3A4*-Aktivität bei Stimulation mit 10 μ M Rifampicin nachgewiesen. Die Immunfluoreszenzfärbung von *CYP2D6* führte zu unerwarteten extrazellulären Färbesignalen, die Expression konnte jedoch durch Western-Blot-Analyse bestätigt werden.

Beide hiPSC-Linien wurden erfolgreich in funktionelle HLCs differenziert, die ein typisches, eher fötales Hepatozyten-ähnliches Genexpressionsprofil und funktionelle Aktivität aufweisen. Die Matrix / Medien-Kombination von Laminin-Mix in Kombination mit einem supplementierten Differenzierungsmedium auf Leibovitz-L15-Basis zeigte die robusteste Unterstützung der Leberdifferenzierung. Für alle Matrix / Medium-Kombinationen konnte eine Hochregulierung der

CYP2D6-Expression bestätigt werden, der Nachweis seiner ordnungsgemäßen Funktionalität lag jedoch außerhalb des Rahmens dieses Projekts. Für die Verwendung abgeleiteter HLCs als Teil eines *In-vitro*-Testsystems ist eine weitere Optimierung des Herstellungsprozesses erforderlich.

Abstract

The polymorphic enzyme Cytochrome P450 2D6 (CYP2D6) is predominantly involved in the hepatic metabolism of 20-25% of all clinically applied medication, including >160 different pharmaceuticals of major drug classes like tricyclic antidepressants, opioids, antiarrhythmics and β -blockers. Its genetic variability, however, results in substantial interindividual differences regarding effective blood levels of a given drug and, therefore, its safety and efficacy. For drug induced liver injury (DILI) being the most frequent reason of drug withdrawal from the market, the establishment of a cell-based *in-vitro* test system that adequately reflects drug metabolism and hepatotoxic effects of investigational new drug (IND) candidates imposes huge potential for indicating adverse drug reactions (ADR) at early stages of drug development, reducing the necessity of animal testing and increasing the patient's safety.

In this study, two induced pluripotent stem cell (hiPSC) lines carrying different *CYP2D6* variants were differentiated into hepatocyte-like cells (HLCs) using three different matrix/medium combinations. After undergoing the three-step differentiation protocol mimicking physiological hepatogenesis, the derived HLCs were assessed for their molecular and biochemical constitution. Special focus was laid on the expression of CYP2D6.

Using quantitative real time PCR (qRT-PCR), upregulation of hepatocyte-associated gene expression (*HNF4A*, *ALB*, *AFP*, *CYP3A4*, *CYP2D6*) and downregulation of the pluripotency marker *OCT4* reflected the morphological changes seen throughout the differentiation process from hiPSC into HLCs. Expression of the hepatocyte-associated biomarkers was confirmed by immunofluorescence staining (HNF4 α , E-Cadherin, AFP, ALB) and flow cytometry (HNF4 α , AFP). Metabolic activity of derived HLCs was proven by indocyanine green (ICG) uptake and release within 24 hours upon application, performing PAS staining for glycogen storage, detection of urea secretion into differentiation media and measuring CYP3A4 activity upon stimulation with 10 μ M rifampicin. Immunofluorescence staining of CYP2D6 resulted in unexpected extracellular staining signals but expression could be confirmed by Western blot analysis.

Both hiPSC lines were successfully differentiated into functional HLCs exhibiting a typical rather fetal hepatocyte-like gene expression profile and functional activity. The matrix/media combination of a Laminin-mix in combination with a growth-factor supplemented Leibovitz-L15-based differentiation medium indicated the most robust support of hepatic differentiation. For all matrix/medium combinations, upregulation of CYP2D6 expression could be confirmed but proving proper functionality was beyond the scope of this project. For using derived HLCs as part of an *in-vitro* testing system, further process development for producing a more mature cell type is necessary.

Abbreviations

A	Ampere
A.	Arteria
ADR	Adverse Drug Reaction
AF	Alexa Fluor
AFP	Alpha Fetoprotein
AHMC	8-acetyl-7-hydroxy-4methylcoumarin
ALB	Albumin
APC	Allophycocyanin
APS	Ammonium Persulfate
Asp	Aspartate
ATMPs	Advanced Therapeutic Medicinal Products
BCA	Bicinchoninic Acid
BME	β -mercaptoethanol
BMP-4	Bone Morphogenic Protein 4
°C	Degrees Celsius
Cat. No.	Catalogue Number
CO ₂	Carbon Dioxide
CPIC	Clinical Pharmacogenetics Implementation Consortium
CYP2D6	Cytochrome P450 2D6
CYP3A4	Cytochrome P450 3A4
D	Day
DE	Definite Endoderm
DEC	December
DEX	Dexamethasone
DILI	Drug Induced Liver Injury
DMEM	Dulbecco's Modified Eagle Medium
DMSO	Dimethyl Sulfoxide
DNA	Desoxyribonucleic Acid
DPWG	Dutch Pharmacogenetics Working Group
EGF	Epidermal Growth Factors
ELISA	Enzyme Linked Immunosorbent Assay
EM	Extensive Metabolizer
EMT	Epithelial to Mesenchymal Transition
EPM	Endoderm Priming Medium
ESC	Embryonic Stem Cell
Ex/Em	Excitation / Emission
FBS	Fetal Bovine Serum
FC	Fold change
FFA	Free Fatty Acids
FGF4	Fibroblast Growth Factor 4
FGF8	Fibroblast Growth Factor 8
FL	Fetal Liver
FSC	Front Scatter
Fwd	Forward
FXR	Farnesoid X receptor
GFR	Growth Factor Reduced
GLUT	Glucose Transporter
HE	Hepatic Endoderm
hESC	Human Embryonic Stem Cell
HGF	Hepatocyte Growth Factor
hiPSC	Human Induced Pluripotent Stem Cell
HLC	Hepatocyte Like Cells
HMG	High Mobility Group
hMSC	Human Mesenchymal Stem Cell
HNF4 α	Hepatocyte Nuclear Factor 4 alpha
hPSC	Human Pluripotent Stem Cells

HRP	Horseradish Peroxidase
HSA	Human Serum Albumin
ICC	Immunocytochemistry
ICG	Indocyanine Green
ICM	Inner Cell Mass
IM	Intermediate Metabolizer
IND	Investigational new drug
iPSC	Induced Pluripotent Stem Cells
ISRM	Institute of Stem Cell Research and Regenerative Medicine
IVF	<i>In-Vitro</i> Fertilization
kDa	Kilo Dalton
kg	Kilogram
KO-DMEM	KnockOut™ Dulbecco's Modified Eagles Medium
KOSR	KnockOut™ Serum Replacement
L15M	Leibovitz 15 Medium
LG	Lactoglobulin
LN	Laminin
LN111	Laminin 111
LN521	Laminin 521
mAb	Monoclonal Antibody
MDMA	Methylenedioxyamphetamine
MDS	Material Data Sheet
MFI	Mean Fluorescent Intensity
MG	Matrigel
min	Minute
miR	Micro RNA
mM	Milli Molar
MPTP	1-methyl-4phenyl-1,2,3,6-tetrahydropyridine
NaCl	Sodium Chloride
NADPH	Nicotinamide Adenine Dinucleotide Phosphate
NAFLD	Non-alcoholic fatty liver disease
NDS	Normal Donkey Serum
NEAA	Non-Essential Amino Acids
NGS	Normal Goat Serum
NO	Nitric oxide
O/N	Overnight
OATP-C	Organic Anion Transporting Polypeptide C
OCT	October
OCT4	Octamer Binding Transcription Factor 4
OSM	Oncostatin M
PAGE	Polyacrylamide Gel Electrophoresis
PAS	Periodic acid-Schiff
PBB	Permeabilisation/Blocking Buffer
PBS (+/+)	Phosphate Buffered Saline + Magnesium + Calcium
PBS (-/-)	Phosphate Buffered Saline -Magnesium -Calcium
PFA	Paraformaldehyde
PGx	Pharmacogenomics
PHH	Adult Primary Human Hepatocytes
PKA	Protein Kinase A
PM	Poor Metabolizer
PTM	Posttranslational Modification
P/S	Penicillin / Streptomycin
qRT-PCR	Quantitative Real Time Polymerase Chain Reaction
rb	Rabbit
resp.	Respectively
Rev	Reverse
RIPA	Radioimmunoprecipitation Assay
RNA	Ribonucleic Acid
ROCK	Rho Kinase
RT	Room Temperature

s	Second
SD	Standard Deviation
SDS	Sodium Dodecyl Sulphate
SEP	September
Ser	Serine residue
SNP	Single Nucleotide Polymorphism
SOX2	SRY box Transcription Factor 2
SOX17	SRY box Transcription Factor 17
SSC	Side Scatter
TBS-T	Tris-base Buffered Saline Tween 20
TEMED	Tetramethylethylenediamine
TGF- β	Transforming Growth Factor beta
T _M	Melting Temperature
UGB	Upper Gel Buffer
UGT1A1	Glucuronosyltransferase 1A1
UM	Ultrafast Metabolizer
U-PGx	Ubiquitous Pharmacogenomics
UAW	Unerwünschte Arzneimittelwirkungen
USA	United States of America
UV	Ultraviolet
V.	Vena
VEGF	Vascular Endothelial Growth Factors
w/o	Without
Wnt	Wingless-related integration site
WT	Wild Type
xg	Times G-Force

List of Figures

<i>Fig. 1 – Segmental anatomy of the liver according to Couinaud’s division</i>	2
<i>Fig. 2 – Microanatomy of the human liver</i>	3
<i>Fig. 3 – Different models describing the functional unit of the human liver</i>	4
<i>Fig. 4 – Concept of induced pluripotent stem cells</i>	17
<i>Fig. 5 - Schematic timeline of hepatic differentiation protocol</i>	31
<i>Fig. 6 – Assembly of SDS-PAGE gel, Blotting membrane, Filter Papers and Sponges for Western Blot</i>	38
<i>Fig. 7 – Morphology of hiPSC lines</i>	43
<i>Fig. 8 – Representative brightfield images of hepatic differentiation of human iPSC</i>	44
<i>Fig. 9 – Morphology of HepG2 cells</i>	45
<i>Fig. 10 – Quality control of isolated RNA by 1% agarose gel-electrophoresis</i>	46
<i>Fig. 11 - Expression of hepatocyte- and pluripotency-associated transcripts in pluripotent stem cell derived HLCs</i>	47
<i>Fig. 12 – Quality control of quantitative real time polymerase chain reaction</i>	48
<i>Fig. 13 – Immunocytochemistry of derived cells at definitive endoderm stage</i>	49
<i>Fig. 14 – Immunocytochemistry of derived cells at hepatic endoderm stage</i>	50
<i>Fig. 15 – Immunocytochemistry of HepG2</i>	52
<i>Fig. 16 – Immunocytochemistry of S12_13B HLCs derived using MG/L15M</i>	53
<i>Fig. 17 – Immunocytochemistry of S12_13B HLCs derived using LN/HepatoZYME</i>	54
<i>Fig. 18 – Immunocytochemistry of UJiPS13 HLCs derived using MG/L15M</i>	55
<i>Fig. 19– Immunocytochemistry of UJiPS13 HLCs derived using LN/L15M</i>	56
<i>Fig. 20 – Immunocytochemistry of UJiPS13 HLCs derived using LN/HepatoZYME</i>	57
<i>Fig. 21 – Gating of parental cell population of S12_13B derived hepatocyte-like cells for flow cytometry</i>	58
<i>Fig. 22 – Dotplots and histograms for gated cell populations</i>	59

Fig. 23 – Indocyanin green (ICG) uptake and release by derived hepatocyte-like cells within 24h.	60
Fig. 24 – Glycogen storage detection by periodic acid Schiff reaction.	61
Fig. 25 – CYP3A4 activity assay of derived hepatocyte-like cells and HepG2 cells.	62
Fig. 26 – Concentration of urea (in mg/dl) in supernatant medium from three different time points (DE (D4), HE (D7), HLC (last day of differentiation)) throughout the hepatic differentiation process.	63
Fig. 27 – Albumin secretion detected by enzyme-linked immunosorbent assay (ELISA).	64
Fig. 28 – Expression of CYP2D6 transcripts in pluripotent stem cell derived HLCs.	65
Fig. 29 – Immunocytochemical staining of derived hepatocyte-like cells and the biological positive control cell line HepG2.	66
Fig. 30 – Photographs from nitrocellulose membranes of Western Blot analysis.	67
Fig. 31 – Ratios of CYP2D6/Actin expression of derived hepatocyte-like cells and HepG2 cells.	68
Fig. 32 – Comparison of different gating strategies for flow cytometric data from S12_13B.	90
Fig. 33 – Complete depiction of gels produced for assessment of RNA quality.	109
Fig. 34 – Standard curve of the Urea Quantichrome Assay.	109

List of Tables

Table 1 – List of major classes of pharmaceuticals metabolized by CYP2D6.	11
Table 2 – Equipment used during the experimental phase of the thesis.	22
Table 3 – Software.	23
Table 4 – Consumables.	24
Table 5 – Primary antibodies used for immunofluorescence staining.	25
Table 6 – Secondary antibodies used for immunofluorescence staining.	25
Table 7 – Primer list.	26
Table 8 – CYP2D6 genotype and phenotype of S12_13B and UJiPS13.	27
Table 9 – Grading system of hiPSC.	29
Table 10 – Ingredients of qRT-PCR reaction mix.	34
Table 11 – Layout of tubes for primary antibody staining of flow cytometry.	35
Table 12 – Dilution row for Albumin ELISA.	36
Table 13 – Components and volumes of 4X Loading buffer, SDS resolving and stacking gel used for SDS-PAGE.	38
Table 14 – Differentiation runs performed during course of the thesis.	42
Table 15 – Common CYP2D6 allele variants and their corresponding activity value.	72
Table 16 – Comparison of CPIC and DPWG genotype to phenotype attribution.	72
Table 17 – Comparison of employed matrix-media combinations for hepatic differentiation of induced pluripotent stem cells.	86

Table of Content

Zusammenfassung.....	I
Abstract.....	III
Abbreviations	IV
List of Figures.....	VI
List of Tables.....	VII
1 Introduction	1
1.1 The liver	1
1.1.1 Macroanatomy	1
1.1.2 Microanatomy	2
1.1.3 Hepatogenesis	5
1.1.4 Metabolic function	7
1.2 Cytochrome P450 family	9
1.2.1 Cytochrome P450 2D6 (CYP2D6).....	10
1.3 Induced pluripotent stem cells (iPSC).....	16
1.3.1 Hepatic differentiation of hiPSC <i>in vitro</i>	18
1.4 Aim of this thesis	21
2 Materials and Methods	22
2.1 Equipment and Consumables	22
2.2 Cell culture	26
2.2.1 Cell Source	26
2.2.2 Non-Pluripotent Cells	27
2.2.3 Human Induced Pluripotent Stem Cells (hiPSC)	28
2.3 Hepatic differentiation	31
2.4 Molecular Biology Assays	32
2.4.1 Isolation of RNA	32
2.4.2 cDNA synthesis.....	33
2.4.3 Quantitative Real Time Polymerase Chain Reaction (qRT-PCR)	33
2.5 Immunoassays.....	34
2.5.1 Immunocytochemistry	34
2.5.2 Flow Cytometry	35
2.5.3 Enzyme linked immunosorbent assay (ELISA) for Albumin	36
2.5.4 Western Blot for CYP2D6.....	37
2.6 Biochemical Activity Assays	39
2.6.1 Indocyanine Green (ICG) Staining	39
2.6.2 PAS staining (Glycogen storage staining)	40

2.6.3	CYP3A4 Activity Assay	40
2.6.4	Urea Quantification (QuantiChrome™ Urea Assay Kit, BioAssay Systems).....	41
3	Results	42
3.1	Morphology of cells changes throughout hepatic differentiation.....	42
3.2	Transcript analysis of derived HLCs for hepatocyte-associated gene expression..	45
3.3	Immunostaining of intra- and extracellular hepatocyte-associated proteins	48
3.4	Biochemical assessment of derived hepatocyte-like cells.....	59
3.4.1	Metabolic functionality of derived HLCs.....	59
3.5	Analysis of CYP2D6 expression on transcriptome and protein level.....	64
4	Discussion.....	69
4.1	Scope of this thesis in relation to current literature	69
4.2	Unharmonized CYP2D6 phenotype prediction may cause opposing dosage adjustment recommendations for similar CYP2D6 genotypes.....	70
4.3	Differentiation of hiPSC carrying different <i>CYP2D6</i> genotype variants into HLCs..	73
4.3.1	Definite Endoderm (DE) derivation.....	73
4.3.2	Hepatic Endoderm (HE) derivation.....	75
4.3.3	HLC maturation.....	75
4.4	Differences in CYP2D6 expression of derived HLCs	78
4.4.1	Higher mRNA expression of CYP2D6 in HLCs derived from UJiPS13 compared to HLCs derived from S12_13B	79
4.4.2	Immunocytochemical staining of CYP2D6 resulted in unexpected, non- specific signaling	80
4.4.3	CYP2D6-specific Western Blot analysis of HLC derived whole cell lysates revealed two additional bands of higher molecular weight and reflected the predicted CYP2D6 phenotypes.....	81
4.5	Comparison of employed matrix-media combinations for hepatic differentiation	84
4.6	Strengths, limitations and outlook of performed study	87
5	Conclusion	93
6	References.....	95
7	Appendix	109
7.1	Appendix 1	109
7.2	Appendix 2.....	109
8	Acknowledgements	110

1 Introduction

1.1 The liver

With a median weight of 1.8 kg for men and 1.4 kg for women, the liver represents the largest gland of the adult human body (1). It plays a central role in a vast range of metabolic processes such as metabolism of carbohydrates, amino acids and lipid nutrients, hormone synthesis and secretion, production of bile for lipid digestion or the body's detoxification from exogenous and endogenous substances.

1.1.1 Macroanatomy

Located in the upper right quadrant of the abdominal cavity right below the diaphragm, the liver is of dark red-brown color, trigonal pyramidal in shape and malleable by adjacent anatomical structures such as heart, right kidney or vena cava. The liver is stabilized by the ligamentous *Glisson capsule* and protected by the rib cage (2). It maintains its position through suspension by several avascular peritoneal reflections such as the falciform ligament attaching the anterior surface of the liver to the anterior abdominal wall and the anterior and posterior coronary ligaments that converge on both the right and left side of the liver to form the right and left triangular ligaments. The right coronary and triangular ligaments attach the liver to the retroperitoneum (3). At the *porta hepatis*, a transverse fissure on the inferior surface of the liver, the afferent blood vessels (hepatic artery, portal veins) and hepatic nervous plexuses are entering and the hepatic ducts and lymph vessels are leaving the liver. Interestingly, 75% of the liver's oxygen supply is covered by the portal vein whereas only 25% of the overall oxygen demand is covered by the hepatic artery (4). All of these incoming and leaving structures at the *porta hepatis* are enveloped within a sheath of loose connective tissue that is continuous to the fibrous *Glisson capsule* as they course through the liver parenchyma. The combination of hepatic artery, portal vein and hepatic bile duct is also called a portal triad. Venous outflow of the liver is conducted by the hepatic veins (5).

Macroanatomically, the liver is divided into four lobes that dominate its visual appearance: right lobe, left lobe, quadrate lobe and caudate lobe. Clinically however, according to Couinaud's division, the liver is divided into eight sections determined by the distribution of portal venous branches in the liver parenchyma (see Fig. 1). This segmental division, although not visible on the organ's surface, allows experienced surgeons the resection of small compartments of the liver (6).

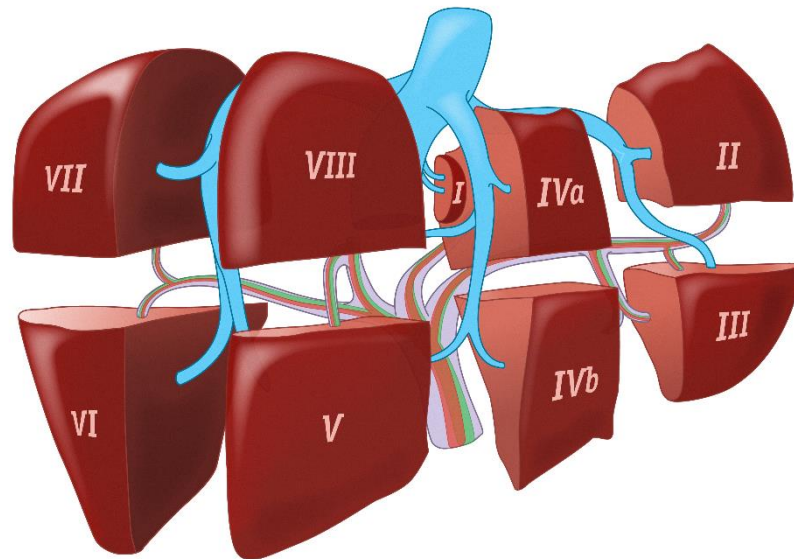


Fig. 1 – Segmental anatomy of the liver according to Couinaud's division. According to Couinaud, the liver can be divided into eight sections determined by the distribution of the portal venous branch in the liver parenchyma (I: caudate lobe, II-IV: left hemiliver, V-VIII: right hemiliver). This segmental division, although not visible on the organ's surface, allows experienced surgeons the resection of small compartments of the liver. (Source: Reiner Bergmann/SEHiGEL.DE, Aachen)

1.1.2 Microanatomy

The human liver consists of a range of epithelial and mesenchymal cells. The dominant cell type, reflecting about 80% of the total mass of an adult, healthy human liver, is hepatocytes, followed by (discontinuous) endothelial cells, cholangiocytes, liver-specific macrophages (or “*Kupffer cells*”) and the stem cell-like stellate cells (or “*Ito cells*”, see Fig. 2). Only 2% of the total mass of a healthy human liver consists of stromal tissue (7).

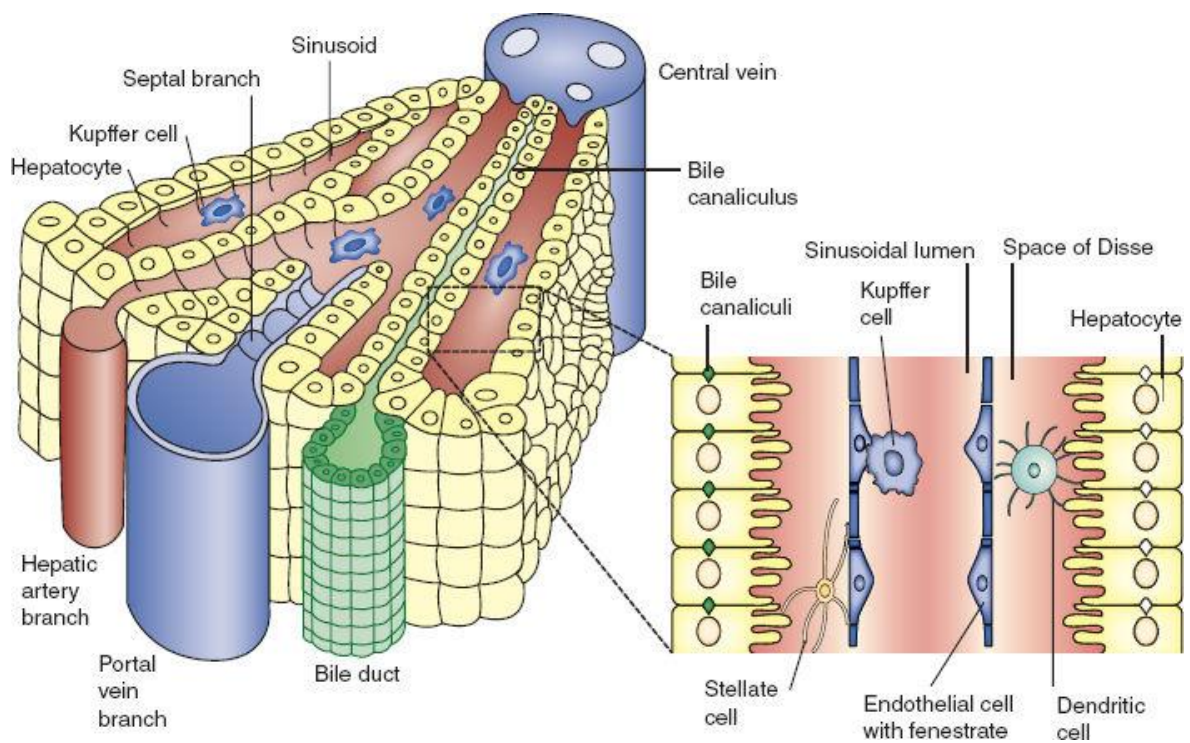


Fig. 2 – Microanatomy of the human liver. The human liver roughly consists of five different cell types, predominantly hepatocytes followed by discontinuous endothelial cells, cholangiocytes, Kupffer cells (liver-specific macrophages) and stellate cells. The liver's blood supply is covered by branches of portal vein and hepatic arteries that terminate in intrahepatic portal tracts. These join into liver sinusoids, the intrahepatic distributing system, draining into the central veins. Liver sinusoids are lined by discontinuous endothelial cells that separate the sinusoidal lumen from the underlying space of Dissé. The space of Dissé harbors extracellular matrix proteins, stellate cells and the liver-specific macrophages. Illustration adapted from Adams et. al. (8).

Hepatocytes are mono-, di-, tetra- or octaploid, may contain up to two nuclei per cell and are arranged in plates. Like other epithelial cells, they are polar – hence containing a basolateral and an apical membrane. Whereas the basolateral membrane is directed towards the blood supplying sinusoids and may even carry surface-enlarging microvilli, the apical membrane is facing towards the bile canaliculi. Hepatic endothelial cells are spindle-shaped cells connected to each other forming sieve-like, transcellular fenestrations which allow sinusoidal blood to be washed around the hepatocytes' basolateral membranes. In between endothelial cells and hepatocytes, the perisinusoidal space (or *space of Dissé*) is formed which is important for proper delivery and residence time of nutrients at the basolateral membrane of hepatocytes. Localized in the perisinusoidal space are also the liver specific macrophages and the Vitamin-A carrying stem cell like stellate cells (see Fig. 2) (7).

During hepatogenesis, liver cells are assembled in repetitive microscopic, functional units to finally form a complex three-dimensional structure. The smallest unit of an organ that can self-sufficiently subserve all functions of a specific organ is called the (structure-)functional unit. Unlike the well-defined nephrons of the kidneys, a similar structure-functional unit describing vascular supply, microarchitectural interfaces and all currently known liver functions, both physiological and pathophysiological, has yet to be identified (9).

The three most commonly described structure-functional units of the liver are Kiernan's classic lobules (10), Mall's portal lobules (11) and Rappaport's acinus (12) (see Fig. 3).

Kiernan's classic lobule model describes the functional unit of the liver as a hexagonal column with peripheral portal triads and a central hepatic vein. In regular intervals along these columns, small arterial and portal venous branches are leaving and bile duct branches are entering the portal triads thereby encircling the hexagonal units. Through both arterial and portal venous branches, oxygenated and nutrient-rich blood is delivered into the intralobular sinusoids and then transported towards the central veins. Embedded in between the sinusoids are the metabolically active hepatocytes. Within adjacent hepatocytes, special canaliculi are built to warrant biliary excretion. In Mall's portal lobule concept instead of the central vein, a portal triad is viewed as the center of a structure-functional liver unit with one portal triad providing oxygen and nutrients for at least three classic lobules. The central veins are located in the periphery.

Rappaport's liver acinus focusses on the microcirculatory supply of a certain group of liver cells that are in direct proximity and supplied by the same blood vessels. This model defines three zones of oxygen and nutrient supply where zone 1 is located around the portal tract, zone 2 represents a transition zone between periportal and pericentral regions, and zone 3 is adjacent to the hepatic venules. The liver acinus model takes into account that metabolic functions of hepatocytes alter depending on their zone affiliation (13). Hepatocytes of zone 1 are responsible for glucose metabolism and ammonia detoxification, zone 3 hepatocytes are involved in lipogenesis, glutamine synthesis and cytochrome P450-associated biotransformation processes. Hepatocytes of zone two may be involved in both processes. This liver acinus concept is capable of describing the pathogenesis of several events such as hepatic cirrhosis more accurate than Kiernan's and Mall's models (9).

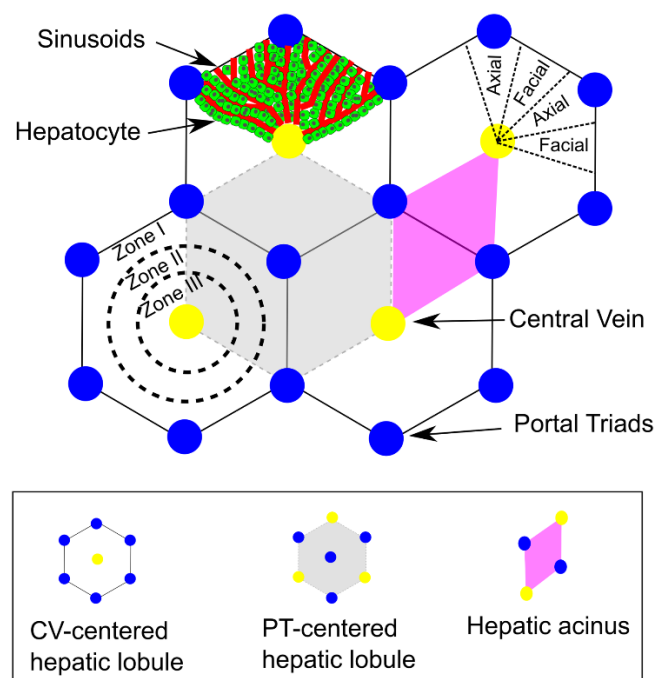


Fig. 3 – Different models describing the functional unit of the human liver. Basic models of the functional unit of the human liver include Kiernan's central vein (CV)-centered liver lobule, Mall's portal triad (PT)-centered liver lobule and Rappaport's liver acinus. All models describe the same morphological structures and liver functions from a different viewpoint (yellow: CV, blue: PT, pink: acinus, green: hepatocyte, red: sinusoid). Blood enters the liver through branches of

the portal vein and liver arteries, flows through sinusoids and drains into central veins. Kiernan's CT-centered lobule model describes the functional unit of the liver as a hexagonal column with peripheral portal triads and a central hepatic vein. In regular intervals along these columns, small arterial and portal venous branches are leaving and bile duct branches are entering the portal triads thereby encircling the hexagonal units. In Mall's portal lobule concept instead of the central vein, a portal triad is viewed as the center of a structure-functional liver unit with one portal triad providing oxygen and nutrients for at least three classic lobules. The central veins are located in the periphery. Rappaport's liver acinus focusses on the microcirculatory supply of a certain group of liver cells that are in direct proximity and supplied by the same blood vessels. This model defines three zones of oxygen and nutrient supply where zone 1 is located around the portal tract, zone 2 represents a transition zone between periportal and pericentral regions, and zone 3 is adjacent to the central venules. Hepatocytes of zone 1 are responsible for glucose metabolism and ammonia detoxification, zone 3 hepatocytes are involved in lipogenesis, glutamine synthesis and cytochrome P450-associated biotransformation processes. Hepatocytes of zone 2 may be involved in both processes. This liver acinus concept is capable of describing the pathogenesis of several pathological events like hepatic cirrhosis more accurate than Kiernan's and Mall's models (9). Illustration adapted from Fu et. al. (13).

1.1.3 Hepatogenesis

Prenatal development of human life from the freshly fertilized oocyte to the new-born fetus can be roughly divided into two phases: embryonal development (week 1 – 8 post fertilization) where all organic primordia are created (organogenesis) and fetal development (week 9 post fertilization – birth) where the created organs grow and mature (14).

To understand hepatogenesis, the structural and functional development of the liver during the first three to eight weeks of embryogenesis, a broad understanding of the early stage of general embryogenesis (gastrulation) and the specific hepatogenesis itself are necessary. Hepatogenesis, again, can be divided into two separate but simultaneously occurring events: the development of hepatic parenchyma and intrahepatic angiogenesis.

1.1.3.1 Embryonal Development (Organogenesis)

At the first three days after fertilization, the newly formed zygote undergoes several rounds of mitosis and, at day 3 (D3), consists of 12- to 16 small, loosely connected cells, the blastomeres. At this stage, the zygote is named morula (15). A fraction of these blastomeres start strengthening their intercellular adhesion by forming tight and gap junctions in a process called compaction. Before reaching the uterus around D6, the embryo already contains two types of cells: an outer layer of trophoblast which shall form the placenta and a tightly connected inner cell mass that shall give rise to the developing embryo. The embryo will now imminently lose its protecting outer envelope, the zona pellucida, thereby marking its transition towards a blastocyst. The blastocyst is capable of nesting into the mucosa of the uterus via its embryonal pole (implantation, still D6) (15). Trophoblast cells express L-selectins that interact with carbohydrate receptors specific for selectins expressed on epithelial cells of the uterus and integrins that interact with laminins and fibronectin of the uterus' stroma. This process is suspected to be comparable to the rolling and migration concept of leukocytes into inflamed tissue sites (16).

The inner cell mass, now called embryoblast, starts to differentiate into two cell layers: the cylindrical epiblast and a layer of polyhedral hypoblast cells (17).

Beginning of week 3 post fertilization, the epiblast starts giving rise to all three germ layers (ectoderm, mesoderm and endoderm) during a process named gastrulation, whereas the hypoblast surrounds the yolk sack (18). Gastrulation starts with a caudal thickening of the epiblast layer which accretes as primitive streak towards the primitive node. Stimulated by paracrine signaling of FGF8 produced by cells of the primitive streak itself and in a process called invagination, epiblast cells undergo epithelial-to-mesenchymal transformation (EMT), round up and migrate into the primitive streak (18). FGF8 downregulates the expression of E-cadherin, a major adhesion molecule for intercellular connections of epithelial cells of the epiblast, and among other signals drives mesodermal differentiation of these cells through upregulation of brachyury (T) expression. A fraction of the invaginated cells replace the polyhedral hypoblast cells and differentiate into a layer called definite endoderm. Key regulators of endoderm formation are the TGF β growth factor Nodal and Wntless-related integration site (WNT) 3a initiating differentiation in a dose dependent manner (19). Low dose signaling of Nodal is associated with mesoderm, high concentrations of Nodal with endoderm formation (20). Nodal stimulates endoderm formation by upregulation of key transcription factors driving endodermal lineage commitment such as SRY box Transcription Factor 17 (SOX17), an HMG domain DNA-binding factor, and HNF3 $\alpha/\beta/\gamma$, for head domain proteins (21). Cells that remain within the epiblast layer will give rise to the ectoderm. Cells invaginating through the primitive node will eventually migrate past the prechordal plate, an important structure for the development of the prosencephalon, and almost completely separate the ecto- and endodermal cell layers only sparing the tightly connected cells of the oropharyngeal membrane that will form the mouth opening (18). The relatively higher mitotic rate of ectodermal cells including the neural tube leads to a craniocaudal and lateral bending that results in an internalization of the endodermal cell derivatives. The resulting internal tract can be divided into fore-, mid- and hindgut. Within the upcoming six weeks, the endodermal cell layer of this tract will proliferate and differentiate into various tissues and organs including the epithelial lining of the respiratory, gastrointestinal and urogenital tract and the parenchyma of the tonsils, thyroid, liver and pancreas (22).

1.1.3.2 Hepatogenesis

Beginning around 18 days post fertilization, bipotential embryonic hepatoblast cells grow ventrally and in plate-like structures out of the anterior part of liver diverticulum of the endodermal foregut into the *ventral mesogastrum* to form the liver bud (23). These cells will give rise to the liver and the intrahepatic biliary tree. Theoretically, the complete endodermal foregut has the capacity to differentiate into hepatocytes but differentiation of the complete foregut into the hepatic lineage is counteracted through inhibiting signaling of the surrounding ectoderm, non-cardiac mesoderm and the notochord. Fibroblast growth factor 2 (FGF-2), excreted paracrinally by cardiac mesoderm and vascular endothelial cells of the nearby liver diverticulum, neutralize this inhibition of hepatic differentiation and defines the prospective liver area. Belonging to the TGF- β superfamily, bone morphogenic growth factor 4 (BMP4) produced by cells of the *septum transversum* seems to enhance

the cell's responsiveness towards FGF-2 and drive cells of the definitive endoderm towards hepatic differentiation (23,24).

The *ventral mesogastrium* is filled with loosely connected mesenchymal cells forming the transversal septum that will give rise to diaphragm, stromal tissue of the liver, hematopoietic cells and stellate cells. The cells secrete several important growth factors for hepatoblast differentiation, migration and survival such as FGF, BMP, HGF, WNT, TGF β and retinoic acid (25). The posterior part of the liver diverticulum shall give rise to the gall bladder and extrahepatic bile ducts (26).

Ten weeks post fertilization, the fetal liver already contributes to approximately 10% of the total body mass of the embryo and is an important site of embryonal hematopoiesis (26). Located in nests between maturing hepatocyte plates and hepatic blood vessels, hematopoietic stem cells proliferate and produce cells of myeloid and lymphatic lineages (23). These hematopoietic stem cells are critically involved in hepatoblast maturation into hepatocytes by producing the IL-6 cytokine family member Oncostatin M (OSM) (27). OSM binds to the OSM receptor (OSMR) which has a high affinity to gp130. The OSMR-gp130 heterodimer activates cytoplasmic tyrosine kinases thereby altering the activity downstream transcription factors (28) leading to the formation of tight junctions and a polarized, epithelial appearance via proteins such as K-Ras and E-Cadherin (29). Together with Hepatocyte Growth Factor (HGF) and glucocorticoid hormones, these factors drive hepatoblast differentiation into hepatocytes (30). Hepatic maturation is counteracted by TNF α which supports the maintenance of the proliferation capacity in more fetal cell types (25). During the last 2 months of embryonic development, hematopoiesis will slowly diminish from hepatic tissue and continue in the primary sites of adult hematopoiesis. Roughly during week 12 post fertilization, hepatocytes start bile production and cystic and hepatic bile ducts merge to form the common bile duct. During this time and in the course of the gastral rotation, the major duodenal papilla, the common outlet of the bile and pancreatic duct, turns its direction at 180° to its final physiological position (23).

The largest part of the intrahepatic vascular system develops from the vitelline veins running first in front of and subsequently on either side of the fetal intestinal canal thereby forming various anastomoses. The cranial part of the vitelline veins will give rise to the intrahepatic part of the inferior *vena cava* and the efferent hepatic veins, the precursors of the hepatic veins. The middle part of the vitelline veins containing the highest density of anastomoses will form the liver sinusoids. The caudal part of the vitelline veins will form the superior mesenteric vein and the portal vein. Two other embryonal blood vessels, the umbilical vein and the venous duct, will obliterate within the first days after birth and form the *teres hepatic ligament* respectively the *ligamentum venosum* (31).

1.1.4 Metabolic function

The liver's extensive importance for the human metabolism is highlighted by receiving around 25% of the cardiac output per minute through the hepatic artery and the main fraction of the venous blood from the digestive system through the portal vein (32). The portal vein, thereby, directs the nutrients

absorbed in the gastrointestinal tract towards the hepatocytes within the liver before they may enter systemic circulation. This tremendous oxygen and nutrient supply is necessary for the homeostasis of various metabolic key processes of the human body including the maintenance of blood glucose levels during rest and exercise, synthesis of ketone bodies, glycerides, cholesterol and serum proteins (i.e. albumin, coagulation factors, complement system protein, acute phase proteins), nitrogen excretion, bile production and phase I and II biotransformation from both exo- and endogenous substances (33). The fetal liver is further also an important location of embryonal hematopoiesis (34). As the detailed description of all metabolic processes regulated by the liver would go far beyond the scope of this thesis, the focus will in this introduction be set on a brief description of metabolic processes important to assess the functionality of the *in vitro* produced hepatocyte-like cells (HLCs).

1.1.4.1 Glucose metabolism

Glucose, sometimes also named dextrose, is a six carbon sugar with the molecular formula $C_6H_{12}O_6$ and the most abundant monosaccharide in nature (35). It is used as an energy source in a vast range of living organisms, from bacteria to vertebrates, including humans where it, through aerobic respiration, is the key source of energy production. 1 g of glucose is capable of providing 16 kJ of food energy (36). Hepatocytes internalize excess serum monosaccharides like glucose, galactose and fructose mainly via the glucose transporter GLUT2 (glucose and galactose) resp. GLUT5 (fructose) to keep blood serum glucose levels within the narrow range of 70 – 110 mg/dl in healthy human adults (37).

In a state of monosaccharide excess, a fraction of the internalized non-glucose monosaccharides can be efficiently metabolized into glucose molecules. Glucose will then undergo enzymatically driven processes to form the glucose storage molecule named glycogen – representing the main storage form of glucose of the human body. A healthy, adult human liver can store up to 150 g of glycogen (33). In a state of glucose deprivation, glycogen may be broken down and glucose be released to elevate serum glucose levels to its physiological range. Simultaneously, the individual would sense a feeling of hunger to further elevate blood glucose level by external supply of (mono-)saccharides. In a state where almost all glycogen reserves are depleted and no external supply is available, hepatocytes can produce glucose *de novo* in a process called gluconeogenesis. During gluconeogenesis, glucose is produced by biochemically transforming glycerin, lactate or various amino acids (33).

1.1.4.2 Urea production

Urea, or also carbamide, is an end product of the hepatocyte-specific urea cycle. It's an amide consisting of two $-NH_2$ groups joined by a carbonyl functional group ($CO(NH_2)_2$), color- and odorless and highly soluble in water. Urea is produced during the urea cycle, also known as ornithine cycle, by hydrolyzation of the amino acid arginine to form urea and the mitochondrial wall passing, non-proteinogenic amino acid ornithine (38).

Urea's main function lies in the storage of nitrogen that, in this soluble form, may be excreted by the kidneys. Accumulation of non-excretable forms of nitrogen like ammonium outside the mitochondrial walls has proven to be toxic to a vast range of human cells and organs (39).

1.1.4.3 Synthesis of human serum albumin

Human serum albumin (HSA) is encoded by the albumin gene (*ALB*) on chromosome 4 of the human genome, translates to a protein with a total mass of 66 kDa and is mainly produced by the liver (40). Once secreted, it is of crucial importance for the maintenance of oncotic pressure inside the blood vessels thereby indirectly regulating the distribution of water molecules between the intraluminal and interstitial space throughout the human body. Reduced serum albumin results in increased intraluminal water loss and the formation of edema. Like many other serum proteins, HSA also functions as carrier molecule for free fatty acids (FFA), bilirubin, lipophilic pharmaceuticals and approximately 50% of the plasmatic calcium ions (41).

1.1.4.4 Phase I and II biotransformation

Organic and inorganic environmental molecules which cannot be used as nutrients, are metabolically inactive or even toxic within the human organism, must be metabolized to either form usable, mostly more soluble agents or form biologically less active molecules. The metabolized molecules may be eliminated from the body more easily due to their now increased solubility. The processing of unusable or (in-)active molecules in this context is called biotransformation. Most reactions belonging to biotransformation are performed in hepatocytes but in smaller extent also in cells of lungs, intestine and kidneys (42–44).

In general, two types of biotransformation are distinguished: phase I and phase II biotransformation (45). Phase I biotransformation describes the introduction of polar groups by oxidation, reduction or hydrolytic reactions to the educt. A key family of enzymes involved in phase I biotransformation reactions are members of the Cytochrome P450 family (see section 1.2). Phase II biotransformation involves the covalent conjugation of hydrophilic endogenous molecules such as glycine, sulphate or glucuronic acid. Ultimate goal of phase II reactions is to further increase the molecule's aqueous solubility making the final product excretable by the kidneys (45,46).

1.2 Cytochrome P450 family

The large and diverse monooxygenase superfamily Cytochrome P450 consists of 18 families encoding for 57 genes and 58 pseudogenes in the human genome with the biggest family in humans being CYP2 with 13 subfamilies and 16 functional genes (44,47,48). CYP enzymes are grouped into the same family when sharing more than 40%, and to the same subfamily when sharing more than 55% of the amino acid sequence (47). All CYP enzymes have a molecular weight between 45 and 60 kDa, contain a noncovalently bound heme group and share a common overall fold and topology.

The heme group acts as the catalytic center of the enzyme where molecular dioxygen and electrons are utilized to oxidize target structures (49).

CYPs were first discovered in 1958 and named for their typical Soret peak at 450 nm ("Pigment at 450 nm"; P450) in absorption spectroscopy (50). They are believed to originate from an ancestral gene existing approximately 3.5 billion years ago which coded for a protein protecting early life forms from toxic levels of accumulating atmospheric oxygen. It evolved through various rounds of among other gene duplication, programmed frameshift, alternative splicing and RNA editing. Still, CYPs are phylogenetically one of the most rapidly evolving genes in humans thereby assuring cellular protection against increasing xenobiotic compound exposition (51).

Although being expressed in many tissues of the human body (e.g. lung, intestine, kidney, heart), enzymes of the P450 family are primarily expressed in the liver (42). The relative abundance of hepatic CYP enzymes was determined as CYP1A2 (13%), CYP2A6 (4%), CYP2D6 (2%), CYP2E1 (7%) and CYP3A4 (30%) (52). Within the liver, CYPs are localized in the inner membrane of mitochondria (Type I) (47), the endoplasmic reticulum (Type II) (47) or the cytoplasm (Type III). Both mitochondrial and endoplasmic CYPs are translated on membrane-free ribosomes in the cytoplasm. Localization is determined by the sequence of the individual NH₂-terminal region of the enzyme which is recognized by site-specific signal-recognition particles (SRPs). SRPs mediate the integration of the final protein at the appropriate site within the cell (53).

Whereas mitochondrial P450s are involved in synthesis and metabolism of internal substances (also called B-Type), e.g. steroid hormone production from cholesterol, endoplasmic P450s mainly metabolize external substances such as medication and environmental toxins (also called D-Type) (54). The heme iron of endoplasmic (Type II) CYPs is reduced by receiving an electron donated from nicotinamide adenine dinucleotide phosphate (NADPH) via the di-flavin (FAD-FMN) protein P450 oxidoreductase (POR). Reduced heme irons transfer the obtained electrons onto molecular dioxygen, the terminal electron acceptor. The produced reactive oxygen species finally mediate catalysis of nearby molecules (47).

In fact, the human Cytochrome P450 superfamily is the most important phase I drug metabolizing system thereby producing more hydrophilic metabolites from endogenous substances and xenobiotics. Six different Type II CYP enzymes, namely CYP1A2, CYP2C9, CYP2C19, CYP2D6, CYP3A4 and CYP3A5, are ultimately responsible for the metabolism of >90% of currently applied clinical pharmaceuticals, with CYP3A4 and CYP2D6 being the most significant ones (55).

1.2.1 Cytochrome P450 2D6 (CYP2D6)

The enzyme Cytochrome P450 2D6 is a major variant of this electron transferring superfamily and mainly expressed in human liver tissue. Although only accounting for 2% of the total hepatic CYP content, CYP2D6 is involved in the hepatic metabolism of around 25% of currently clinically applied pharmaceuticals including major drug classes such as β -blocker, tricyclic antidepressants,

opioids, antiarrhythmics and anti-cancer drugs such as tamoxifen (see Table 1) (44). *CYP2D6* expression at low to moderate levels has also been identified in other human tissues such as kidney, intestine, breast, lung, placenta and the brain (56).

Major pharmaceutical classes	Major class members
Antiarrhythmics	Propafenone Flecainide Lidocaine
Anti-cancer drugs	Tamoxifen Vinblastine Paclitaxel
Anticoagulant	Warfarin
Antidepressants	Amitriptyline Paroxetine
Antiemetics	Ondansetron
Antihistamines	Loratadine Promethazine
Anti-HIV agents	Ritonavir Nevirapine Delavirdine
Antipsychotics	Aripiprazole Risperidone
β-blockers	Atenolol Carvedilol Metoprolol Bisoprolol
Drugs of abuse	Methamphetamine Methylenedioxymethamphetamine (MDMA) Nicotine
Hypnotic	Zolpidem
Neuroleptics	Haloperidol Thioridazine Clozapine
Neurotoxins	1-methyl-4phenyl-1,2,3,6-tetrahydropyridine (MPTP)
Opioids	Codeine Tramadol

Table 1 - List of major classes of pharmaceuticals metabolized by *CYP2D6* with prominent class members (43,44).

1.2.1.1 The *CYP2D6* gene locus: allelic and ethnic variability

In the human genome, the *CYP2D6* gene locus is located on chromosome 22q13.1, consists of nine exons plus eight introns and encodes for a polypeptide consisting of 497 amino acids (43,56). Restricted food intake in sophisticated human societies led to selection pressure against keeping *CYP2D6* and the adjacent pseudogenes *CYP2D7P* and *CYP2D8P* active (51). *CYP2D7P* and *CYP2D8P* were completely and *CYP2D6* in the following partially inactivated. Whereas rodents carry up to nine active copies of *CYP2D6* within their genome, most humans only have one active copy left. The one remaining human gene, however, is highly polymorphic with more than 100

known allelic variants and even more subvariants being reported until 2017. These alleles include fully functional, reduced functional and null alleles (51).

The common nomenclature of *CYP2D6* allelic variants involves the addition of an asterisk and an allele number for variants that share key mutations, e.g. *CYP2D6*1* (57). Variants sharing the same key mutations but exhibiting additional sequence variation are distinguished by capital letters, e.g. *CYP2D6*1A* (58). The **1A* refers to the wild type reference haplotype and shows normal enzyme activity.

Null alleles do not encode for a functional protein and have acquired mutations, single base pair mutations or small insertions/deletions, causing reading frame interruptions or interference with correct transcript splicing which may terminate functional protein production. Only rarely full-length proteins will be produced (*CYP2D6*7*, **12*, **14*, **18*). The by far most common null allele (allele frequency: 25%) in European Caucasians is *CYP2D6*4* (59).

*CYP2D6*9*, for example, lacks codon 281 resulting in a functional protein with reduced enzymatic activity. It has an allele frequency of 1-2% in Caucasians. *CYP2D6*10*, **36*, **37* are characterized by a C100T mutation resulting in Pro³⁴Ser altering the hinge region between the hydrophobic membrane anchor and the globular heme-binding region of the enzyme, also resulting in reduced enzyme activity. *CYP2D6*10* has an allele frequency of up to 50% in oriental populations. *CYP2D6*17* shares two nonsynonymous mutations with *CYP2D6*2* and an additional mutation leading to T¹⁰⁷I amino acid change resulting in decreased enzymatic activity. This allele is nearly absent in European Caucasians but has a frequency of approximately 30% in the African and Afro-American populations (59).

CYP2D6 genes with multiple copies (*CYP2D6xN*) of normal functioning alleles such as **1*, **2*, **35* or *41*, as well as specific single base pair mutations, e.g. -1584 C>G, are associated with increased *CYP2D6* enzyme activity (59).

1.2.1.2 Regulation of *CYP2D6* gene expression and activity

As mRNA expression levels of *CYP2D6* correlate well with *in vitro* and *in vivo* enzyme activity (60), not only its allelic constitution contributes to interindividual *CYP2D6* activity variability but also up- and downregulation of its expression. In contrast to other major CYP enzymes such as *CYP3A4*, *CYP2D6* expression and activity is not influenced by smoking, alcohol induced cirrhosis, herbal medicines or physiological factors such as adult age and gender (61,62). Human *CYP2D6* is further largely unresponsive to typical CYP enzyme inducers such as rifampicin, phenobarbital and dexamethasone (63). However, there is evidence of alterations in CYP expression and activity during human ontogeny. It seems that *CYP2D6* activity is gradually increased within the first year of life with the enzyme reaching adult expression levels and functionality after approximately six to twelve month of age (64). For first and second trimester (<26 weeks of gestation), no to very low *CYP2D6* activity is detected, whereas around 70% of fetal samples show low *CYP2D6* activity in third trimester (65).

On a transcriptional level, *CYP2D6* expression is known to be upregulated by hepatocyte nuclear factor 4 alpha (HNF4 α), a nuclear receptor that plays a key role in hepatocyte differentiation and adult liver homeostasis, and CCAAT/enhancer binding protein alpha (C/EBP α), a transcription factor involved in, amongst others, nutrient metabolism, cell cycle control and liver regeneration. HNF4 α regulates synthesis of apolipoproteins, coagulation factors and CYPs involved in lipid transport, glucose and drug metabolism, e.g. CYP3A4. It directly interacts with the promoter region of *CYP2D6* and upregulates its expression (63). C/EBP α is a transcription factor expressed in later stages of hepatocyte development and overexpression is correlated with increased formation of *CYP2D6* mRNA in HepG2 cells. Knock-down of C/EBP α is associated with decreased mRNA levels. A binding site for this factor could be identified in 2012 in the *CYP2D6* promoter region (66).

The orphan receptor SHP can downregulate *CYP2D6* gene expression by formation of non-active heterodimers that compete with and repress several important hepatocyte specific transcription factors such as RAR α , RXR α or HNF4 α . Farnesoid X receptor (FXR), a nuclear hormone receptor involved in bilirubin metabolism, and NO in a concentration dependent manner are other factors that negatively influence *CYP2D6* expression (43).

Further, epigenetic modifications such as CpG hypermethylation and histone acetylation as well as various miRNAs (miR-140-3p, miR-149, has-miR-370-3p) are discussed for being involved in up- and downregulation *CYP2D6* expression (67,68).

1.2.1.3 Characteristics of CYP2D6 on protein level

The mature CYP2D6 protein has a molecular weight of approximately 56 kDa and is embedded in the phospholipid bilayer of the endoplasmic reticulum facing the cytosol. The crystal structure has been determined first in 2006 (69) and shows a characteristic cytochrome P450 folding pattern with a well-defined substrate binding cavity above the heme group. This cavity contains two negatively charged residues (Asp-301, Glu-216) playing key roles in binding typical substrates of CYP2D6. These are usually lipophilic bases bearing planar hydrophobic aromatic ring and a protonated nitrogen atom at physiological pH. This nitrogen atom is essential for the electrostatic interaction of the substrate with carboxylate groups within the active center of the enzyme. CYP2D6 has a half-life of 46.6 to 51 h and any factor changing this half-life time will modify drug metabolism of the affected individual (51).

1.2.1.4 Clinical implications of allelic and ethnic variability

Due to its substantial allelic variability, the CYP2D6 enzyme is characterized by a large inter-individual difference in enzyme activity. When exposed to equal drug dosages, subjects with multiple gene copies may metabolize target pharmaceuticals more rapidly than slow metabolizers resulting in too low drug blood levels to achieve a medicinal effect. Subjects with low to none enzyme activity, e.g. through missense mutations, however, may exhibit impaired drug metabolism and therefore show increased adverse drug reactions (ADR) or no efficacy at all to similar doses of a given

pharmaceutical. ADRs may occur through drug accumulation in the blood stream, loss of efficacy through impaired pro-drug activation (56).

Individuals can therefore be categorized into four general phenotypes: poor metabolizers (PM) with no, intermediate metabolizers (IM) with decreased, extensive metabolizers (EM) with normal and ultrafast metabolizers (UM) with increased enzyme functionality. The final CYP2D6 activity phenotype depends on the highest functioning allele of an individual which, as mentioned before, varies considerably across the major ethnic groups (70). Globally speaking, 0.4-5.4% of humans are PM, 0.4-11% IM, 67-90% EM and 1-21% UM (59).

The clinical impact of the interindividual variability in CYP2D6 activity can be tremendous and depends on whether the drug is solely metabolized by CYP2D6 and the relative activity and potency of the given pharmaceutical respectively any of its metabolites.

The antiarrhythmic drug encainide, for instance, is less potent than its metabolites. Upon CYP2D6-dependent biotransformation, an increased prevalence of QRS prolongation is visible in EMs compared to PMs. In contrast, propafenone, a potent class Ic antiarrhythmic with intrinsic β -blocker capacity, shows more negative chronotropic potency in PMs than in EMs as the parental drug exhibits a higher potency than its metabolites (71). The antitumoral agent tamoxifen is more prone to therapeutic failure in PMs, whereas UMs are more likely to experience ADRs upon administration. This is the result of the prodrug character of tamoxifen where the derived metabolites endoxifen and 4-OH-tamoxifen are responsible for antitumoral potency of the drug. PM have higher rates of recurrences of breast cancer and shorter relapse-free periods (71). Several clinical studies further indicated a relationship between CYP2D6 genotype and steady-state concentrations of several antipsychotics such as risperidone and haloperidol (71). Antiemetic pharmaceuticals such as ondansetron have shown reduced efficacy in UMs indicating why post-operative vomiting might be of higher incidence in some patients upon ondansetron treatment than others (71). Gefitinib, an antitumoral agent applied during therapy of EGFR-positive NSCLC, even showed increased hepatotoxicity in PMs (72).

1.2.1.5 Evaluation of drug metabolism and safety in vitro

A recent study by Onakpoya et. al. (73) indicated that more than 450 pharmaceuticals had to be withdrawn from the market between 1950 and 2013 with the most common reason being hepatotoxicity (18%) followed by immune related reactions (17%) and cardiotoxicity (14%).

The current gold standard for preclinical prediction of the safety of a new drug compound still involves mainly animal-based experiments which are barely transferable to the human system (74). Two famous examples of drugs erroneously deemed safe through animal testing are thalidomide and the monoclonal antibody TGN1412. Thalidomide, better known under the name Contergan, was introduced in 1956 for the treatment of morning sickness during pregnancy and caused severe congenital abnormalities in infants born upon Contergan usage. This teratogenic effect was not seen on the prenatal development in rodents (74,75). TGN1412, a CD28-specific monoclonal antibody

for treatment of multiple sclerosis or rheumatoid arthritis, led to systemic organ failure in six patients enrolled in a phase 1 clinical trial in 2006 although being previously tested in various animal models including primates (76,77).

Given the fact that bringing a new drug onto the market is estimated to take approximately 12 years with costs of US\$ 800 million to 12 billion (78), effective prediction of human ADRs, including drug induced liver injury (DILI), caused by new drug candidates imposes a tremendous economic benefit and increases the patients' safety. It would allow for the correct identification of unsuitable new drug candidates at very early stages of drug development and before becoming applied to human beings as investigational new drug (IND) in phase I-III clinical trials.

An alternative to animal-based hepatotoxicity testing is seen in human *in vitro* assays. A major bottleneck in identifying human liver associated ADRs in such assays is the lack of a model adequately representing the physiological function of the liver. Many of the currently used models depend on recombinant pure enzyme solutions, isolated liver fractions such as liver microsomes or immortalized respectively cancer cell lines characterized by their inherent metabolic difference to primary human hepatocytes (79,80). Whereas recombinant enzymes and liver fractions do not account for the cellular complexity of drug metabolism, the tumorigenic origin of immortalized cell lines is accompanied by metabolic dysregulation and dysfunctional apoptosis pathways that make them more resistant to toxicological effects of pharmaceutical compounds and unsuitable for drug screening applications (80,81). Primary human hepatocytes (PHH) isolated from adult living or recently deceased patients are morphologically and metabolically comparable to healthy human hepatocytes *in vivo* (82). Being cultured over an extended period of time, however, these cells show a decline in many hepatocyte-specific proteins including CYP enzymes and assimilate to other hepatic cell lines. Within 4 h after plating only 15% of initial mRNA levels and within 48 h after plating only 20-40% of initial CYP enzyme activity are detectable (83). Due to their limited availability and *in vitro* metabolic instability, PHH are barely suitable to meet the quantitative need for reproducible, large scale experiments.

A potential solution for above mentioned limitations could be using human induced pluripotent stem cell (hiPSC) derived hepatocyte-like cells (HLCs) which are obtained from various genetic backgrounds thereby accounting for, among others, the genetic diversity of the CYP enzyme superfamily. Promising the availability of sufficient cell quantities and accounting for a broader range of the human genetic diversity in high-throughput compound screening experiments, appropriately differentiated HLCs may more accurately resemble adverse effects of new drug candidates on human liver tissue (84–86).

1.3 Induced pluripotent stem cells (iPSC)

Pluripotent stem cells are defined by their capacity to indefinitely proliferate in a pluripotent state when kept under stable, pluripotency-preserving conditions but to differentiate into cells of all three germ layers (ectoderm, mesoderm and endoderm) once this environment is changed. Therefore, pluripotent stem cells can differentiate into all 220 somatic cell types occurring in the human body (87,88).

The first, and probably most famous, pluripotent stem cell type discovered was the embryonic stem cell (ESC). In 1981, Martin et al. were capable of isolating and establishing a murine pluripotent stem cell line from the inner cell mass (ICM) of a normal preimplantation mouse embryo *in vitro* (89). For technical and ethical reasons, it took until 1998 for the first human embryonic stem cell lines to be established by James A. Thomson et al. at the University of Wisconsin, Madison (90). Interestingly, one of the 14 cell lines generated during these experiments has subsequently been used in clinical trials for many years (91). Again, the pluripotent stem cells were obtained from the ICM of preimplantation human embryos. The method of acquiring ESC by destructing the embryo, which has been produced during *in vitro* fertilization (IVF), raised major ethical and moral considerations on all levels of society: scientist, physicians, ethicists, politicians, governments and the general public alike (92–94). Although promising great potential for tissue repair and the treatment of a wide range of common diseases, the destructive influence on potential human life in its early stage found itself to be a major roadblock for progression of this technique into clinical application. Despite ethical and legislative issues, until 2011 roughly 60 hESC lines have been produced world-wide. These cell lines have been used for differentiation studies into a vast range of different cell types (95) including mature neurons (96), insulin producing pancreatic β -cells (97) and cardiomyocytes (98). In 2004, Karin Hübner et al. were even capable of producing germ cells from ESC (99).

In 2006 resp. 2007, pluripotent stem cell science was revolutionized by the induction of pluripotency in somatic cells of mice (100) resp. humans (101,102). This was shown by the two independent, almost simultaneously publishing groups of Shinya Yamanaka and James A. Thomson. Through forced expression of four transcription factors (Oct4, Sox2, Klf4 and c-Myc; resp. Oct4, Sox2, Nanog and LIN28) somatic cells of the human body, in both cases human dermal fibroblasts, could be transformed into a pluripotent-like state, comparable to that of hESC (see Fig. 4). This method circumvents some of the major roadblocks of the clinical application of previous hPSC including ethical issues regarding the need of destructing human embryos and concerns of immune rejection of the derived advanced therapeutic medicinal products (ATMPs). The major impact of this invention was finally obvious when Shinya Yamanaka received the Nobel Prize for Physiology or Medicine in 2012 for the induction of pluripotency in somatic cells (103).

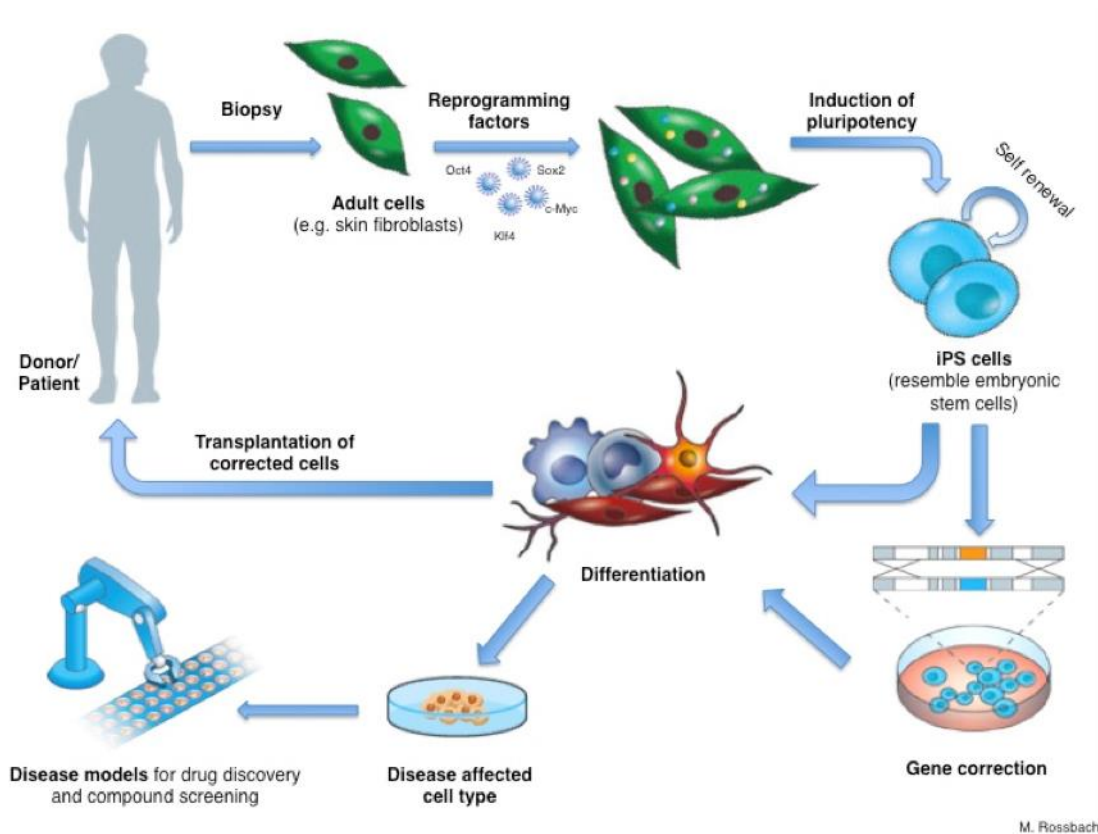


Fig. 4 – Concept of induced pluripotent stem cells. Tissue biopsies from informed healthy donors or patients can be reprogrammed into a pluripotent state comparable to the current gold standard of embryonic stem cells by forced overexpression of a panel of transcription factors such as OCT4, SOX2, KLF4 and c-MYC. These induced pluripotent stem cells (iPSC) are capable of (theoretically) indefinite self-renewal and differentiation into somatic cells of all three germ layers (meso-, endo-, ectoderm). Derived cell types may be used for a variety of applications including disease modelling, drug toxicity screening, or in the scope of advanced therapy medicinal products. Illustration adapted from Rossbach et. al. (104).

Despite its great potential, the induction of pluripotency needed improvement on various levels of the derivation protocol before iPSC and derived tissues could be ever taken into consideration for a wide range of applications. Some of these roadblocks of iPSCs usability have now already been addressed:

The original protocol from 2007 was based on the usage of integrating vectors from adeno- (101) and lentiviruses (102) to drive somatic cells into a pluripotent state thereby disrupting the cells genetic integrity questioning the general comparability of derived tissues to somatic cells and raising tumorigenic safety issues for any clinical usage. To overcome this issue, several non-integrating reprogramming techniques have been developed including episome (105), Sendai virus (106), modified mRNA (107) and protein (108) based approaches.

Initially, iPSC have been cultured on a feeder layer consisting of inactivated murine fibroblasts (101,102). This method is time consuming, expensive and not considered to be a defined growth environment for cultured cell lines. Since 2007, several feeder- and xenofree matrices, culture media and passaging systems have been developed offering fully defined culturing conditions for derived iPSC (109–112) thereby reducing batch to batch variety of employed materials. Even automated culturing approaches and suspension culture in bioreactors have been described (113,114).

To increase low reprogramming efficiencies ranging from 0.013% for episome to 2.1% for modified mRNA based reprogramming (115), several small molecule combinations have been tested (116). A mixture of three small molecules (A-83-01, PD0325901, CHIR99021) inhibiting TGF β , MEK and GSK3 β pathways indicated to significantly enhance episomal reprogramming of human somatic cells (117).

Since its invention, iPSCs are considered or are being assessed for a broad range of applications including *in vitro* disease modelling (85,118,119), *in vitro* toxicity studies (74,120,121) and clinical usage for tissue repair (122–124). This introduction will further focus on the use of human iPSC for the *in vitro* production of hepatocyte-like cells and their potential for drug-toxicity screenings.

1.3.1 Hepatic differentiation of hiPSC *in vitro*

In 2003, Rambhatla et al. for the first time described the successful derivation of a homogenous cell population featuring hepatocyte-like features from human embryonic stem cells without an intermediate embryoid body formation usually resulting in heterogenous cell populations (125). Since then, various hepatic differentiation protocols have been developed (126–129) which, in the dawn of induced pluripotent stem cells, could also be converted onto differentiating hiPSC into HLCs (130,131). In 2011, Jozefczuk et al. compared hESC- and hiPSC-derived HLCs (132). Although certain differences could be detected when using the same differentiation protocol, common hepatocyte-specific gene expression important for liver physiology was observed.

As *in vivo* hepatogenesis is a highly complex process depending on a controlled cascade of signaling events, most *in vitro* hepatic differentiation protocols mimic basic hepatic differentiation events by conducting a three-step approach: generation of definitive endoderm (DE), generation of hepatic endoderm (HE) and maturation of HLCs. Herefore, various growth factors and/or small molecules are employed.

Definitive endoderm (DE) formation is induced in pluripotent stem cells through Nodal and Wnt3a signaling. As sufficiently active protein sources of Nodal itself is difficult to obtain, the TGF- β family member Activin A, showing a comparable receptor binding profile and triggering similar intracellular signaling pathways, may be used instead (133,134). WNT signaling is usually induced by the glycogen synthase kinase (GSK)-3 inhibitor CHIR99021 which is favored over adding WNT3A into DE differentiation for its cost effectiveness with comparable DE induction efficiency (135,136). Upon treatment for 72 h, cells lose pluripotency associated biomarkers such as OCT4 and NANOG, change their morphology and express the DE markers FOXA2, SOX17, CXCR4 and HHEX (137).

Following establishment of definitive endoderm, hepatic endoderm (HE) may be derived by adding the small molecule dimethyl sulfoxide (DMSO), a amphipathic molecule commonly employed for transdermal delivery of hydro- and lipophilic medication or as cryopreservation additive, to a basal serum-free culture medium (125,138,139). Although its biological effect during hepatic endoderm

derivation is not fully elucidated yet, DMSO application to DE cells induces vast morphological changes and proliferation. Within 4-5 days, the majority of treated cells should express the hepatic endodermal markers AFP, HNF4 α , GATA4 and CEBPA and exhibit typical hepatic endodermal morphology (137).

Hepatic maturation, the final step of the typical hepatic differentiation protocol, may be performed with addition of various growth factors including BMP4, EGF, FGF2, FGF4, HGF, OSM and/or VEGF (137) respectively hormones such as dexamethasone (137) or insulin (140) to hepatocyte maturation media such as, for example, HepatoZYME, a proprietary medium from ThermoFisher Scientific, or a modified Leibovitz L-15 medium (137,141). After several days of culture in growth factor supplemented media, derived cells morphologically resemble hepatocytes with large and angular cells exhibiting bright junctions and multiple nuclei. Derived HLCs express hepatocyte marker such as albumin, HNF4 α , A1AT, CYP3A4 and AFP (137,139). The HLC derivation process employed during this thesis is adapted from Wang et al. (142).

Although currently known protocols are capable of efficiently generating cells with hepatocyte-like morphology and functional activity, PSC-derived HLCs are known to exhibit a rather fetal phenotype. HLCs indicate detectable expression of fetal hepatocyte markers such as AFP and immature functionality especially regarding biotransformation processes. These features usually become visible when derived HLCs are compared to freshly plated primary human hepatocytes (PHH) (82,143).

Due to limited availability and rapid dedifferentiation *in vitro* of primary human hepatocytes respectively limited comparability for metabolic functions in hepatoma cell lines such as HepG2, much effort has been undertaken to increase pluripotent stem cell derived HLC maturity. This involves scaled 3D cell culture models in various matrices including collagen, alginate, hydrogels or Matrigel, co-culture of hepatic endodermal cells with human umbilical vein endothelial cells (HUVECs) or human mesenchymal stem cells (hMSCs), co-culture of HLCs with endothelial, stellate or biliary cells to better mimic the *in vivo* extracellular architecture or inhibiting signals driving differentiation into other germ lineages (144).

Despite the rather fetal phenotype of derived HLCs from currently available hepatic differentiation protocols, PSC-derived HLCs have been successfully employed in *in vitro* studies of infectious diseases such as hepatitis B (145) and C (146) and malaria (147) as well as metabolic diseases such as Wilson's Disease (148), α 1-antitrypsin deficiency, hypercholesterolemia, glycogen storage disease type 1a (149) or non-alcoholic fatty liver disease (NAFLD) (150). For the large multinational and intercontinental efforts that are being undertaken to employ human pluripotent stem cell derived tissues for preclinical testing (151), it can be assumed that *in vitro* obtained toxicological data will soon become a valuable part of regulatory submissions for new pharmaceutical compounds. However, current *in vitro* toxicity studies mostly rely on single donor derived tissues which obviously cannot account for the complex, individual (patho-)physiological, pharmacogenetic and/or ethnic differences (152).

Human iPSC-derived HLCs derived from patients with different CYP2D6 phenotypes may, therefore, harbor great potential to support the development of a testing procedure allowing for the identification of suitable INDs without the necessity for time and labor expensive animal testing and more adequately reflecting human hepatic response. Until conduction of the experiments belonging to this thesis from June 2017 to February 2018, to our best knowledge, no investigation was performed on the establishment of a testing kit consisting of iPSC-derived HLCs harboring varying CYP2D6 phenotypes, where the employed iPSC lines were episomally reprogrammed from fibroblasts respectively urine cells.

1.4 Aim of this thesis

For drug induced liver injury (DILI) being the most frequent reason of drug withdrawal from the market, the establishment of a cell-based *in vitro* test system that adequately reflects drug metabolism and hepatotoxic effects of investigational new drug (IND) candidates imposes huge potential for indicating adverse drug reactions (ADR) at early stages of drug development, reducing the necessity of animal testing and increasing patient's safety.

Being predominantly involved in the hepatic metabolism of 20-25% of all clinically applied medication, including >160 different pharmaceuticals of major drug classes like tricyclic antidepressants, opioids, antiarrhythmics and β -blockers, the polymorphic enzyme Cytochrome P450 2D6 may be an ideal candidate for the development of such a cell-based (pre-)clinical toxicity assay. Due to its genetic variability, however, substantial interindividual differences can be observed influencing effective blood levels of a given drug candidate and, therefore, its safety and efficacy.

During this thesis, two episomally reprogrammed, fully characterized and published induced pluripotent stem cell lines were chosen for their distinct CYP2D6 genotype and used to derive hepatocyte like cells (HLCs). Aim of this thesis is to lay the foundation of the development of a cell-based testing kit for the effect of pharmaceutical compounds on human liver tissue phenotypically representing two different CYP2D6 variants.

To achieve this, the following main objectives will be addressed:

1. Selection of two induced pluripotent stem cell lines for their different CYP2D6 geno- and predicted phenotypes
2. Differentiation of selected induced pluripotent stem cell lines into HLCs using the ISRM's current standard protocol and materials (Matrigel™ and supplemented modified Leibovitz L15 medium) and a completely defined matrix (LN111/LN521 mix) and medium (HepatoZYME) combination
3. Characterization of derived HLCs using various molecular and biochemical assays including RT-qPCR, immunocytochemistry, flow cytometry, Western Blot analysis, ICG uptake/release, urea detection and a CYP3A4 activity assay
4. Assessment of CYP2D6 expression of derived HLCs on transcriptional and proteomic level
5. Comparing ISRM's standard materials to a more defined matrix and medium combination (Laminin 111/521 mixture and HepatoZYME medium)

2 Materials and Methods

2.1 Equipment and Consumables

Equipment	Model	Company, City, Country
Agarose Gel Electrophoresis System	Perfect Blue Gel System	PEQLAB Biotechnology, Erlangen, Germany
Class II Biosafety Cabinet	Biowizard	Kojair®, Vilppula, Finland
Class II Biosafety Cabinet	Labogene Scanlaf MARS	GKS KlimaService GmbH, Sturh, Germany
Microcentrifuge	Microcentrifuge 5418	Eppendorf AG, Hamburg, Germany
Camera	AxioCam ICC3	Zeiss, Jena Germany
Centrifuge	Centrifuge 5810R	Eppendorf AG, Hamburg, Germany
Chemical Safety Cabinet	23-201260-401	Düperthal, Karlstein, Germany
Counting Chamber	Neubauer 0.0025 mm ²	Superior, Marienfeld, Germany
ELISA Plate Reader	AF2200	Eppendorf AG, Hamburg, Germany
Flow Cytometer	CyAn ADP Flow Cytometer	Beckman Coulter, Brea, USA
Fluorescence Microscope	LMS700	Zeiss, Jena, Germany
Freezer (-80°C)	Temperature U725	Eppendorf, Hamburg, Germany
Freezer (-20°C)		Liebherr Premium, Ochsenhausen, Germany
Incubator (37°C / 5% CO ₂)	INNOVA CO-170	New Brunswick Scientific, Edison, USA
Incubator (37°C / 5% CO ₂)	CB150	Binder GmbH, Tuttlingen, Germany
Inverted Microscope	Leica DMIL	Leica Microsystems, Wetzlar, Germany
Liquid Nitrogen Tank	BioSafe®	Cryotherm GmbH, Kirchen, Germany
Luminometer	Lumat LB 9507	Berthold Technologies, Bad Wildbad, Germany
Mr. Frosty	NALGENE™ Cryo 1°C Freezer Container	ThermoFisher Scientific, Waltham, USA
Nanodrop	Nanodrop 2000c	ThermoFisher Scientific, Waltham, USA
Pipettes	2.5, 10, 20, 200, 1000 µl	Eppendorf AG, Hamburg, Germany
Pipetting aid	PIPETBOY acu 2	INTEGRA, Bioscience, Fernwald, Germany
Real Time PCR machine	StepOnePlus™	AB Applied Biosystem, California, USA
Shaking Plate	SeaStar® Orbital Shaker	Thomas Scientific, New Jersey, USA
Thermoblock	Thermomixer comfort®	Eppendorf AG, Hamburg, Germany
Thermocycler	peqSTAR 96X Universal	PEQLAB, Erlangen, Germany
Vortex	Vortex Genie 2 T	Scientific Industries, New York, USA

Table 2 – **Equipment used during the experimental phase of the thesis.** In alphabetical order, a list of all equipment used including general description of equipment, model, manufacturer, city and country of origin

Software	Company, City, Country
ELISA Plate Reader AF2200 1.1.24	Eppendorf AG, Hamburg, Germany
FlowJo™	Becton Dickinson, Ashland, USA
ImageJ Fiji	Max-Planck Institute, Dresden, Germany
Microsoft 365	Microsoft, Redmond, USA
Microsoft Office 2010	Microsoft, Redmond, USA
NanoDrop 2000	ThermoFisher Scientific, Waltham, USA
Zen Blu 2.5	Zeiss, Jena, Germany
ViiA™ 7 Software	ThermoFisher Scientific, Waltham, USA

Table 3 – **Software**. In alphabetical order, all software used throughout the experimental and data analysis phase of the thesis including name of the software, developer, city and country of origin

Consumable	Supplier, City, Country
0.05% Trypsin/EDTA	ThermoFisher Scientific, Waltham, USA
β-Mercaptoethanol	ThermoFisher Scientific, Waltham, USA
A-83-01	Tocris Bioscience, Bristol, UK
Activin A	PeproTech Inc., Hamburg, Germany
Acrylamide/Bisacrylamide (30%)	Carl Roth GmbH KG, Karlsruhe, Germany
Agarose Powder	Biozym Scientific GmbH, Oldendorf, Germany
Amersham™ ECL™ Primary Western Blotting Detection Reagent	GE Healthcare UK Ltd., Buckinghamshire, UK
B-27™ -retinoic acid (50X supplement)	ThermoFisher Scientific, Waltham, USA
Basic fibroblast growth factor (bFGF)	ThermoFisher Scientific, Waltham, USA
Bovine Serum Albumin (BSA)	Sigma-Aldrich, Taufkirchen, Germany
Bromophenol Blue	Merck, Darmstadt, Germany
CHIR99021	Stemgent, Cambridge, USA
DEPC-treated nuclease-free water	Promega Corporation, Wisconsin, USA
Dexamethasone	Sigma-Aldrich Chemicals, Taufkirchen, Germany
Dimethyl Sulfoxide	Sigma-Aldrich, Steinheim, Germany
Direct-zol™ RNA Mini-Prep Kit	Zymo Research, Irvine, USA
Distilled Water	Fischar® GmbH & Co., Saarbrücken, Germany
Dulbecco's Modified Eagle Medium (DMEM)	ThermoFisher Scientific, Waltham, USA
Dulbecco's Modified Eagle Medium Nutrient Mixture F-12 (DMEM F-12)	ThermoFisher Scientific, Waltham, USA
DNA Loading Buffer 10X	ThermoFisher Scientific, Waltham, USA
Dulbecco's Phosphate Buffered Saline [-]MgCl ₂ [-]CaCl ₂ (DPBS)	ThermoFisher Scientific, Waltham, USA
Ethanol 95%	Zentralapotheke Universitätsklinikum, Düsseldorf, Germany
Ethylenediaminetetraacetic acid (EDTA)	Carl Roth GmbH & Co. KG, Karlsruhe, Germany
Falcon™ 5 ml round bottom polystyrene test tube	Corning, New York, USA
Fetal Bovine Serum (FBS)	ThermoFisher Scientific, Waltham, USA
Gelatine	Sigma-Aldrich, Taufkirchen, Germany
GelRed™ Nucleic Acid Stain	Biotium Inc., California, USA
Glycerol	Sigma-Aldrich, Taufkirchen, Germany
Glucose	ThermoFisher Scientific, Waltham, USA
GlutaMax® (L-alanyl L-glutamine)	ThermoFisher Scientific, Waltham, USA
Glycogen Storage - Periodic Acid Schiff Staining System	Sigma-Aldrich, Taufkirchen, Germany
Go Taq® G2 Hot Start Polymerase kit	Promega Corporation, Wisconsin, USA
Hank's Balanced Salt Solution	MediaTechInc, Corning, VA, USA
Hematoxylin	Sigma-Aldrich Chemicals, Taufkirchen, Germany
Hepatic Growth Factor (HGF)	PeproTech Inc., Hamburg, Germany
HEPES	ThermoFisher Scientific, Waltham, USA
HepG2	ATCC, Manassas, USA
Hoechst 33258	Sigma-Aldrich Chemicals, Taufkirchen, Germany
Human Albumin ELISA Quantification Set	Bethyl Laboratories Inc., Montgomery, USA
Indocyanine Green (ICG)	Sigma-Aldrich Chemicals, Taufkirchen, Germany

Insulin	ThermoFisher Scientific, Waltham, USA
Knock-Out Serum Replacement (KO-SR)	ThermoFisher Scientific, Waltham, USA
Laminin 111	Biolamina, Sundbyberg, Sweden
Laminin 521	Biolamina, Sundbyberg, Sweden
Leibovitz's Medium (L-15)	ThermoFisher Scientific, Waltham, USA
Lucia Broth (LB)	Lennox Deutschland GmbH, Rattigen, Germany
Matrigel®, hESC Qualified Matrix	Corning, New York, USA
Milk Powder	Carl Roth GmbH & Co KG, Karlsruhe, Germany
mTeSR™1 Basal Medium	Stem Cell Technologies, Corning, USA
mTeSR™1 Supplement 5X	Stem Cell Technologies, Corning, USA
N2 Supplement	Gibco® Thermo Fisher Scientific, Waltham, USA
NaCl	Carl Roth GmbH & Co, KG, Karlsruhe
NaOH	Carl Roth GmbH & Co, KG, Karlsruhe
NEAA	Lonza, Velvier, Belgium
Normal Donkey Serum (NDS)	Sigma-Aldrich Chemicals, Taufkirchen, Germany
Normal Goat Serum (NGS)	Sigma-Aldrich Chemicals, Taufkirchen, Germany
NucleoSpin Plasmid (NoLid) Kit	Macherey-Nagel GmbH, Düren, Germany
Nunc MaxiSorb™ flat bottom 96-well plate	ThermoFisher Scientific, Waltham, USA
Oncostatin M (OSM)	ImmunoTools, Friesoythe, Germany
One Shot® TOP10 Competent cells	ThermoFisher Scientific, Waltham, USA
P450 Glo Assay™, CYP3A4	Promega Corporation, Wisconsin, USA
Paraformaldehyde (PFA)	USB Corporation, Cleveland, USA
PD0325901	Tocris Bioscience, Bristol, UK
Penicillin/Streptomycin (P/S)	ThermoFisher Scientific, Waltham, USA
Perfect™ 100bp DNA Ladder	EURx, Poland
Perfect Plus™ 1Kb DNA Ladder A30	EURx, Poland
Phosphatase Inhibitor Cocktail	Sigma-Aldrich, Missouri, USA
Pierce™ BCA Protein Assay Kit	ThermoFisher Scientific, Waltham, USA
Ponceau Solution S	Sigma-Aldrich Chemicals, Steinheim, Germany
Power SYBR® Green	ThermoFisher Scientific, Waltham, USA
Protease Inhibitor Cocktail	Sigma-Aldrich, Missouri, USA
Proteinase K	Sigma-Aldrich Chemicals, Taufkirchen, Germany
Protein Marker V (Pre-stained)	PEQLAB Biotechnology, Erlangen, Germany
QuiAquick Gel Extraction Kit	Qiagen, Cologne, Germany
Radioimmunoprecipitation Assay Buffer (RIPA)	Sigma-Aldrich, Missouri, USA
RPMI 1640	Thermo Fisher Scientific, Waltham, USA
Reverse Transcription TaqMan® Kit	Applied Biosystems Roche, Foster City, USA
Sodium Dodecyl Sulfate (SDS)	Carl Roth GmbH & Co, KG, Karlsruhe
Sodium Hydrogen Carbonate (NaHCO ₃)	Carl Roth GmbH & Co, KG, Karlsruhe
Stem Macs™ iPS-Brew XF	Miltenyi Biotech, Bergisch Gladbach, Germany
Stem Macs™ iPS-Brew XF Supplement 50X	Miltenyi Biotech, Bergisch Gladbach, Germany
Test tube, round bottom, polystyrene, 5 ml	Sarstedt AG & Co KG, Nümbrecht, Germany
Tris-HCl	Carl Roth GmbH & Co, KG, Karlsruhe
Triton X-110	Sigma-Aldrich, Taufkirchen, Germany
TRIzol™	Thermo Fisher Scientific, Waltham, USA
Trypan Blue	Sigma-Aldrich, Missouri, USA
TrypLE™ Express	Thermo Fisher Scientific, Waltham, USA
Trypsin	Thermo Fisher Scientific, Waltham, USA
Tryptose Phosphatase Broth (TPB)	Thermo Fisher Scientific, Waltham, USA
Tween20	Sigma-Aldrich, Taufkirchen, Germany
Urea Colorimetric Assay, QuantiChrome™	BioAssay Systems, Hayward, USA
Y-27632	Tocris Bioscience, Bristol, UK

Table 4 – **Consumables**. In alphabetical order, all consumables used throughout the experimental and data analysis phase of the thesis including name of the consumable, supplier, city and country of origin

Name	Host-Species	Dilution	Catalogue Number	Supplier	Stage
α -AFP antibody	Rabbit	1:250	HPA023600	Sigma Aldrich	DE, HE, HLC
Monoclonal α -Albumin antibody	Mouse	1:500	A6684-.2ml	Sigma Aldrich	HLC
Invitrogen™ Cytochrome P450 2D6 antibody	Rabbit	1:100	PA5-39598	ThermoFisher Scientific	HLC
E-Cadherin (24E10)	Rabbit	1:300	3195	Cell Signaling Technology	HLC
α -HNF4 α antibody (EPR3648)	Rabbit	1:300	ab92378	Abcam	DE, HE, HLC
Human SOX2 antibody	Mouse	1:200	4900S	Cell Signaling Technology	DE
Human SOX17 Antibody	Goat	1:50	AF1924	R&D Systems	DE, HE
Human Glucuronosyltransferase 1A1/UGT1A1 Antibody	Mouse	1:200	MAB6490	R&D Systems	HLC

Table 5 – **Primary antibodies used for immunofluorescence staining** (immunocytochemistry and flow cytometry) including applied dilutions in PBB/PBS (-/-, ratio 1:1), catalogue numbers, suppliers. DE – Definitive Endoderm, HE – Hepatic Endoderm, HLC – Hepatocyte-like cells

Name	Host-Species	Dilution	Catalogue Number	Supplier
Anti-goat IgG, Alexa Fluor 488	Donkey	1:500	A11055	ThermoFisher Scientific
Anti-rabbit IgG, Alexa Fluor 488	Goat	1:500	A27034	ThermoFisher Scientific
Anti-rabbit IgG, Alexa Fluor 555	Goat	1:500	A21428	ThermoFisher Scientific
Anti-goat IgG, Alexa Fluor 555	Donkey	1:500	A21432	ThermoFisher Scientific
Anti-mouse IgG, Cy3	Goat	1:2000	A10521	ThermoFisher Scientific
Anti-goat IgG, Alexa Fluor 647	Donkey	1:500	A21447	Thermo Fisher Scientific

Table 6 – **Secondary antibodies used for immunofluorescence staining** (ICC and FC) including applied dilutions in PBB/PBS (-/-, ratio 1:1), catalogue numbers and suppliers

Primer		Sequence (5' – 3')	Length (in bp)	T _M (in °C)	% GC	Product Length (in bp)
AFP	Fwd	AGCAGCTTGGTGGTGGATGA	20	54	55	88
	Rev	CCTGAGCTTGGCACAGATCCT	21	56	57	
ALB	Fwd	AGCTGTTATGGATGATTTTCGCAG	23	53	43	77
	Rev	CCTCGGCAAAGCAGGTCTC	19	55	63	
β-actin	Fwd	TCAAGATCATTGCTCCTCCTGAG	21	61	52	87
	Rev	ACATCTGCTGGAAGGTGGACA	23	57	52	
CYP2D6	Fwd	TTCCTGCCTTTCTCAGCAGG	20	60	55	185
	Rev	GCACAAAGCTCATAGGGGGA	20	60	55	
CYP3A4	Fwd	GTGACTTTGCCCATTTGTTTAGAAAG	25	54	40	79
	Rev	CAGGCGTGAGCCACTGTG	18	55	67	
HNF4α	Fwd	GTGCGGAAGAACCACATGTACTC	23	57	52	102
	Rev	GAAGCATTTCTTGAGCCTGCAGTA	24	56	46	
OCT4	Fwd	AGTTTGTGCCAGGGTTTTTG	20	57	45	113
	Rev	ACTTACCTTCCCTCCAACC	20	59	55	
RPL37a	Fwd	GTGGTTCCTGCATGAAGACAGTG	23	62	52	84
	Rev	TTCTGATGGCGGACTTTACCG	21	60	52	
RPS16	Fwd	GCTATCCGTCAGTCCATCTCCAA	22	57	52	73
	Rev	CCTTCTTGAAGCCTCATCCAC	20	57	55	

Table 7 – **Primer list.** List of primers used for qRT-PCR for transcripts. Stated are name of transcript, sequence (5' → 3' direction), length in base pairs (bp), melting temperature, relative GC content and product length. Supplier for all primers was Eurofins Genomics, Ebersberg, Germany. Fwd – Forward, Rev – Reverse, Bp – Base pairs, T_M – Melting temperature, % GC – Percentage Guanine and Cytosine, °C – Degree Celsius

2.2 Cell culture

2.2.1 Cell Source

The pluripotent stem cell lines used throughout this study are fully characterized and published cell lines of the Institute for Stem Cell Research and Regenerative Medicine (ISRM) of Heinrich-Heine University Düsseldorf and referred to as UJiPS13, also named HHUUKDi001-A or ISRM-UM51, and S12_13B. Both cell lines were derived and used under ethical approval of the ethical committee of the medical faculty of Heinrich-Heine University Düsseldorf, Germany (UJiPS13 approval number: 5704; S12_13B approval number: 5013).

UJiPS13 was derived from SIX2-positive renal cells isolated from urine of a 51 years old male of African origin (153). S12_13B was derived from primary fibroblasts of a 50 years old female suffering from low-grade hepatosteatosis (154,155). Briefly, both cell lines were reprogrammed by nucleofection of two episomal plasmids expressing OCT4, SOX2, NANOG, LIN28, C-MYC and KLF-4 (102). Pathway inhibition by a three component small molecule cocktail (A-83-01 (TGFβ-inhibitor), PD0325901 (MEK-inhibitor), CHIR99021 (GSK3β)) was used to enhance reprogramming efficiency for S12_13B but not UJiPS13. Both cell lines were assessed for the respective CYP2D6 genotype through analysis of genomic DNA performed by CeGat GmbH (Tübingen, German; see Table 8). According to the Pharmacogenomics Organizations (PGx) CPIC and DPWG, S12_13B can be classified as Extensive Metabolizer (EM) and UJiPS13 as Intermediate Metabolizer (IM).

Cell line	Gene	Genotype	Phenotype	Pharmacogenomics (PGx) organization
S12_13B	CYP2D6	*1 / *2	EM	CPIC, DPWG
UJiPS13	CYP2D6	*4 / *17	IM	CPIC, DPWG

Table 8 – CYP2D6 genotype and phenotype of S12_13B and UJiPS13. Genomic DNA was analyzed by CeGat GmbH for the individual CYP2D6 genotype and used to determine their associated phenotype. S12_13B is classified as extensive metabolizer (EM), whereas UJiPS13 is an intermediate metabolizer (IM). PGx: Pharmacogenomics, CPIC – Clinical Pharmacogenetics Implementation Consortium, DPWG – Dutch Pharmacogenetics Working Group

HepG2 cells were used as positive controls for a variety of functionality assays throughout the thesis. This cell line is an immortalized human liver carcinoma cell line acquired from the liver tissue of 15 year old Caucasian male (156). HepG2 cells were obtained from ATCC (HB-8065™).

2.2.2 Non-Pluripotent Cells

HepG2 cells were routinely cultured as monolayers on cell culture treated plastic ware without growth matrix and in low glucose (1 g/l), pyruvate containing Dulbecco's Modified Eagle Medium supplemented with 10% FBS (both Thermo Fisher Scientific) – referred to as HepG2 Medium. HepG2 Medium was exchanged twice per week. HepG2 cells were kept at 37°C / 5% CO₂ under humidified atmosphere (INNOVA CO-170 Incubator, New Brunswick Scientific, Edison, USA).

2.2.2.1 Passaging non-pluripotent cells

HepG2 cells were passaged as single cells when approximately 80% confluent. Cells were washed twice with 5 ml/T75 flask PBS (-/-), incubated with 2 ml/T75 flask 0.05 % Trypsin/EDTA (both Thermo Fisher Scientific) for 4 min at 37°C/5% CO₂, washed off gently using a 5 ml stripette and transferred into a 15 ml conical tube containing 5 ml HepG2 medium. The cell suspension was then centrifuged at 600xg for 5 min, supernatant discarded and the cell pellet gently resuspended in 4 ml fresh HepG2 medium. The cells were transferred into a fresh T75 cell culture treated plastic flask containing 20 ml fresh HepG2 Medium. Routinely a split ratio of 1:8 was applied. HepG2 cells were split every 7 days.

2.2.2.2 Freezing and Thawing non-pluripotent cells

For freezing, 80% confluent cultures were washed twice with 5 ml/T75 flask PBS(-/-), incubated with 2 ml/T75 flask 0.05 % Trypsin/EDTA at 37°C/5% CO₂ for 5 min, washed off gently with 5 ml HepG2 medium, transferred to a 15 ml conical tube and centrifuged at 300xg for 5 min. The supernatant was discarded, the cell pellet resuspended in 5 ml of HepG2 medium supplemented with 10% DMSO (Sigma Aldrich, Steinheim, Germany) and transferred into a cryovials (1 ml/cryovial). The cryovials were stored in a MrFrosty™ isopropanol box at -80°C (-1°C/min) O/N and in liquid nitrogen (-160°C) from there on until further usage.

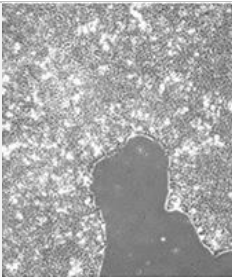
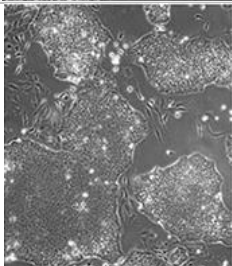
For thawing, a cryovial was removed from liquid nitrogen and incubated at RT until only a small ice clump was left. The cell suspension was carefully pipetted into a 15 ml conical tube containing 10 ml of HepG2 medium at RT. After centrifugation at 300xg and RT for 5 min, the supernatant was discarded and the cell pellet resuspended into 10 ml HepG2 medium. The cell suspension was added into a fresh T75 flask containing 10 ml HepG2 medium. Cultures were incubated at 37°C/5% CO₂ and medium exchanged as described before (2.2.2. Non-pluripotent cells).

2.2.3 Human Induced Pluripotent Stem Cells (hiPSC)

Human iPSC lines S12_13B and UJiPS13B (153) were routinely cultured feeder-free either on Matrigel (MG, Corning Inc., New York, USA) and in StemMACS iPS-Brew (Miltenyi Biotec GmbH, Bergisch-Gladbach, Germany) or in the completely defined matrix / medium combination Laminin 521 (LN521, Biolamina, Sundbyberg, Sweden) and StemMACS iPS-Brew. Pluripotent stem cell culture medium was exchanged daily. All hiPSC cultures were kept in an incubator (INNOVA CO-170 Incubator, New Brunswick Scientific) at 37°C / 5% CO₂ under humidified atmosphere.

2.2.3.1 Daily Assessment of hiPSC (“Scoring”)

HiPSC cultures have been assessed for morphology and occurrence of differentiation on a daily basis using a Leica DMIL inverted microscope (Leica Microsystems, Wetzlar, Germany; see Table 9). Depending on the morphology of the cells, size of the colonies and amount of differentiation, the cell cultures were graded from A (typical hiPSC-like morphology, big and dense colonies, no differentiation) to D (no hiPSC-like morphology visible, high amount of differentiation). Based on the score of a culture, the cells were either passaged, fed or discarded.

Grade	Description	Pictures
A	Perfect culture (large, dense colonies; low to no differentiation visible) and >70% confluent	
B	Good culture (medium to large colonies; low to medium differentiation visible) and >50% confluent	

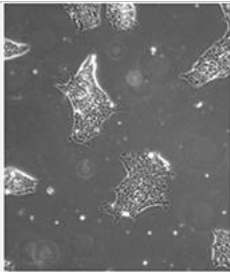
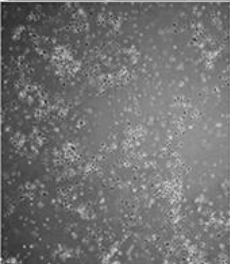
C	Fair culture (small to medium colonies; medium to low differentiation visible) and/or >25% confluent	
D	Poor culture (poor adherence, high amount of differentiation and no iPSC visible)	

Table 9 – Grading system of human induced pluripotent stem cells. Induced pluripotent stem cells (iPSC) grow in sharp-edged, flat colonies and exhibit a characteristic high nucleus to cytoplasm size ratio. Their usual cell doubling time averages at 16-18 hours (157). Daily assessment could therefore reveal changes in phenotype stability and cell cycle regulation – both being an indicator of, amongst others, insufficient cell culture conditions or karyotypic instability.

2.2.3.2 Preparation of Matrigel®-Coated Plates

Matrigel is a basement membrane produced by Engelbreth-Holm-Swarm (EHS) mouse sarcoma cells. It supports maintenance and growth of pluripotent stem cells under feeder-free conditions.

hESC-qualified growth factor reduced (GFR) Matrigel® stock solution was aliquoted into 0.5 mg/tube and stored at -80°C until further usage. One aliquot was sufficient to coat one complete 6-well or 12-well plate. Once an aliquot was retrieved from -80°C and thawed completely, the Matrigel® solution was diluted with ice-cold pipette tips in 6 ml ice-cold KnockOut™ Dulbecco's Modified Eagles Medium (KO-DMEM, ThermoFisher Scientific). 1 ml/6-well resp. 0.5 ml/12-well was added and the plates incubated at 4°C O/N. Immediately prior to adding cells, Matrigel solution was removed and the wells washed once with 1 ml/6-well resp. 0.5 ml/12-well KO-DMEM. If not used directly, 2 ml/6-well or 1 ml/12-well KO-DMEM was added, plates sealed with parafilm and stored at 4°C for up to one week.

2.2.3.3 Preparation of LN521-coated Plates

Laminins are heterotrimeric basement membrane proteins consisting of various combinations of α , β and γ chains. LN521 consists of the specific combination of $\alpha 5$, $\beta 2$ and $\gamma 1$ chains and is known to support pluripotent stem cell maintenance and growth (110).

LN521 stock solution was thawed completely at 4°C and aliquoted into 50 μ l/vial, 100 μ l/vial or 150 μ l/vial. Aliquots were stored at -20°C for up to three years. Per 50 μ l, one well of a 6-well or two wells 12-well plate could be coated. Aliquots were retrieved from -20°C and thawed until completely liquified at RT. For each 50 μ l LN521 stock solution, 950 μ l PBS (+/+ , ThermoFisher Scientific) was added. LN521 working solution was then distributed to coat sufficient amounts of 6-well (1 ml/well) or 12-well plates (0.5 ml/12-well) at 4°C O/N. The final concentration of LN521 was

approximately 0.5 µg/cm². Immediately prior to plating cells, LN521 working solution was removed without letting the wells dry out. If not used directly, 2 ml/6-well or 1 ml/12-well PBS (+/+) was added, the plate sealed with parafilm and stored at 4°C for up to four weeks.

2.2.3.4 Passaging human induced pluripotent stem cells (hiPSC)

Approximately 80% confluent hiPSC cultures were passaged routinely as single cells. Therefore, cell culture treated plastic ware was coated with either Matrigel or LN521 one day prior to usage. Wells containing cells for passaging were washed twice with 1 ml/6-well PBS (-/-, ThermoFisher Scientific), followed by incubation with 1 ml/6-well TrypLE Express (ThermoFisher Scientific) at 37°C / 5% CO₂ for 5 min. Cells were triturated five times to receive single cells and transferred into a 15 ml conical tube containing 4 ml PBS (-/-) per 1 ml TrypLE Express. 10 µl of the cell suspension was entered into a Neubauer chamber for cell counting. The cell suspension was centrifuged at 300xg for 3 min, supernatant discarded and the cell pellet resuspended at a concentration of 1x10⁶ cells/ml in fresh StemMACS iPS-Brew. While plating 0.75 – 2x10⁵/well pluripotent stem cells, a final concentration of 10 µM/well of ROCK-Inhibitor Y-27632 (Sigma-Aldrich, St. Louis, USA) was added to the plating medium.

2.2.3.5 Cell Counting

10 µl of single cell suspension was mixed with 10 µl 0.4% Trypan blue and subsequently entered into a Neubauer chamber for cell counting and discrimination of living cells from dead cells. Trypan blue is an anionic cell dye that can only be excluded by cells with uncompromised cell membranes. Using the 10X magnification of the Leica DMIL inverted microscope (Leica Microsystems), viable, not blue cells were counted in each of the four corners of the chamber. Final cell count was determined using equation 1.

$$\text{Equation 1: Total Cell Count (viable cells)} = \left(\frac{(X1+X2+X3+X4)}{4} \right) \times 10^4 \times V$$

X1 – X4: Cell counts of Neubauer chamber corners V: Total volume of cell suspension (in ml)

2.2.3.6 Freezing and Thawing Pluripotent Stem Cells

For cryopreservation, 80% confluent pluripotent cell cultures were washed twice with 1 ml/6-well PBS (-/-), followed by incubation with 1 ml/6-well TrypLE Express (ThermoFisher Scientific) at 37°C / 5% CO₂ for 5 min. Cells were triturated five times to receive single cells and transferred into a 15 ml conical tube containing 4 ml PBS (-/-) per 1 ml TrypLE Express. 10 µl of the cell suspension was entered into a Neubauer chamber for cell counting. The cell suspension was centrifuged at 300xg for 3 min, supernatant discarded and the cell pellet resuspended at a concentration of 1x10⁶ cells/ml in StemMACS iPS-Brew containing 10% DMSO. The cryovials were stored in an “Mr. Frosty” isopropanol box at -80°C (-1°C/min) O/N and in liquid nitrogen (-160°C) from there on until further usage.

For thawing pluripotent stem cells, a cryovial was removed from liquid nitrogen and incubated at RT until only a small ice clump was left. The cell suspension was carefully pipetted into a 15 ml conical tube containing 3 ml of StemMACS iPS-Brew at RT. The cryovial was washed with 1 ml fresh StemMACS iPS-Brew and the wash was added to the respective 15 ml conical tube. After centrifugation at 200xg and RT for 5 min, the supernatant was discarded and the cell pellet resuspended into 2 ml fresh StemMACS iPS-Brew supplemented with 10 μ M ROCK inhibitor Y-27632. The cell suspension was added into one well of a 6-well plate. Cultures were incubated at 37°C/5% CO₂ and medium exchanged as described before (2.2.3. Human induced pluripotent stem cells (iPSC)).

2.3 Hepatic differentiation

For hepatic differentiation (see Fig. 5), one day prior to starting the differentiation $1.5 - 4 \times 10^5$ pluripotent stem cells were plated on cell culture treated plastic ware coated with either Matrigel or a 3:1 mixture of LN111 and LN521 (both Biolamina) in PBS +/- (ThermoFisher Scientific). Differentiation was initiated by replacing spent StemMACS iPS Brew with Definitive Endoderm (DE) Medium consisting of RPMI1640 supplemented with 2% B27 w/o retinoic acid, 1% GlutaMAX, 100 μ g/ml Penicillin / Streptomycin (P/S, all ThermoFisher), 100 ng/ml Activin A (Peprotech, Rocky Hill, USA) and, only on the first day of differentiation, 2.5 μ M CHIR99021 (Stemgent, Cambridge, USA). DE Medium was replaced daily for three days in total. On Day 4, medium was switched to Hepatic Endoderm (HE) Medium consisting of KnockOut™ DMEM, 20% KnockOut™ Serum Replacement (KOSR), 0.5% GlutaMAX, 0.1 mM β -Mercaptoethanol, 1% P/S, (all ThermoFisher Scientific) and 1% DMSO (Sigma Aldrich) and exchanged daily for four days. From day eight on, medium was switched to either L15 Maturation Medium (L15M) consisting of Leibovitz L-15 medium supplement with 8% FBS, 8% Tryptose Phosphate Broth, 1% GlutaMAX, , 1% P/S (all ThermoFisher Scientific), 0.01% Insulin (Sigma Aldrich), 10 ng/ml Hepatocyte Growth Factor (HGF), 20 ng/ml Oncostatin M (OSM) and 25 ng/ml Dexamethasone (DEX, all Peprotech, Hamburg, Germany) or HepatoZYME™ supplemented with 1% GlutaMAX, 1% P/S (all ThermoFisher Scientific), 10 ng/ml HGF, 20 ng/ml OSM and 25 ng/ml DEX (all Peprotech). L15M respectively HepatoZYME™ were exchanged every other day for eleven days.

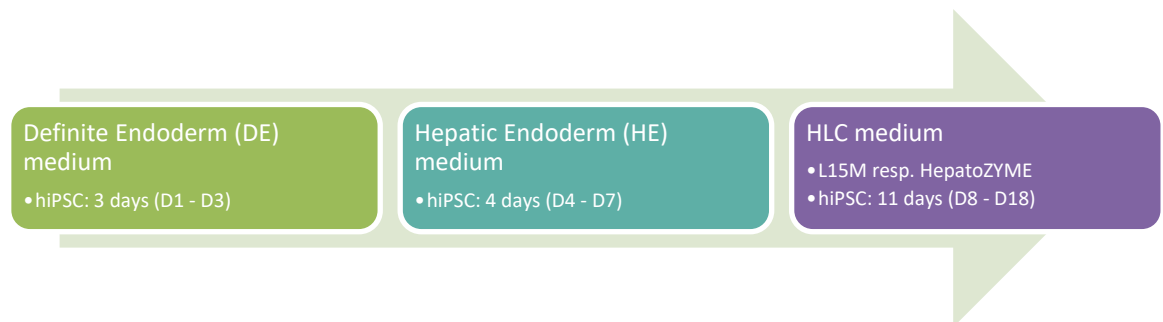


Fig. 5 - Schematic timeline of hepatic differentiation protocol. Pluripotent stem cells were seeded $1.5-4 \times 10^5$ cells/well onto Matrigel® respectively LN111/521 (3:1) and cultured for three days in DE Medium consisting of RPMI1640

supplemented with 2% B27 w/o retinoic acid, 1% GlutaMAX, 100 µg/ml Penicillin / Streptomycin (P/S, all ThermoFisher), 100 ng/ml Activin A (PeproTech, Rocky Hill, USA) and, only on the first day of differentiation, 2.5 µM CHIR99021 (StemCell Technologies, Vancouver, Canada). From day 4 to day 7, medium was changed to HE Medium (KnockOut™ DMEM, 20% KnockOut™ Serum Replacement (KOSR), 0.5% GlutaMAX, 0.1 mM β-Mercaptoethanol, 1% P/S, (all ThermoFisher Scientific) and 1% DMSO (Sigma Aldrich)). The remaining 11 days of hepatic differentiation, cells were cultured with either L15 Maturation Medium (L15M) consisting of Leibovitz L-15 medium supplemented with 8% fetal bovine serum (FBS), 8% Tryptose Phosphate Broth (TPB), 1% GlutaMAX, , 1% P/S (all ThermoFisher Scientific), 0.01% Insulin (Sigma Aldrich), 10 ng/ml Hepatocyte Growth Factor (HGF), 20 ng/ml Oncostatin M (OSM) and 25 ng/ml Dexamethasone (DEX, all Peprotech) or HepatoZYME™ supplemented with 1% GlutaMAX, 1% P/S (all ThermoFisher Scientific), 10 ng/ml HGF, 20 ng/ml OSM and 25 ng/ml DEX (all Peprotech). During DE and HE stages, medium was exchanged on a daily basis. Both HLC media were exchanged every other day. µg – microgram, ng – nanogram, ml – milliliter, mM – millimolar, P/S – Penicillin/Streptomycin

2.4 Molecular Biology Assays

For molecular biology assays, cell pellets of all cell lines have been produced on the last day of hepatic differentiation. Therefore, two wells of a 6-well plate containing HLCs or HepG2 cells were stored in a chemical safety cabinet on ice and wells were washed twice with 2 ml / 6-well PBS (-/-) for 3 min. After adding 800 µl / 6-well TRIzol™ reagent (ThermoFisher Scientific), cells were incubated at RT for 5 min and then detached from the surface area by scratching using a cell scraper. The cell suspension was transferred to two properly signed 1.5 ml Eppendorf tubes per used 6-well and immediately stored at -80°C until further usage.

2.4.1 Isolation of RNA

RNA was isolated according to Direct-zol™ RNA Mini-Prep Kit's (Zymo Research, Montgomery, USA) instruction. Briefly, samples to be used during qRT-PCR were thawed at RT until no ice clumps were visible. Then, 400 µl / tube 100% ethanol was added and resuspended by triturating five times. 700 µl / sample Ethanol / Trizol (1:1) cell suspension was added onto Zymo-Spin IIC columns in a collection tube and centrifuged at 9000 xg for 1 min. Flow through was discarded and centrifugation repeated until no cell suspension per sample remained. Then, columns were washed twice using 400 µl RNA wash buffer and centrifugation at 9000 xg for 30 s. 80 µl / tube DNase I reaction buffer containing 1:16 DNase I in DNase Reaction buffer was added directly to the matrix of the columns and incubated tubes at RT for 20 min. After centrifugation at 9000 xg for 30 s, columns were washed twice using 400 µl / tube RNA PreWash followed by centrifugation at 9000 xg for 1 min. 700 µl / tube RNA wash buffer was added and centrifuged at 9000 xg for 1 min. Tubes were centrifuged dry at maximum speed for another 1 min and RNA suspended in 30 µl dH₂O in RNase-free Eppendorf tubes. RNase tubes were kept on ice and RNA concentration and quality determined using Nanodrop 2000c. An Abs^{260/280} ratio nearing 2 was considered pure RNA. Gel electrophoresis on 1% agarose gel was employed to confirm RNA integrity (2:1 ratio of S28:S18; Ladder: Perfect Plus 100 kb DNA ladder A30 (EURx, Gdansk, Poland). RNA samples were stored at -80°C until further usage.

2.4.2 cDNA synthesis

cDNA was synthesized from isolated RNA employing the Reverse Transcription TaqMan® Kit (Applied Biosystems Roche, Foster City, USA) according to manufacturer's instructions.

Briefly, 500 ng / sample of isolated RNA but a maximum of 4 µl was transferred into a fresh, RNase free PCR tube and mixed with 6 µl MasterMix (1 µl 10X buffer, 2.2 µl MgCl₂, 2 µl dNTPs, 0.5 µl oligoDT primers, 0.2 µl RNase inhibitor (20 U/µl), 0.25 µl Reverse Transcriptase). Samples were loaded onto a Thermocycler running following protocol for 32 cycles of amplification: denaturation (94°C, 15 seconds), annealing (T_M, 30 seconds), elongation (68°C, 60 seconds), termination (68°C, 7 minutes), storage at 4°C. Each sample was diluted to a final concentration of 5 ng/µl with nuclease-free water and stored at -80°C until further usage.

2.4.3 Quantitative Real Time Polymerase Chain Reaction (qRT-PCR)

Using qRT-PCR, it is possible to assess the expression level of genes of interest within a cell population. All reactions were prepared in triplicate in 384-well plates containing 10 µl/well reaction mix (see Table 10). As negative control, 1 µl of water was added in lieu of cDNA for every primer pair. Amplification was performed using following PCR program: 95°C for 10 minutes, then 40 cycles of:

- I. Denaturation (95°C for 30 s)
- II. Annealing (60°C for 30 s)
- III. Extension (72°C for 30 s)

Melting curves were generated by increasing the temperature at 0.05°C / s to 95°C, holding the 95°C for 15 s and reducing the temperature to 60°C for 1 min. Samples were stored at 4°C until further usage. The PCR products were finally loaded onto a 1% agarose gel containing 1:10000 GelRed™ nucleic acid stain (Biotium Inc., Fremont, USA) and run at 70V for 4 minutes and 100 V for another 2 h. Electrophoresis was stopped when the loading dye reached roughly 75% of the gel. Visualization was performed under UV using the Fusion FX image capturer.

Ingredient	Volume
1X Power SYBR® Green	5 µl
Primer 3'	0.5 µl
Primer 5'	0.5 µl
DNase/RNase free water	3 µl
cDNA (sample)	1 µl

Table 10 – **Ingredients of quantitative real time polymerase chain reaction mix.** Volumes described are needed for 1 well of a 384 well plate. µl - microliter

Acquired data was analyzed using Microsoft Excel (Microsoft, Redmond, USA) and the $\Delta\Delta Ct$ method (158). Briefly, the ΔCt value for each gene and matrix/medium condition was determined by subtracting the mean of the triplicate Ct values of the gene interest from the mean Ct value of the house keeping gene *RPL37a*. The $\Delta\Delta Ct$ was determined by subtracting ΔCt of each condition from the ΔCt of the biological negative control (iPSC) for each gene of interest. The *fold change* could be determined by calculating the power of two of $-\Delta\Delta Ct$ ($2^{-\Delta\Delta Ct}$).

2.5 Immunoassays

2.5.1 Immunocytochemistry

On the fourth, seventh and last day of hepatic differentiation, wells dedicated for immunocytochemistry have been washed twice with 0.5 ml/well PBS (-/-) for 3 min and fixed by adding 200 µl/well 4% paraformaldehyde (PFA) at RT for 15 min. After two washing steps using 0.5 ml/well PBS (-/-) for 5 min, fixed cells could either be stored in PBS (-/-) +1% P/S at 4°C until further usage or used directly for immunofluorescence staining.

For immunofluorescence staining of intracellular proteins, fixed cells were incubated with 400 µl/well Permeabilisation/Blocking Buffer (PBB) consisting of PBS (-/-) supplemented with 10% normal goat or donkey serum (NGS resp. NDS, both ThermoFisher Scientific), 0.5% Triton-X-100 and 0.05% Tween-20 (both Sigma Aldrich) at RT for 2 h. For extracellular staining, no detergents were added to PBS (-/-) and 10% NGS resp. NDS. Once the 2 h incubation period had lapsed, the cells were incubated O/N at 4°C in the dark in 250 µl/well primary antibody solutions (see Table 1) prepared in PBB/PBS (-/-, ratio 1:1). Solutions added to wells designated as negative control did not contain primary antibodies.

Next morning, cells were washed twice using 0.5 ml/well PBB/PBS (-/-, ratio 1:1) at RT for 5 min and subsequently incubated with 250 µl/well secondary antibody solutions in PBB/PBS (-/-, ratio 1:1, see Table 2) in the dark for 1 h. Solutions added to wells designated as negative control did not contain secondary antibodies. After washing wells twice with 0.5 ml/well PBB/PBS (-/-, ratio 1:1), 0.5 ml/well PBS (-/-) + 1% P/S was added. Cell were visualized using a Zeiss LMS 700 microscope

connected to camera for microscopy, model AxioCam ICC3. Pictures were analyzed using the software Zen Blu 2.5 and ImageJ Fiji (159).

2.5.2 Flow Cytometry

For flow cytometry, two wells of a 6-well plate were washed twice with 2 ml/well PBS (-/-) and incubated in 1 ml/well TrypLE Select (ThermoFisher Scientific) at 37°C/5% CO₂ for 5 min. The cells were washed off the bottom of the wells viciously by trituration and the suspension transferred into 8 ml PBS (-/-). Routinely, a cell count using a hemocytometer was performed at this stage to calculate the appropriate volume of fixative. After centrifugation at 300xg for 3 min, produced cell pellet was resuspended at 1x10⁷ cells / ml in 2% PFA and incubated at RT for 15 min. The cells were washed twice with 5 ml PBS (-/-), resuspended at 1x10⁷ cells / ml 0.5% Triton-X-100 (Sigma Aldrich) in PBS (-/-, PBS-T) and incubated at RT for 20 min. After another two washing steps using 5 ml PBS (-/-) and centrifugation conditions of 500xg for 5 min, the cells were blocked in 1 ml 10% NGS in PBS (-/-) at RT for 20 min. The cells were washed once, resuspended in 5 ml PBS (-/-), counted using a hemocytometer and distributed at 2x10⁵ cells/tube in an appropriate amount of fresh 15 ml conical tubes. After centrifugation at 500xg for 5 min, cells were incubated in 300 µl/15 ml tube primary antibody solutions (see Table 11) at 4°C O/N.

Tube	Condition	Primary Ab	Dilution
1	Unstained	N/A	N/A
2	HNF4α single	α-HNF4α antibody (EPR3648)	1:300
3	ALB single	Monoclonal α-Albumin antibody	1:500
4	HNF4α + ALB	α-HNF4α antibody (EPR3648)	1:300
		Monoclonal α-Albumin antibody	1:500
5	AFP + UGT1A1	α-AFP antibody	1:250
		Human Glucuronosyltransferase 1A1/ UGT1A1 Antibody	1:200

Table 11 – **Layout of tubes for primary antibody staining of flow cytometry analysis of derived hepatocyte-like cells.** HNF4α – hepatocyte nuclear factor 4 alpha, ALB – albumin, AFP – alpha fetoprotein.

On the next morning, cells were washed twice using 1 ml/tube PBS-T/PBS (ratio 1:1) and incubated in 400 µl/tube secondary antibody solution (see Table 6) for 1 h. After washing the cells with 1 ml/tube PBS-T/PBS (ratio 1:1), the cells were resuspended in 200 µl/tube PBS (+/+) and transferred to the respective flow cytometry tubes (Corning, New York, USA). Flow cytometry was performed on the CyAn ADP Flow Cytometer. Unstained cells (tube 1) were used to address autofluorescence of derived HLCs and used to define the border between expression negative and positive populations. Single color stained samples (tube 2 and 3) were used for compensation of spectral overlap between AF488 and PE. Final analysis and visualization was performed using FlowJo.

2.5.3 Enzyme linked immunosorbent assay (ELISA) for Albumin

An ELISA has been used for the detection of human albumin within supernatant media samples collected throughout the differentiation process of human iPSC towards HLCs, precisely on days 3, 7 and on the last day of differentiation. HepG2 cells have been used as positive control.

1 μ l of affinity purified antibody A80-129A diluted in 99 μ l ELISA coating buffer (0.05 M sodium hydrogen carbonate, pH 9.6) was added to each well to be used and incubated at 4°C O/N. Every well was washed five times using 300 μ l/96-well ELISA wash solution (50 mM Tris, 0.14 M NaCl, 0.05% Tween 20, pH 8.0). Then, 200 μ l/96-well of ELISA blocking solution (5% milk powder in PBS (-/-) containing 0.05% Tween 20) was added. After 30 min of incubation at RT, blocking solution was discarded and all wells washed five times using 100 μ l/96-well ELISA wash solution. A standard curve (400 ng/ml, 200 ng/ml, 100 ng/ml, 50 ng/ml, 25 ng/ml, 12.5 ng/ml, 6.25 ng/ml) and blanks were produced in triplicate using Human Reference Serum from the Human Albumin ELISA Quantitation Set from Bethyl Biotechnologies (see Table 12).

Standard	ng/ml	RS10-110-4 (22 mg/ml Albumin)	Sample Diluent
Initial	10,000	5 μ l	11 ml
1	400	100 μ l from initial	2.4 ml
2	200	500 μ l from std 1	500 μ l
3	100	500 μ l from std 2	500 μ l
4	50	500 μ l from std 3	500 μ l
5	25	500 μ l from std 4	500 μ l
6	12.5	500 μ l from std 5	500 μ l
7	6.25	500 μ l from std 6	500 μ l
8	0	Blank	500 μ l

Table 12 – Dilution row for Albumin ELISA using the Human Albumin ELISA Quantitation Kit from Bethyl Biotechnologies. Std – Standard, ng – nanogram, mg – milligram, ml - milliliter

100 μ l of standards or samples were added in triplicate to assigned wells of the prepared 96-well plate and incubated at RT for 1 h. After incubation, standards and samples were removed and all wells washed five times using 300 μ l/96-well ELISA wash solution.

HRP Detection Antibody (A80-129P) was diluted 1:100000 in sample/conjugate diluent (PBS (-/-), 0.05% Tween-20) and 100 μ l of this secondary antibody solution added to each well. After 1 h of incubation at RT, secondary antibody solution was removed and all wells washed five times using 100 μ l/96-well ELISA wash solution. 100 μ l of TMB substrate solution was added to each well and the plate subsequently incubated at RT in the dark for exactly 15 min. Then the reaction was stopped by adding 100 μ l of ELISA stop solution (5 M H₂SO₄).

Absorbance of each well was measured at 490 nm using the ELISA plate reader AF2200 within 30 min after adding ELISA stop solution.

2.5.4 Western Blot for CYP2D6

2.5.4.1 Protein isolation

Wells containing material for Western Blotting were washed twice with 2 ml/well PBS (-/-). Cells were collected into 1.5 ml Eppendorf tubes using a cell scraper and spun down at 20000xg for 2 min. The supernatant was discarded, the cell pellet snap frozen on dried ice and stored at -80°C until further usage.

Proteins from cell pellets were obtained by retrieving samples from -80°C and adding 100 µl/sample RIPA buffer / Protease inhibitor (10:1). After triturating three times, vials were incubated on ice for 20 min with thoroughly triturating each sample another four times using a glass syringe. Samples were centrifuged at 20000xg and 4°C for 20 min. Supernatant was collected in ice-cold, properly labelled 1.5 ml Eppendorf tubes. 8 µl/sample was used for BCA-mediated protein quantification, the rest stored at -80°C until further usage.

2.5.4.2 Pierce Bicinchoninic Acid Protein Assay (BCA Assay)

All samples for quantification were diluted 1:10 in ice cold PBS (-/-) and kept on ice until further usage. All standards and samples were prepared in triplicate.

The BSA standard curve ranging from 2000 to 67.5 µg/ml was prepared in PBS (-/-). A final volume of 25 µl per standard or sample was added to an ice cold flat bottom 96-well plate. After adding 200 µl Master Mix reagent prepared according to manufacturer's instruction to each well, the 96-well plate was placed onto a rocking plate at RT in the dark for 30 s and subsequently incubated at 37°C/5% CO₂ for 30 min. The plate was equilibrated to RT in the dark for 5 min and absorption of each well measured at 562 nm wavelength using the ELISA plate reader AF2200 (Eppendorf). Protein concentrations could be calculated by inserting absorbance values into the linear regression curve retrieved from the standard values (see Equation 2)

$$\text{Equation 2: Protein concentration in } \frac{\mu\text{g}}{\text{ml}} = m * \text{Abs}_{562} + b$$

m: slope of linear regression Abs₅₆₂: absorbance (562 nm) b: y-intercept of linear regression

2.5.4.3 Sodium Dodecyl Sulphate Polyacrylamide Gel Electrophoresis (SDS-PAGE)

One day prior to Western Blot analysis, a 10% SDS resolving gel (see Table 13) was poured into a fully assembled Western Blot cassette and incubated at 4°C under wet paper O/N. Next morning, 3.5 % stacking gel (see Table 13) and a pouch comb was added to the Western Blot cassette and incubated at RT for 60 min.

Prior to loading the gel, 50 µg protein / sample was diluted in RIPA buffer containing 4X loading buffer to produce a final volume of 40 µl. All samples were incubated in a thermoblock at 95°C for 3 min and then, alongside 4 µl of the Protein Marker V protein ladder (PEQLAB Biotechnology,

Erlangen, Germany), loaded onto the polymerized SDS gel. Gel electrophoresis was performed at 100V until samples reached the resolving gel and at 200V until samples run through gel completely.

	Loading buffer (4X)	SDS Resolving Gel (10%)	SDS Stacking gel
Final Volume	10 ml	10 ml	5 ml
Ingredients	2.5 ml Tris 1M (pH 6.8) 0.8 g SDS 4 ml Glycerol 2 ml β -Mercaptoethanol 1 mg Bromophenol blue Adjusted to 10 ml with dH ₂ O	4.167 ml H ₂ O 2.5 ml LG 3.3 ml Acrylamide (30%) 30 μ l APS (10%) 3 μ l TEMED	3.315 ml H ₂ O 1 ml UGB 0.58 ml Acrylamide (30%) 50 μ l APS 50 μ l SDS (10%) 5 μ l TEMED

Table 13 – Components and volumes of 4X Loading buffer, sodium dodecyl sulphate (SDS) resolving and stacking gel used for sodium dodecyl sulphate polyacrylamide gel electrophoresis (SDS-PAGE). SDS – Sodium dodecyl sulphate, LG – Lactoglobulin, UGB – Upper Gel Buffer, APS – Ammonium persulfate, TEMED – tetramethylethylenediamine, M – molar, ml – milliliter

2.5.4.4 Membrane Transfer and Blotting

The SDS-PAGE gel was removed from the gel electrophoresis device, laid onto a 1X 0.45 μ M nitrocellulose blotting membrane and both together embedded in between two 2X Whatman papers and sponges (see Fig. 6). Membrane transfer found place in transfer buffer (0.25mM Tris-base and 0.192mM Glycine, pH 8.3, 20% methanol) at 0.2A for 1.5 h and was confirmed by Ponceau Solution S staining of the blotting membrane after disassembly on a rocking plate at RT for 30 min. Membranes were washed twice with Millipore water for 5 min. Ponceau Solution S staining was removed by washing membranes three times with 0.05% TBS-Tween-20 (TBS-T).

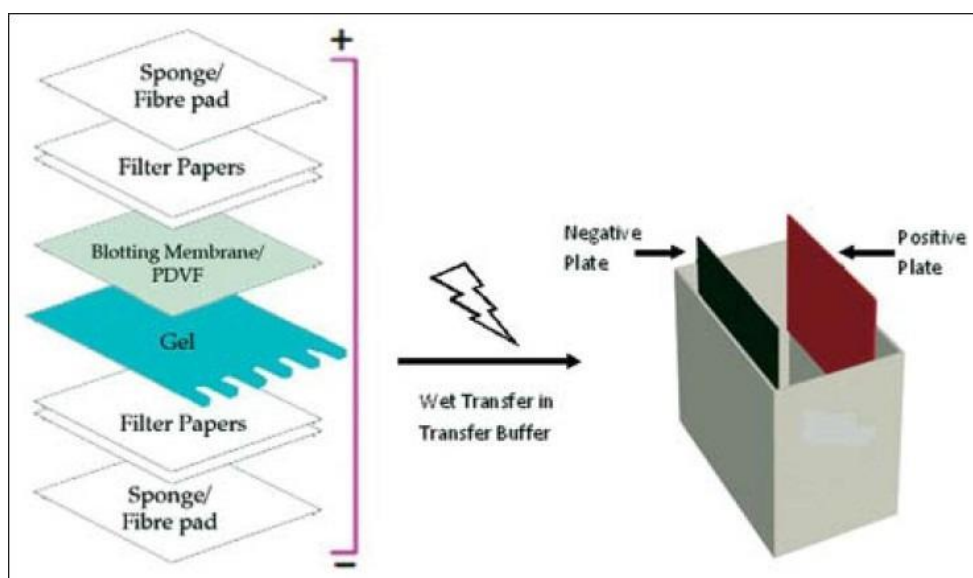


Fig. 6 – Assembly of SDS-PAGE gel, Blotting membrane, Filter Papers and Sponges for Western Blot (8). The SDS-PAGE gel was removed from the gel electrophoresis device, laid onto a 1X 0.45 μ M nitrocellulose blotting membrane and both together embedded in between two 2X Whatman papers and sponges. Membrane transfer found place in transfer buffer (0.25mM Tris-base and 0.192mM Glycine, pH 8.3, 20% methanol) at 0.2A for 1.5 hours. SDS-PAGE - sodium dodecyl sulphate polyacrylamide gel electrophoresis, μ M – micromolar, mM – millimolar, A – Ampere.

The membranes were subsequently blocked by incubating in 5% milk powder/TBS-T at RT on a rocking plate for 2 h. Primary antibody staining of CYP2D6 was performed using a 1:800 dilution of Invitrogen™ Cytochrome P450 2D6 antibody (PA5-39598, ThermoFisher) in 5% milk powder/TBS-T O/N. Next day, all membranes were washed three times using 0.1% PBS-T (1X) on a rocking plate for 10 min. Secondary antibody staining was performed using 1:2000 dilution of a sheep α -rabbit HRP (Abcam plc, Cambridge, UK) in 5% milk powder/TBS-T on a rocking plate at RT for 2 h. Signaling was visualized using FusionCapt Advance FX7. Photographs taken of the blots were corrected for background signaling by applying the rolling ball technique and used to quantify signal intensities of derived single bands belonging to housekeeping protein and CYP2D6. The ratio of CYP2D6 and actin expression was calculated by dividing mean signal intensity of CYP2D6 and actin using Microsoft Excel. Standard deviations (SD) were calculated when more than two biological replicates were available. Ratios and SD were visualized as bar graphs. Raw data was analyzed for statistical significance where possible employing the Mann-Whitney U test in Microsoft Excel. P values ≤ 0.05 were considered statistically significant.

2.6 Biochemical Activity Assays

2.6.1 Indocyanine Green (ICG) Staining

Indocyanine Green (Cardiogreen, Sigma Aldrich) is a cyanine dye and organic anion used for assessing viability and metabolic activity of hepatocytes in vitro. Once applied to the cell culture medium, ICG rapidly binds noncovalently to plasma proteins, such as Albumin or Transferrin, thereby forming fluorescent complexes. These fluorescent complexes are internalized by metabolically active hepatocytes via Na⁺-independent basolateral (sinusoidal and lateral) membrane transport systems, mainly the organic anion transporting polypeptide C (OATP-C) or the liver-specific organic anion transporter (LST-1, 7) and excreted apically into the biliary canaliculi by multidrug resistance protein 2 (MDR-2, 8). Viable, metabolically active hepatocytes should be capable of internalizing ICG-protein complexes within 30 min after application and excrete ICG within 24 h (160,161).

25 mg Cardiogreen (Sigma Aldrich) was dissolved in 5 ml DMSO (Sigma Aldrich), aliquoted at 1 ml/vial and stored at -80°C until further usage. Prior to ICG staining, one vial was retrieved from -80°C and thawed for 5 min at RT. Photographs were taken from one well of a 12-well plate of the HLC differentiation on D17 an Olympus CK2 phase contrast microscope (Olympus, Hamburg, Germany) connected to a Zeiss AxioCam ERc 5s camera. 1.6 ml HLC medium was removed from the well of interest. 100 μ l of 5 mg/ml ICG stock solution was added to the remaining 400 μ l HLC medium producing a final concentration of 1 mg/ml ICG in HLC Medium. The wells were incubated

at 37°C / 5% CO₂ for 30 min. After washing the wells twice with PBS (+/+), 1 ml/well PBS (+/+) was added and the cells assessed using the Olympus CK2 microscope. PBS (+/+) was exchanged with 2 ml/12-well HLC Medium and cells stored at 37°C / 5% CO₂ for 24 h. After 24 h, wells were washed twice with 1 ml/12-well PBS (+/+) and assessed again 1 ml/12-well PBS (+/+) using the Olympus CK2 microscope. Photographs were taken again using a Zeiss AxioCam ERc 5s camera.

2.6.2 PAS staining (Glycogen storage staining)

PAS staining is a histochemical staining method to detect carbohydrate(-containing) macromolecules, such as glycogen. Periodic acid oxidizes residues of glucose molecules to form aldehydes. These aldehydes are capable of recoloring a Schiff reagent producing a magenta color (162).

On the last day of differentiation, one dedicated well of a 12-well plate was washed twice with 0.5 ml PBS (+/+) and fixed with 200 µl 4% PFA at RT for 15 min. Cells were washed twice again with 0.5 ml PBS (+/+). Then, the Periodic Acid-Schiff (PAS) Staining System (Sigma Aldrich) was used according to manufacturer's instruction. Briefly, after fixation 300 µl/well Periodic Acid solution was added and the cells were incubated at RT for 5 min. The cells were washed three times with 0.5 ml/well distilled water at RT for 3 min and then incubated with Schiff's reagent at RT for 15 min. After another three washing steps with 0.5 ml distilled water for 3 min, cells were counterstained with 300 µl/well hematoxylin for 90 s. Cells were washed three times with 0.5 ml/well distilled water, stored in PBS (+/+) and visualized using an Olympus CK2 phase contrast microscope. Pictures were taken using a Zeiss AxioCam ERc 5s camera.

2.6.3 CYP3A4 Activity Assay

To measure the activity of Cytochrome P450 3A4 (CYP3A4), the P450-Glo™ CYP3A4 Assay kit (Promega, Mannheim, Germany) was used. One day prior to measuring, CYP3A4 activity was induced by exchanging spent medium with 1.5 ml of fresh HLC medium supplemented with 10 µM rifampicin. On the last day of HLC differentiation, the medium of one well of a 12-well plate was exchanged with 585 µl HLC Medium + 15 µl Luciferin-PFBE to obtain a final concentration of 50 µM Luciferin-PFBE. Luciferin-PFBE is a pro-luciferin activated through metabolization by CYP3A4. After incubation at 37°C / 5 % CO₂ for 4 h, 150 µl of the medium was aliquoted at 50 µl/tube into three 5 ml round bottom, polystyrene test tubes (Sarstedt, Nürnbrecht, Germany) and diluted 1:1 with 50 µl/tube detection reagent. After incubation at RT in the dark for 20 min, light signaling was measured in technical triplicates using the luminometer Lumat LB 9507 (Berthold Technologies, Bad Wildbad, Germany). As negative controls medium and Luciferin-PFBE was added to an empty well of the 12-well plate and treated as described above.

Luminescence signaling of medium samples were corrected for background signaling by subtraction of the mean luminescence of the negative controls using Microsoft Excel. The mean of sample signaling after background correction and associated standard deviation was represented as bar graph.

2.6.4 Urea Quantification (QuantiChrome™ Urea Assay Kit, BioAssay Systems)

The production of urea, a major hepatic end product of protein catabolism, indicates adequate functionality of produced HLCs and can be measured employing the QuantiChrome™ Urea Assay Kit from BioAssay Systems (Hayward, USA). This kit utilizes a chromogenic reagent that specifically binds to urea, thereby forming colored complexes. The resulting color intensity of the solution can be measured spectrophotometrically at 520 nm and is directly proportional to the urea concentration of the sample.

A standard dilution row of urea (50 mg/dl, 40 mg/dl, 20 mg/dl, 10 mg/dl, 5 mg/dl, 2.5 mg/dl, 1.25 mg/dl and 0 mg/dl) was prepared in duplicate in Millipore water. 5 µl/well of standards, culture medium controls and supernatant sample medium from three time points of differentiation (DE, HE, HLC stage) were pipetted in duplicate into a flat bottom 96-well plate. 200 µl of 1:1 mixture of reagent A and B of the QuantiChrome™ Urea Assay Kit was added to each well to be analyzed. The plate was incubated at RT in the dark for 20 min and absorbance was measured at 520 nm using the ELISA plate reader AF2200. Using Microsoft Excel, the mean of the duplicates of the standard dilution row was corrected for the background by subtraction the absorption of the mean blank. Resulting values were plotted and the trendline of curve used to calculate sample urea concentrations (see Appendix 2, Fig. 34) after correction for background absorption of the respective medium.

3 Results

During three differentiation experiments, the two iPSC lines S12_13B and UJiPS13 were differentiated twice each into HLCs using different matrix-media systems (Matrigel + L15M; Laminin-111/521 + L15M; Laminin-111/521 + HepatoZYME™) in order to obtain a more detailed insight into the influence of different matrix-media systems on the establishment of an *in-vitro* toxicity testing assay for CYP2D6-metabolized substances (see Table 14).

Differentiation runs	Cell lines	Conditions	Date
HepDif#1	S12_13B P14 UJiPS13 P20	MG + L15M	18JUL17 – 07AUG17
HepDif#2	S12_13B P17	LN + L15M LN + HepatoZYME	27SEP17 – 14OCT17
HepDif#3	UJiPS13 P14	LN + L15M LN + HepatoZYME	22NOV – 07DEC17

Table 14 – Differentiation runs performed during course of the thesis. HepDif experiment #1 included differentiation of both cells lines (S12_13B and UJiPS13) on MG and L15M medium. HepDif experiment #2 was performed on S12_13B employing two different matrix / medium combinations (LN + L15M or HepatoZYME). HepDif experiment #3 was performed on UJiPS13 employing two different matrix / medium combinations (LN + L15M or HepatoZYME). P – Passage, MG – Matrigel, LN – Laminin, L15M – Leibovitz 15 Maturation Medium, JUL – July, AUG – August, SEP – September, OCT – October, NOV – November, DEC – December

During HepDif#1, the experimental outlay did not include the addition of insulin to the HLC medium. Produced HLCs were subsequently characterized for their biochemical functionality.

3.1 Morphology of cells changes throughout hepatic differentiation

Both pluripotent cell lines, S12_13B and UJiPS13, have shown stable growth throughout the cell culturing phase of the project independent from the employed growth matrix (LN521, MG) when cultured in pluripotent stem cell medium (StemMACS iPS-Brew). They exhibited high nucleus to cytoplasm ratio, prominent nucleoli, scant cytoplasm and a small and round morphology of the single cells throughout the course of this thesis. Colonies were round, compact and flat with well-defined and smooth edges (see Fig. 7 A+B). Spontaneous differentiation of pluripotent cells was only seen on rare occasions and has, therefore, been considered negligible.

Colonies of cell line UJiPS13 featured a slightly less packed morphology during lower confluency but adjusted to typical iPSC colony morphology when reaching higher densities within a colony (see Fig. 7 B).

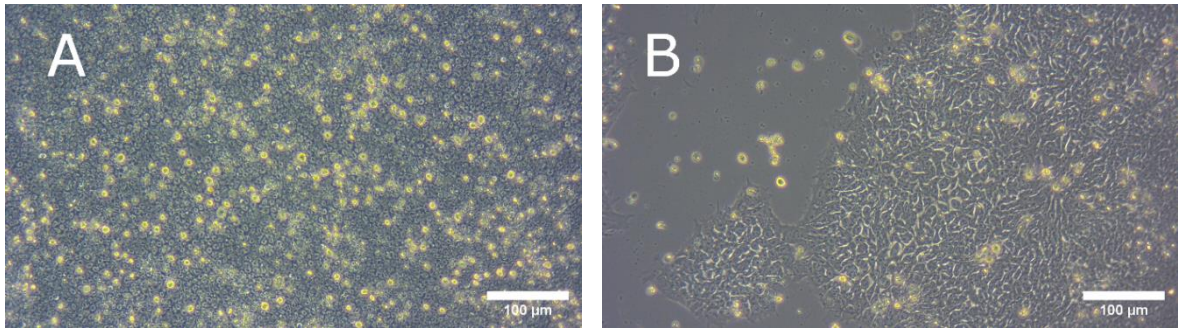


Fig. 7 – Morphology of hiPSC lines. (A) S12_13B P17 5 days after splitting. Cells exhibited high nucleus to cytoplasm ratio, prominent nucleoli, scant cytoplasm and a small and round morphology of the single cells. Colonies were round, compact and flat with well-defined and smooth edges. (B) UJiPSC13 P13 3 days after splitting. Cells exhibited high nucleus to cytoplasm ratio, prominent nucleoli, scant cytoplasm and a small and round morphology of the single cells. Colonies were slightly less packed morphology during phases of lower confluency but adjusted to typical iPSC colony morphology when reaching higher densities within a colony. P – Passage

Upon media conversion to DE medium, morphological changes and vast proliferation was initiated. Single cells started to migrate out of the former colonies exhibiting a more stretched morphology with dendritic outgrowths. The formerly tightly packed colonies began to disband. S12_13B cultures reached full confluency within 3 days of culturing in DE medium. UJiPSC13B exhibited a slightly slower growth profile and usually reached confluency at day four post initiation of differentiation. Once reaching confluency, cells stopped proliferating and remained as single layers. Differentiated cells generally lost their high nucleus to cytoplasm ratio, their round-flat colony structure and became a more heterogenous, irregularly shaped cell population. Some cells developed a second nucleus during DE stage (see Fig. 8, white arrows), a typical sign of the beginning of hepatic differentiation. The number of binucleated cell increased throughout the course of the differentiation protocol. HLCs finally adopted a polygonal three-dimensional shape that is characteristic of human hepatocytes derived at the ISRM. Especially HLCs derived from S12_13B exhibited a recognizable amount of cells containing lipid droplets within their cytoplasm (see Fig. 8, red arrows).

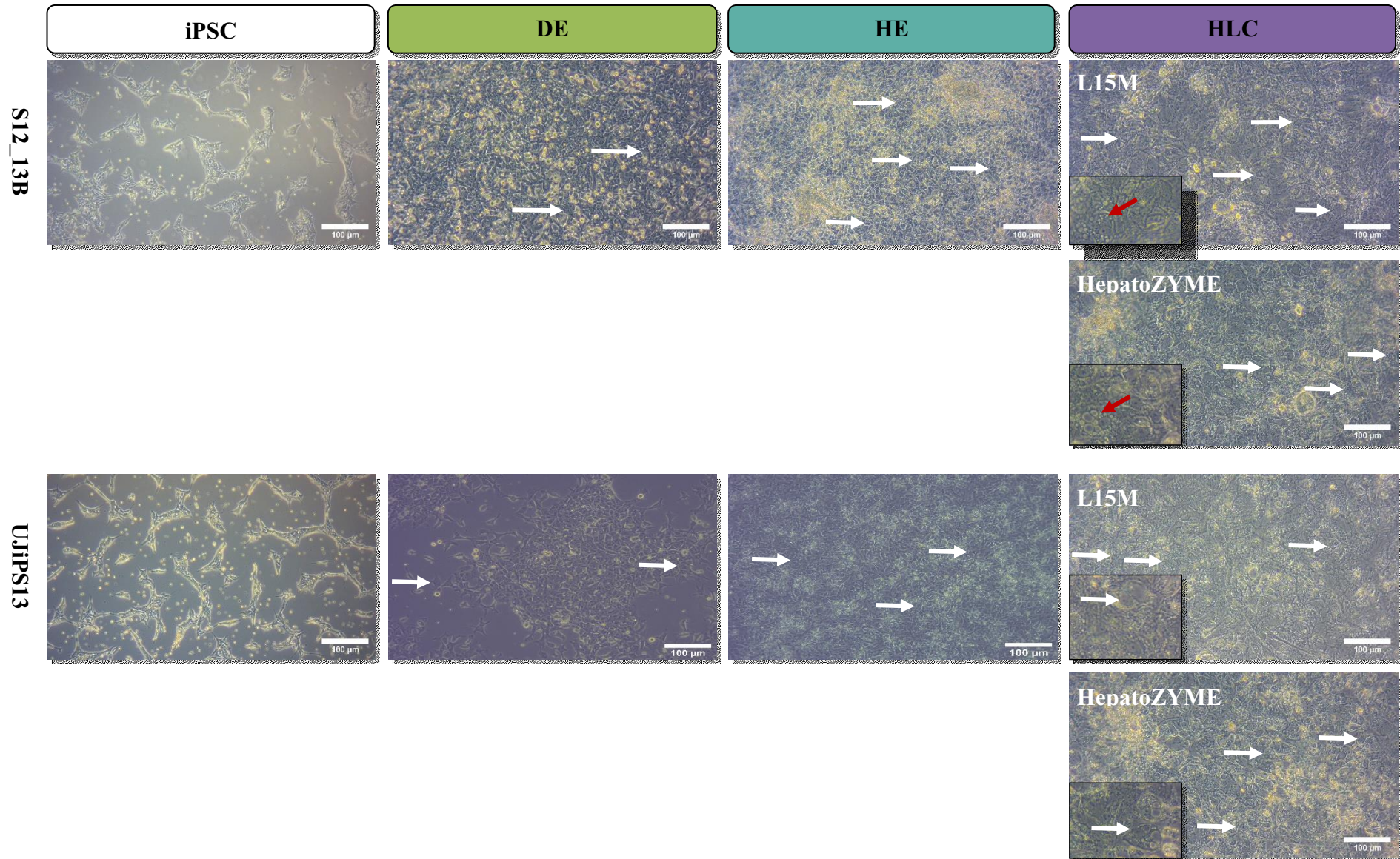


Fig. 8 - Representative brightfield images of hepatic differentiation of human iPSC. Pluripotent stem cells were seeded onto Matrigel® respectively Laminin-111/521 (3:1) and cultured for three days in Definitive Endoder (DE) Medium. From day 4 to day 7, medium was changed to Hepatic Endoder (HE) Medium. The remaining 11 days of hepatic differentiation, cells were cultured with either L15 Maturation Medium (L15M) consisting of L-15 medium or HepatoZYME™. During DE and HE stages, medium was exchanged on a daily basis. Both Hepatocyte-like cells (HLC) media were exchanged every other day. After cell culture in DE medium for 1-2 days, the formerly in colonies growing hiPSC started to migrate out of the cell clusters and change their morphology to a more spindle-shaped cell type mostly reaching 100% confluency between day 3 to 5. After 4 days of culture in HE medium, a homogenous cell population could be observed exhibited a morphology typical for cells at this stage of differentiation. Derived cells were polygonal in shape, showed several binucleated cells (white arrows) and bright cell membranes. During maturing and until D18, cells flattened and became more heterogenous. S12_13B derived HLCs exhibited a large number of cells containing multiple small lipid droplets (red arrows). UJiPS13-derived HLCs showed less lipid droplets with larger diameters. Pictures displayed are obtained from cells derived on LN mixture.

The biological positive control cell line, HepG2, grew adherent on cell culture treated plastic ware and maintained an epithelial morphology throughout various passages. As expected, they tended to grow in small aggregates of irregularly shaped, microscopically almost indistinguishable cells (see Fig. 9). Singularized cells did not attach and were washed off during media changes. Cultures of HepG2 cells reached 60-80% confluency within 4-5 days after passaging and were split roughly once a week.

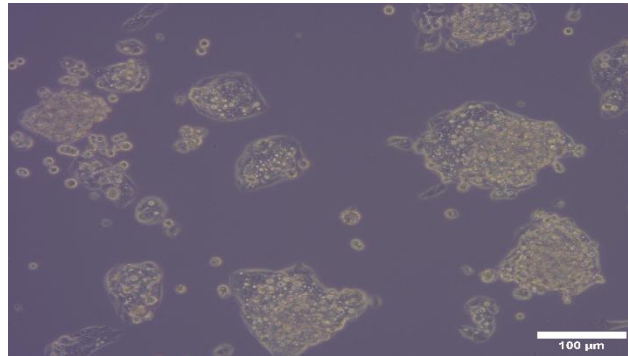


Fig. 9 - Morphology of HepG2 cells two days after passaging. HepG2 cells tend to grow in small aggregates of irregularly shaped, hardly distinguishable cells on cell culture treated plastic ware without growth matrix. Cells were passaged when reaching 60-80% confluency, mostly after 4-5 days after splitting. Scale bar: 100 μm

3.2 Transcript analysis of derived HLCs for hepatocyte-associated gene expression

To evaluate the expression of the hepatocyte-associated genes *ALB*, *AFP*, *CYP3A4* and *HNF4a* and the pluripotency gene *OCT4* on transcript level, RNA was isolated at the last day of differentiation. The RNA was quality controlled, transcribed into cDNA and analyzed using RT-qPCR. The fold change in gene expression, normalized to the house keeping gene *RPL37a* and relative to gene expression in human PSCs, was calculated using the $\Delta\Delta\text{Ct}$ method in Microsoft Excel and visualized as bar graph with logarithmic y-axis.

Although each differentiation was planned to yield three RNA samples per differentiation condition, multiple wells per run were lost due to cellular lift off or contamination. For several differentiation runs and conditions the anticipated triplicates could therefore not be obtained.

The quality of RNA isolated from cells on the last day of differentiation was assessed through separation of S28 and S18 bands on a 1% agarose gel (see Fig. 10). The ratio S28/S18 for each RNA sample equaled approximately 2:1 and besides the two visible bands, no additional bands or smear was visible on respective gels (see Appendix 1, Fig. 33). RNA quality was therefore assumed as not degraded and sufficient for use in RT-qPCR experiments.

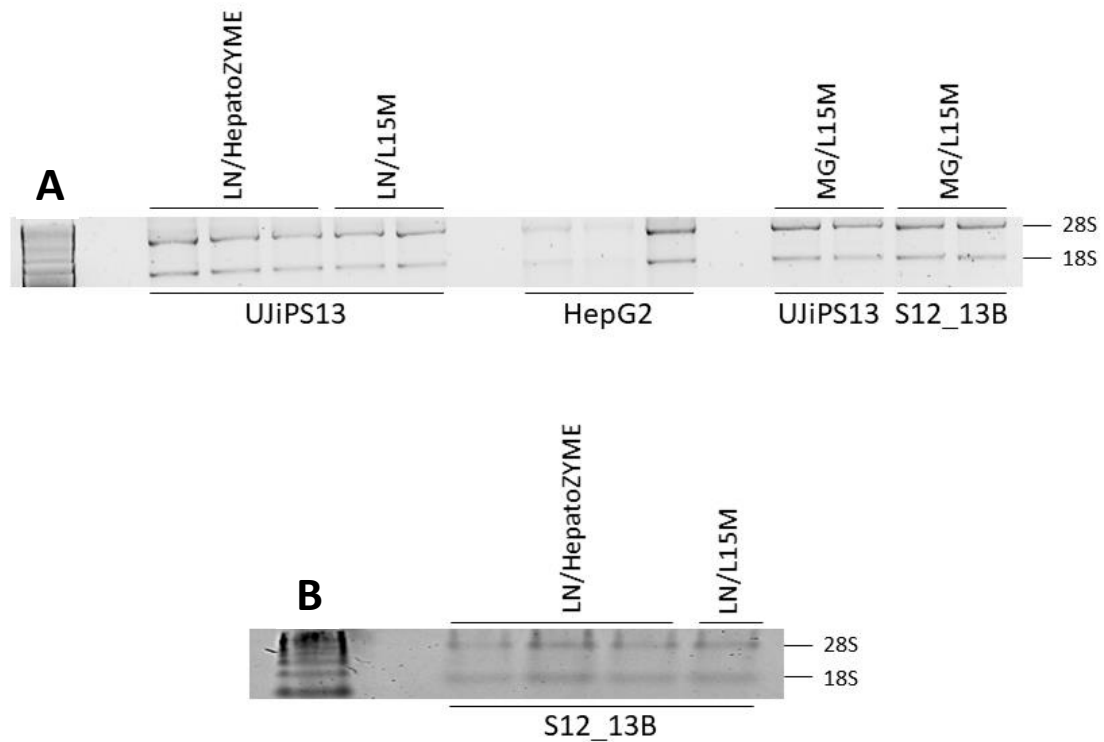


Fig. 10 – Quality control of isolated RNA by 1% agarose gel-electrophoresis. For each sample, two bands were visible exclusively on the prepared gels representing 28S and 18S RNA at a ratio of approximately 2:1. **A.** 28S (upper band) and 18S (lower band) RNA from UJiPS13 differentiated using Laminin (LN) 111/521 mixture and HepatoZYME® respectively Leibovitz 15 Maturation Medium (L15M), the biological positive control cell line HepG2, UJiPS13 differentiated using Matrigel (MG) and L15M and S12_13B differentiated using MG and L15M. **B.** 28S and 18S from S12_13B differentiated using LN-111/521 mixture and HepatoZYME® respectively L15M. For HepG2, three RNA samples could be obtained for further analysis. UJiPS13 differentiated on MG/L15M yielded two, LN/L15M two and LN/HepatoZYME three replicates. For S12_13B HLCs derived on MG/L15M two replicates, LN/L15M one and LN/HepatoZYME three replicates could be obtained. Ladder: Perfect Plus 100 kb DNA ladder.

Upon differentiation of S12_13B and UJiPS13 into HLCs, expression of the key pluripotency marker *OCT4* was downregulated consistently and at least for 96,7% (S12_13B, LN/L15M) for all differentiation conditions (see Fig. 11A). S12_13B derived HLCs exhibited comparable *OCT4* expression levels to adult primary human hepatocytes (PHH). In UJiPS13 derived HLCs and S12_13B differentiated employing MG/L15M, *OCT4* expression was downregulated more than 99%.

Hepatocyte-associated gene expression in contrast was upregulated for each cell line and culture condition. For *Albumin*, the fold change in gene expression ranged from 84 (S12_13B LN/HepatoZYME) to 1590 (UJiPS13 LN/HepatoZYME). Although there is a relevant increase in *ALB* expression of derived HLCs when compared to pluripotent stem cells, the biological positive controls showed higher *ALB* expression ranging from 900000 (HepG2) to 9246000 (PHH) fold change compared to hiPSC (see Fig. 11B). *AFP* expression in both cell lines and all applied conditions was comparable to fetal liver and HepG2 cells but recognizably higher than in adult PHH (see Fig. 11C). *CYP3A4* expression was highest in adult hepatocytes followed by fetal liver cells. An

increase in *CYP3A4* expression could, to lesser extent, also be detected in derived HLCs. Especially S12_13B differentiation using LN/L15M and LN/HepatoZYME exhibited comparable *CYP3A4* expression to HepG2 cells. Throughout all differentiation conditions, UJiPS13 exhibited the lowest upregulation of *CYP3A4* gene expression ranging from 5 to 20 fold change (see Fig. 11D). *HNF4α* expression was upregulated most in HepG2 cells (1686) when compared to iPSC. UJiPS13-derived HLCs when differentiated using LN/L15M (393) or LN/HepatoZYME (186) showed comparable *HNF4α* expression levels to PHH. Other cell lines and differentiation conditions exhibited *HNF4α* expression levels more comparable to fetal liver (see Fig. 11E).

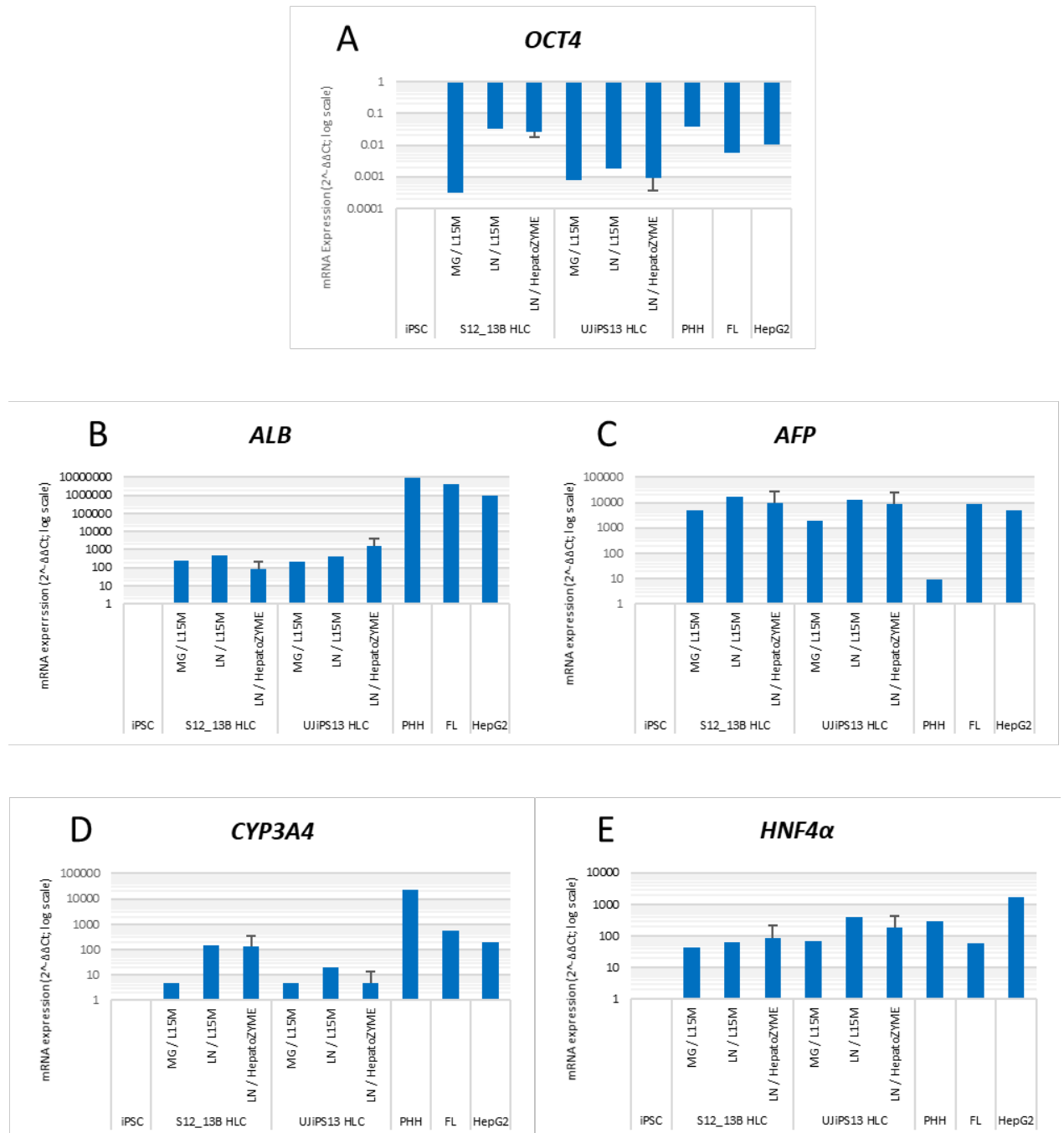


Fig. 11 - Expression of hepatocyte- and pluripotency-associated transcripts in pluripotent stem cell derived HLCs at the end of the hepatic differentiation process and three biological controls (PHH, FL, HepG2). The fold change in gene expression, normalized to the house keeping gene *RPL37a* and relative to gene expression in human PSCs, was calculated using the $\Delta\Delta C_t$ method in Microsoft Excel and visualized as bar graph with logarithmic y-axis. UJiPS13 differentiated on

MG/L15M was analyzed using two, LN/L15M using two and LN/HepatoZYME using three replicates. For S12_13B HLCs derived on MG/L15M two replicates, LN/L15M one and LN/HepatoZYME three replicates were employed. **A.** Fold Change of pluripotency-associated marker OCT4 **B-E.** Fold Change of hepatocyte-associated markers ALB (**B**), AFP (**C**), CYP3A4 (**D**) and HNF4 α (**E**). HLC – Hepatocyte-like cells, PH – primary human hepatocytes, FL – fetal liver, MG – Matrigel, LN – Laminin, L15M – Leibovitz 15 Maturation Medium, PSC – pluripotent stem cells

To check whether the amplicons of the RT-qPCR experiments corresponded to the expected size of the gene of interest, the PCR products were supplemented with 1 μ l loading dye, loaded onto 1,5% agarose gels containing 1X GelRed[®] nucleic acid gel stain and run at 80 mV for 15 min, 100 mV for another 15 min and 120 mV for the last 15 min. PCR products were visualized using UV light and the Fusion FX image capturer.

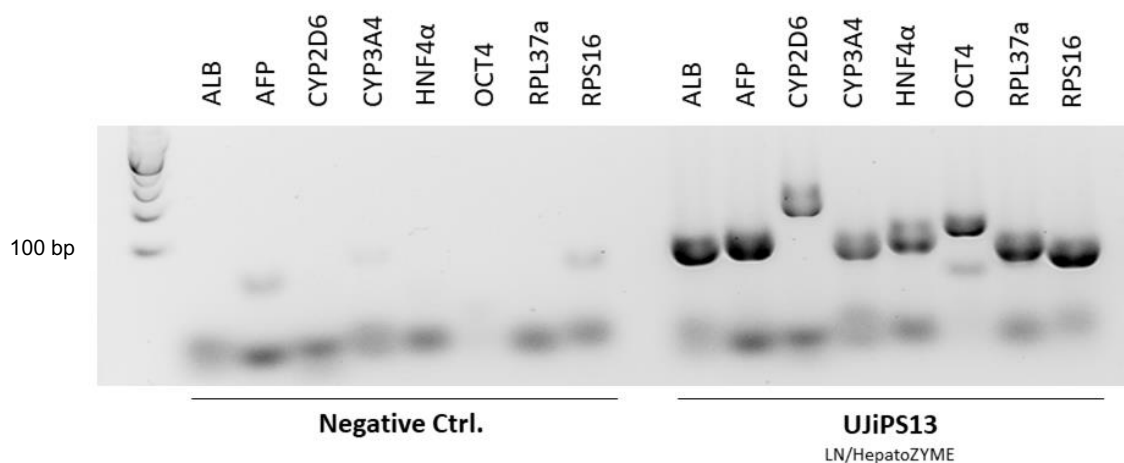


Fig. 12 – Quality control of quantitative real time polymerase chain reaction. Polymerase chain reaction (PCR) products were supplemented with 1 μ l loading dye, loaded onto 1,5% agarose gels containing 1X GelRed[®] nucleic acid gel stain and run together with a Perfect[™] 100 bp DNA ladder at 80 mV for 15 min, 100 mV for another 15 min and 120 mV for the last 15 min. PCR products were visualized using UV light and the Fusion FX image capturer. No bands representing nucleic acid of specific size were detectable within the negative control. Bands representing amplification products of appropriate sizes were visible for UJiPS13 differentiated with LN/HepatoZYME. This result is representative for other cell lines and differentiation conditions. Bp – base pairs, μ l – microliter, mV – Millivolt, min – minute, UV – ultraviolet, LN – laminin, ALB – albumin, AFP – alpha fetoprotein, ctrl - control

A representative result of derived RT-qPCR products, here UJiPS13 differentiated using LN/HepatoZYME, shows bands of expected sizes for the amplification products of all genes of interest (see Fig. 12). Amplification products could not be detected within the respective negative controls.

3.3 Immunostaining of intra- and extracellular hepatocyte-associated proteins

Whereas cells derived during HepDif#1 were only assessed using ICC at the HLC stage, HepDif#2 and #3 were checked for adequate expression of stage-specific biomarkers on the fourth, seventh and last day of hepatic differentiation. HepG2 cells served as positive control. On the last day of hepatic

differentiation, additionally two wells of a 6-well plate were singularized and fixed for flow cytometric analysis.

For ICC of the DE stage (HepDif#2 and #3), cells were fixed on the fourth day of hepatic differentiation and stained for SOX17, AFP, HNF4 α and SOX2. Nuclei were counterstained with Hoechst 33342. Both cell lines, S12_13B and UJiPS13, showed nuclear expression of HNF4 α and no expression of SOX2 upon differentiation on the Laminin mixture (see Fig. 13). They also indicated no expression of SOX17 and AFP (data not shown).

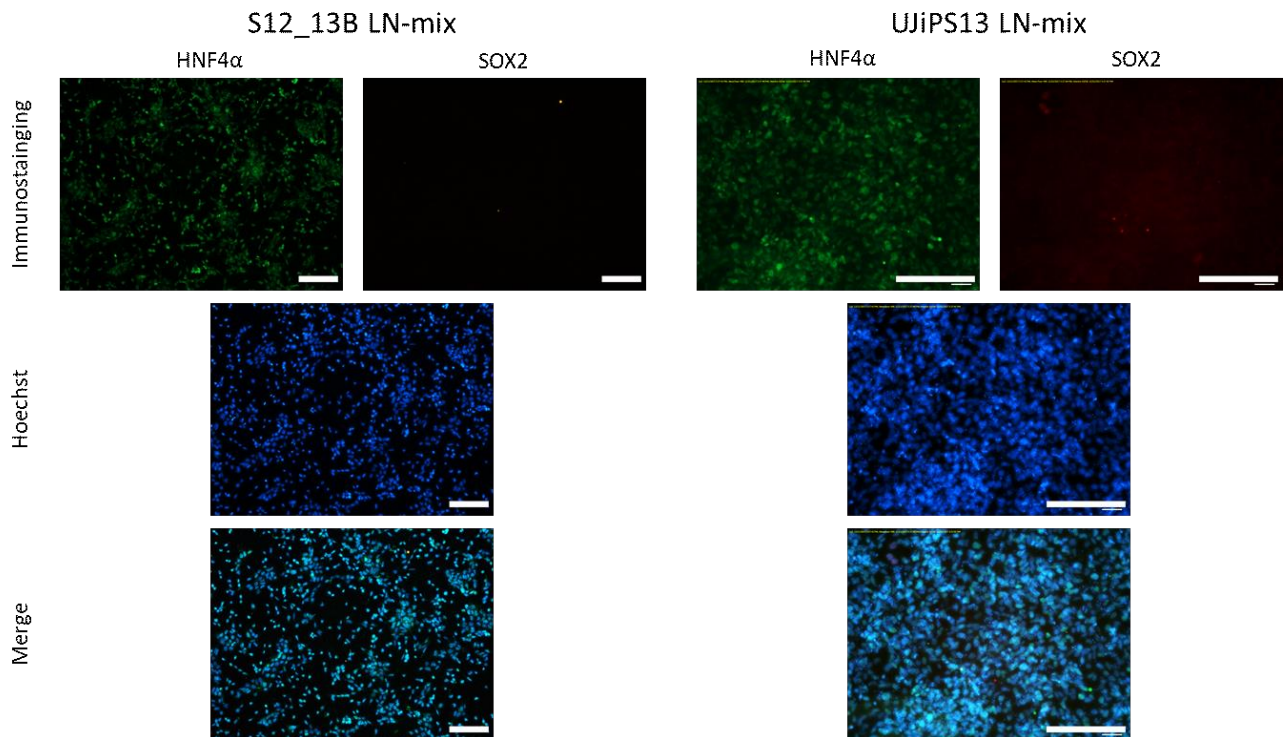


Fig. 13 – Immunocytochemistry of derived cells at definitive endoderm stage. Representative images of hepatic progenitor cells from S12_13B and UJiPS13 at DE stage (D4) stained for HNF4 α (rabbit α -HNF4 α antibody 1:300, goat α -rb-AF488 1:500) and SOX2 (mouse α -SOX2 antibody 1:300, goat α -mouse Cy3 1:500). Nuclei were counterstained with Hoechst 33342. Cells at DE stage of both cell lines expressed HNF4 α with a clearly nuclear localization and were negative for SOX2. Magnification of S12_13B: 10X, Magnification of UJiPS13: 20X, large scale bar: 200 μ m, small scale bar 50 μ m. LN – Laminin, DE – Definitive Endoderm, rb - rabbit

At day seven, cells from HepDif#2 and HepDif#3 were fixated at HE stage of differentiation. During both staining procedures a sheet of cells was lost. While a sufficient amount of cells was left for HepDif#3 derived cells, samples of HepDif#2 were lost completely and results for this differentiation experiment could not be retrieved at HE stage. HE cells from UJiPS13 derived on LN-mix indicated low expression of HNF4 α and AFP but no expression of SOX17 and SOX2 (see Fig. 14).

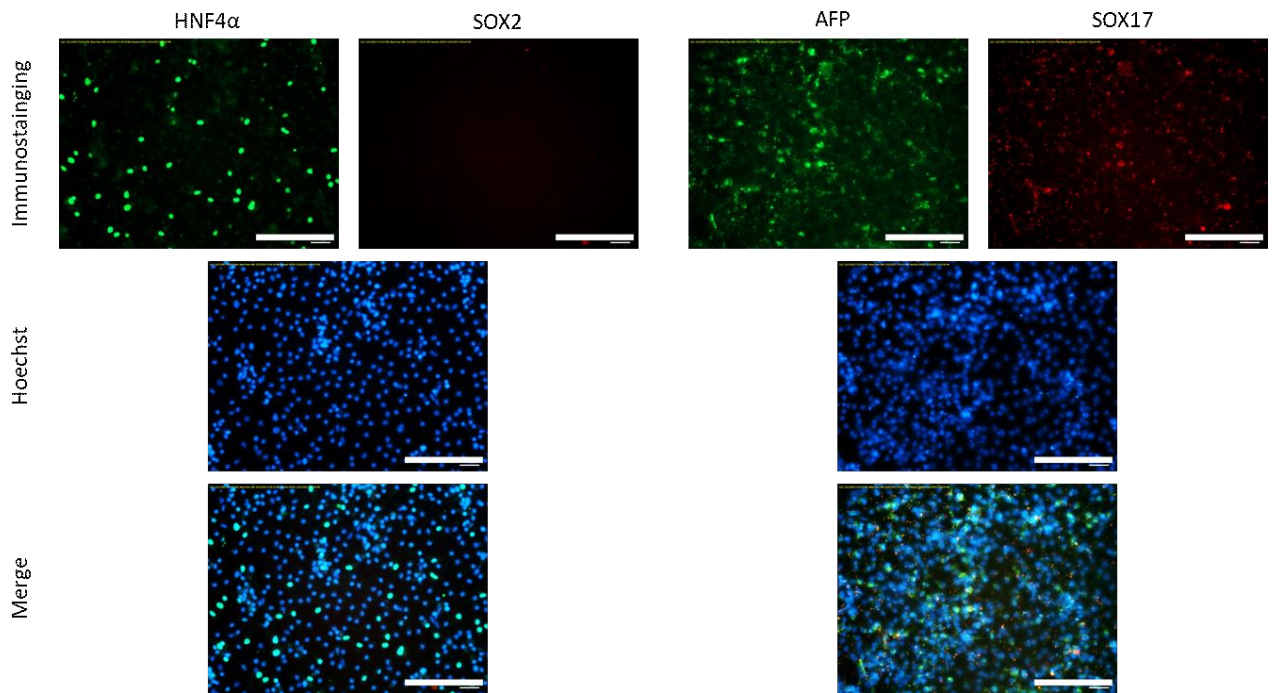


Fig. 14 – Immunocytochemistry of derived cells at hepatic endoderm stage. Representative images of hepatic progenitor cells from UJiPS13 at HE stage (D7) stained for HNF4 α (rabbit α -HNF4 α antibody 1:300, goat α -rb AF488 1:500), SOX2 (mouse α -SOX2 antibody 1:300, goat α -mouse Cy3 1:500), AFP (rabbit α -AFP antibody, 1:250, goat α -rb AF488 1:500) and SOX17 (goat α -SOX17 antibody, α -goat AF555 1:500). Nuclei were counterstained with Hoechst 33342. HE cells from UJiPS13 derived on LN-mix indicated low expression of HNF4 α and AFP but no expression of SOX17 and SOX2. Large scale bar: 200 μ m, small scale bar 50 μ m. HE – Hepatic Endoderm, rb – rabbit, LN – Laminin, AFP – alpha fetoprotein, ALB – albumin

On the final day of differentiation, derived HLCs and the biological positive control HepG2 exhibited varying expression of the hepatocyte-associated markers HNF4 α , E-Cadherin, AFP and Albumin. HNF4 α expression could be detected across all cell lines and differentiation conditions. After producing overlays with Hoechst 33342 counterstained nuclei, this marker showed a clear nuclear localization.

Staining for the membrane-bound epithelial marker E-Cadherin resulted in highlighting of a polygonal meshwork of comb-like structures in HepG2 cells, S12_13B derived HLCs differentiated on LN/HepatoZYME and UJiPS13 derived HLCs differentiated using LN/L15M and LN/HepatoZYME. Overlays with counterstained nuclei revealed that each comb contains one or two nuclei. Explicitly well visible is this comb-like structure on UJiPS13 differentiated using LN and L15M (see Fig. 19). UJiPS13 HLCs differentiated on MG/L15M did not show typical E-Cadherin expression and was therefore considered negative for E-Cadherin expression.

All conditions were further double-stained for the early resp. late-stage cytoplasmic hepatocyte-associated biomarker AFP and ALB. AFP is an early stage marker of hepatic differentiation and ALB seen as late stage marker indicating hepatocyte maturation. AFP was strongly expressed in HLCs derived from S12_13B differentiated using LN/HepatoZYME (see Fig. 17), UJiPS13 derived HLCs using LN/L15M (see Fig. 19) and the biological positive control HepG2 (see Fig. 15). Weak to no expression was detected in HLCs derived using MG/L15M and UJiPS13 HLCs differentiated

employing LN/HepatoZYME (see Fig. 20). ALB expression was strongest in HLCs derived from UJiPS13 using LN/L15M (see Fig. 19), S12_13B using LN/HepatoZYME (see Fig. 17) and in HepG2 cells (see Fig. 15). For S12_13B HLCs differentiated using MG/L15M no ALB expression could be detected, these cells were considered negative for ALB expression in ICC (see Fig. 16). Overall, AFP seems to be more abundant in derived HLCs than ALB and cells which were positive for AFP expression were only in rare occasions double positive for AFP and ALB expression and *vice versa*. Hepatic differentiation on the Laminin matrix, in general, showed stronger expression of both AFP and ALB compared to their Matrigel counterparts. The respective negative controls did not show relevant autofluorescence background staining.

Immunostaining of HepG2 cells

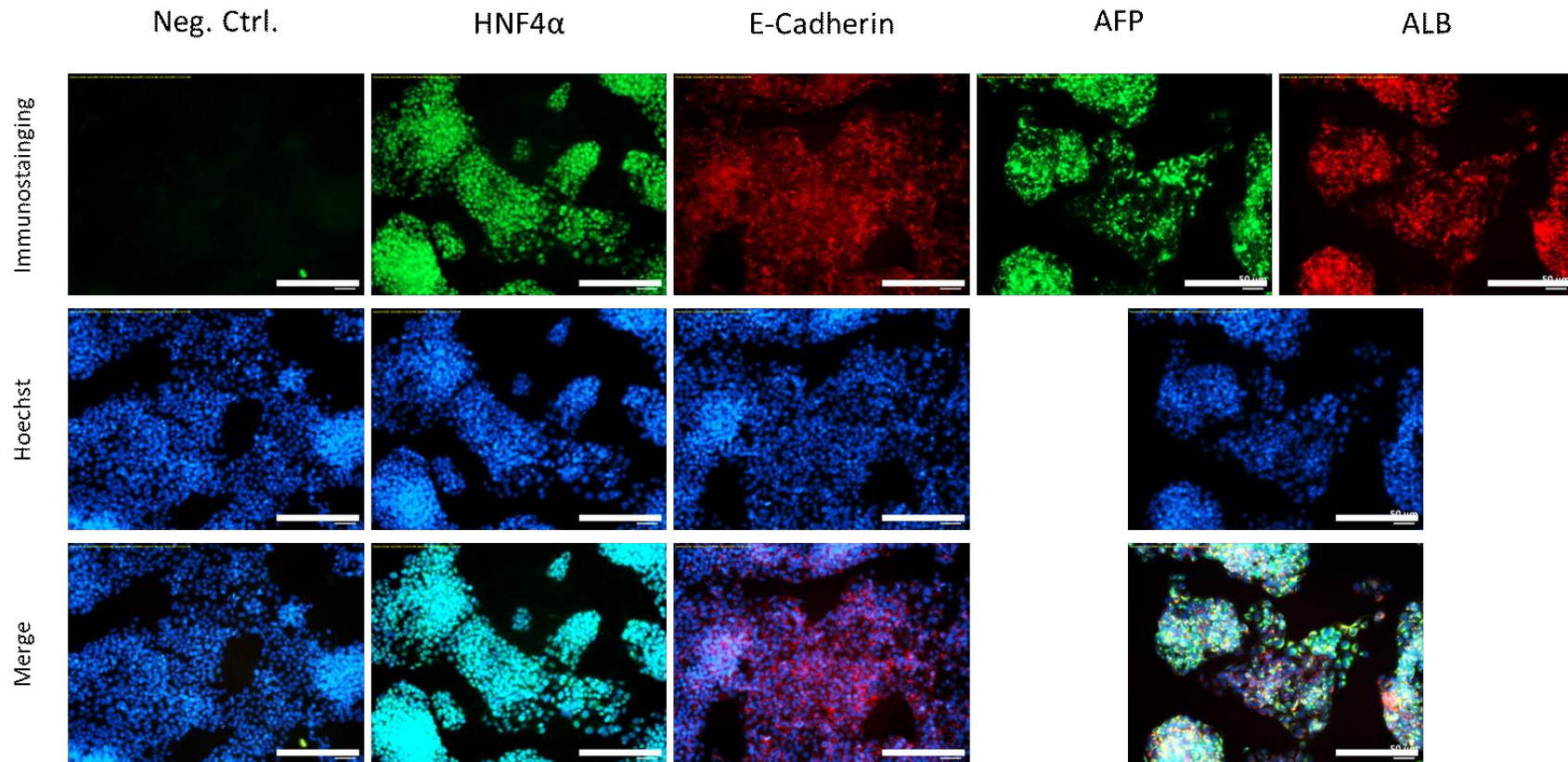


Fig. 15 – Immunocytochemistry of HepG2. Cells were stained for HNF4 α (rabbit α -HNF4 α antibody 1:300, goat α -rb AF488 1:500), E-Cadherin (mouse α -E-Cadherin 1:300, α -mouse Cy3 1:500), AFP (rabbit α -AFP antibody 1:250, α -rb AF488 1:500) and ALB (mouse α -ALB 1:500, goat α -mouse Cy3 1:500). Nuclei were counterstained with Hoechst 33342 (1:5000). HepG2 cells were positive for the hepatocyte-associated transcription factor HNF4 α exhibiting a clearly nuclear expression signaling after producing overlay pictures with Hoechst 33342 counterstained nuclei. E-Cadherin staining showed membrane associated signaling surrounding one or two nuclei per stained structure. Compared to hepatocyte-like cells however, cells were smaller in size and difficult to distinguish in centers of the colonies. AFP and ALB staining resulted in cytoplasmic signaling. Cells that were positive for AFP only in rare occasions were also positive for ALB and vice versa. The negative control was clearly negative for autofluorescence. Large scale bar: 200 μ m, small scale bar 50 μ m. AFP – Alpha Fetoprotein, ALB – Albumin, rb – rabbit, μ m - micrometer

Immunostaining of S12_13B differentiated on MG / L15M

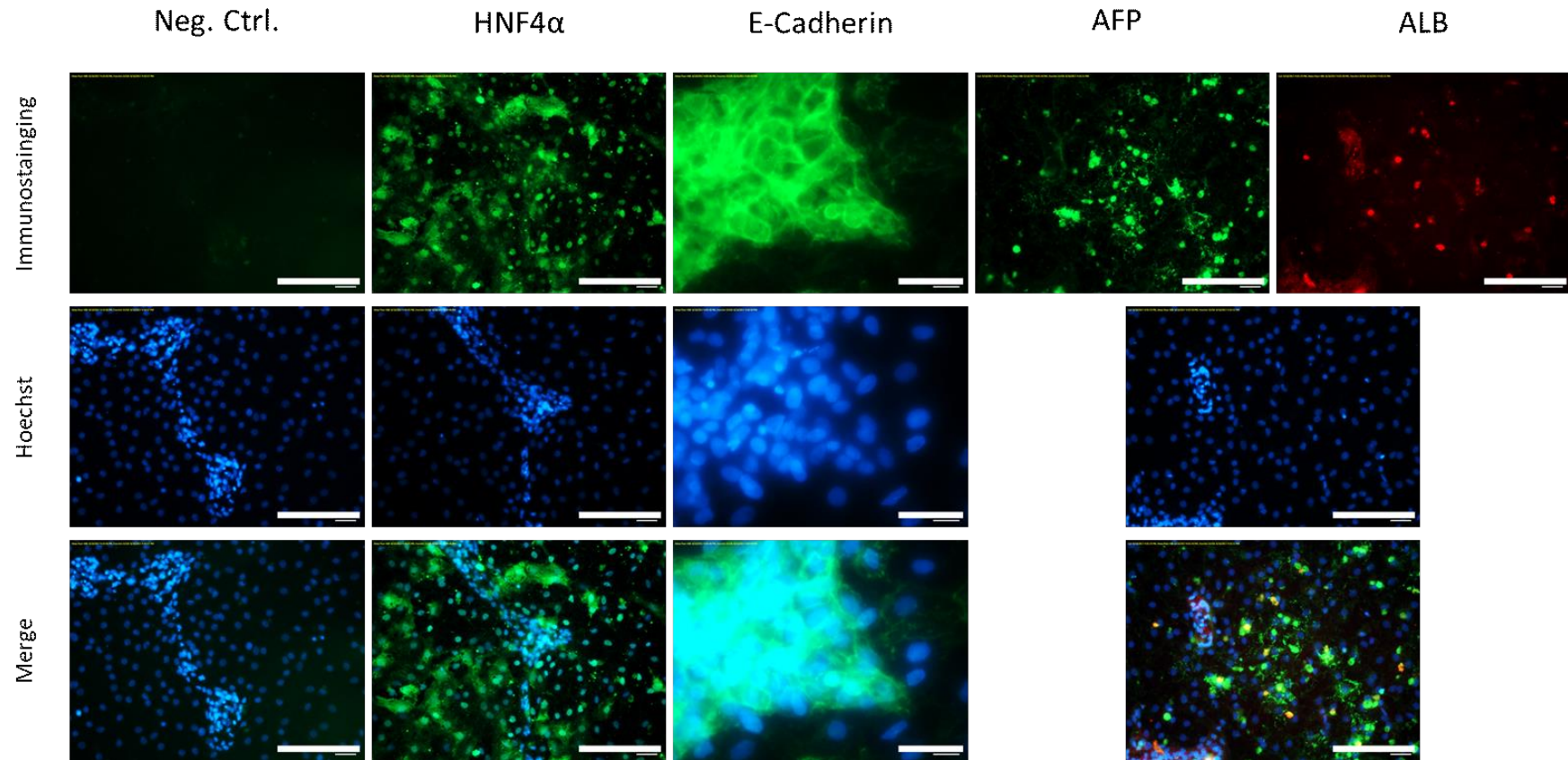


Fig. 16 – Immunocytochemistry of S12_13B HLCs derived using MG/L15M. Cells were stained for HNF4 α (rabbit α -HNF4 α antibody 1:300, goat α -rb AF488 1:500), E-Cadherin (rabbit α -E-Cadherin 1:300, α -rabbit AF488 1:500), AFP (rabbit α -AFP antibody 1:250, α -rb AF488 1:500) and ALB (mouse α -ALB 1:500, goat α -mouse Cy3 1:500). Nuclei were counterstained with Hoechst 33342 (1:5000). HLCs were positive for the hepatocyte-associated transcription factor HNF4 α exhibiting a clearly nuclear expression after producing overlay pictures with Hoechst 33342 counterstained nuclei. E-Cadherin staining showed membrane associated signaling surrounding one or two nuclei per stained structure. AFP and ALB expression was rare. The negative control was negative for autofluorescence. Large scale bar: 200 μ m, small scale bar 50 μ m. For E-Cadherin: large scale bar: 50 μ m, small scale bar: 20 μ m. AFP – Alpha Fetoprotein, ALB – Albumin, HLC – Hepatocyte-like cells, rb – rabbit, μ m - micrometer

Immunostaining of S12_13B differentiated on LN-Mix / HepatoZYME

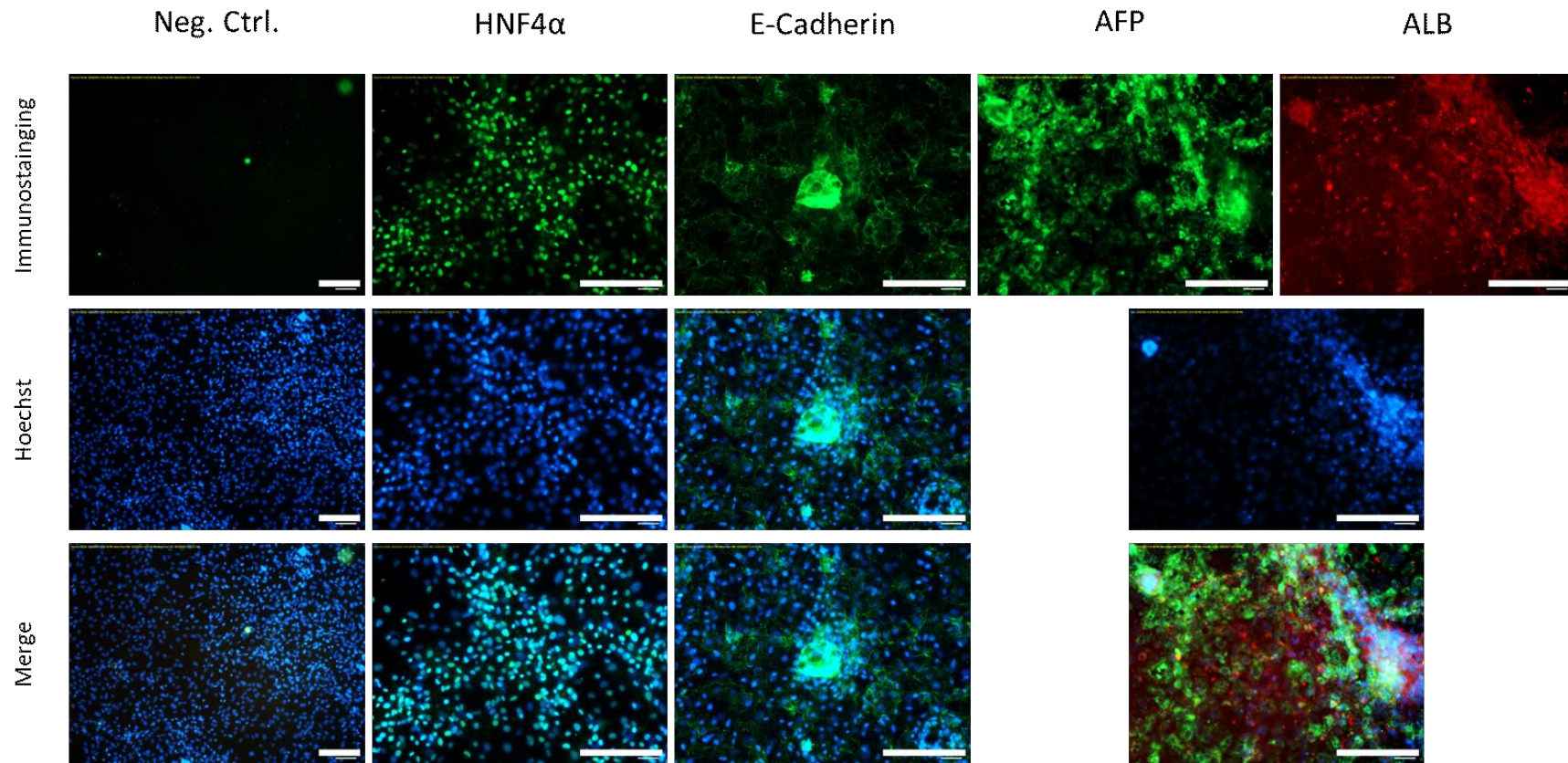


Fig. 17 – Immunocytochemistry of S12_13B HLCs derived using LN/HepatoZYME. Cells were stained for HNF4 α (rabbit α -HNF4 α antibody 1:300, goat α -rbAF488 1:500), E-Cadherin (rabbit (rb) α -E-Cadherin 1:300, α -rabbitAF488 1:500), AFP (rabbit α -AFP antibody 1:250, α -rb AF488 1:500) and ALB (mouse α -ALB 1:500, goat α -mouse Cy3 1:500). Nuclei were counterstained with Hoechst 33342 (1:5000). Scale bar: 50 μ m. Derived HLCs were positive for the hepatocyte-associated transcription factor HNF4 α indicating a clearly nuclear localization after producing overlay pictures with Hoechst 33342 counterstained nuclei. E-Cadherin staining showed membrane associated signaling surrounding one or two nuclei per stained structure. AFP and ALB were expressed in the cytoplasm. Cells that were positive for AFP only in rare occasions were also positive for ALB and vice versa. The negative control was clearly negative for autofluorescence. Large scale bar: 200 μ m, small scale bar 50 μ m.

Immunostaining of UJiPS13 differentiated on MG / L15M

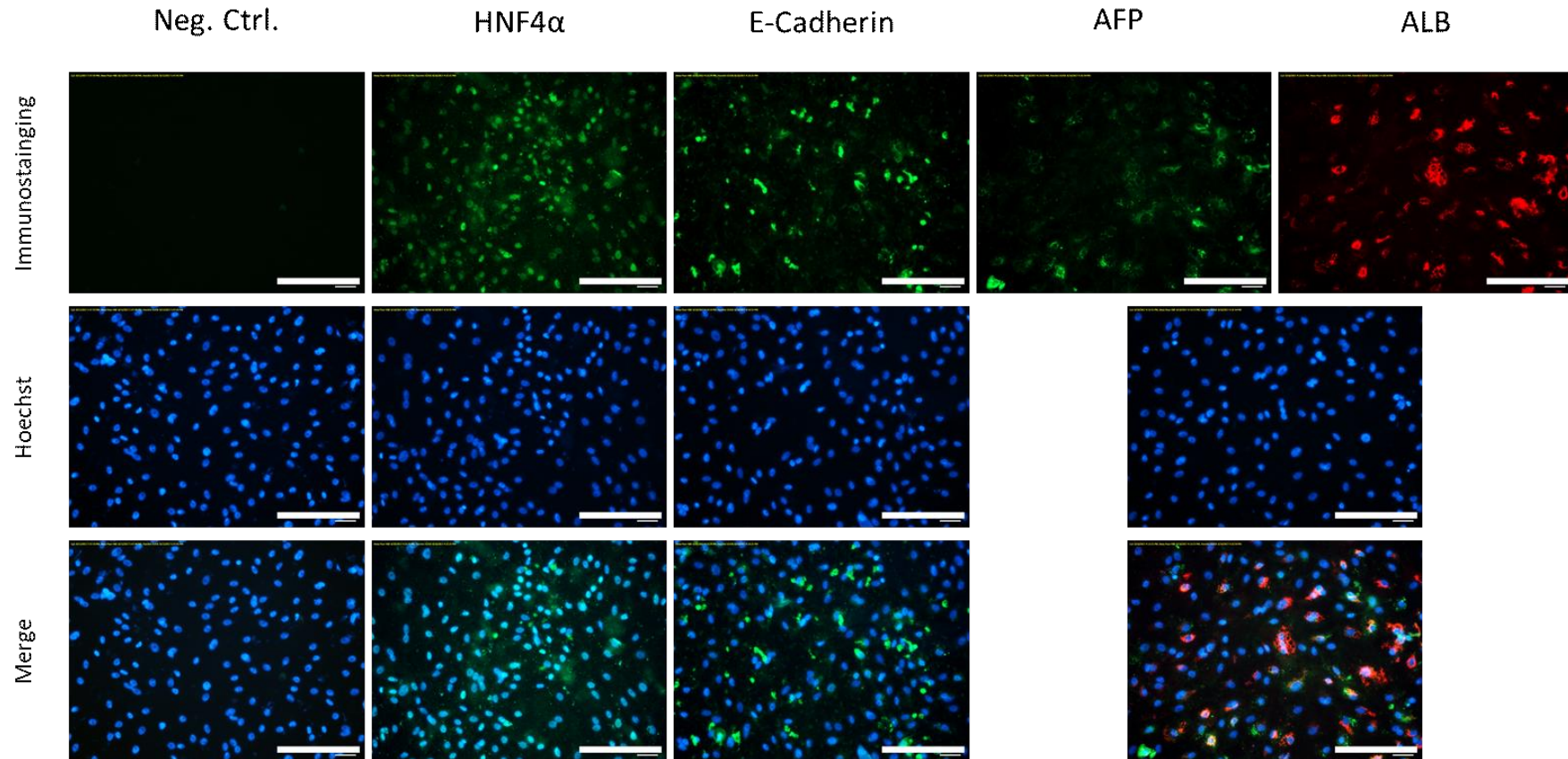


Fig. 18 – Immunocytochemistry of UJiPS13 HLCs derived using MG/L15M. Cells were stained for HNF4 α (rabbit α -HNF4 α antibody 1:300, goat α -rbAF488 1:500), E-Cadherin (rabbit α -E-Cadherin 1:300, α -rabbit AF488 1:500), AFP (rabbit α -AFP antibody 1:250, α -rb AF488 1:500) and ALB (mouse α -ALB 1:500, goat α -mouse Cy3 1:500), nuclei counterstained with Hoechst 33342 (1:5000). Derived HLCs were positive for HNF4 α indicating a clearly nuclear localization after producing overlay pictures with Hoechst 33342 pictures. E-Cadherin staining was dim and did not result in membrane associated signaling. AFP and ALB were expressed rarely in the cytoplasm of derived HLCs. The negative control was negative for autofluorescence. Large scale bar: 200 μ m, small scale bar 50 μ m.

Immunostaining of UJiPS13 differentiated on LN-mix / L15M

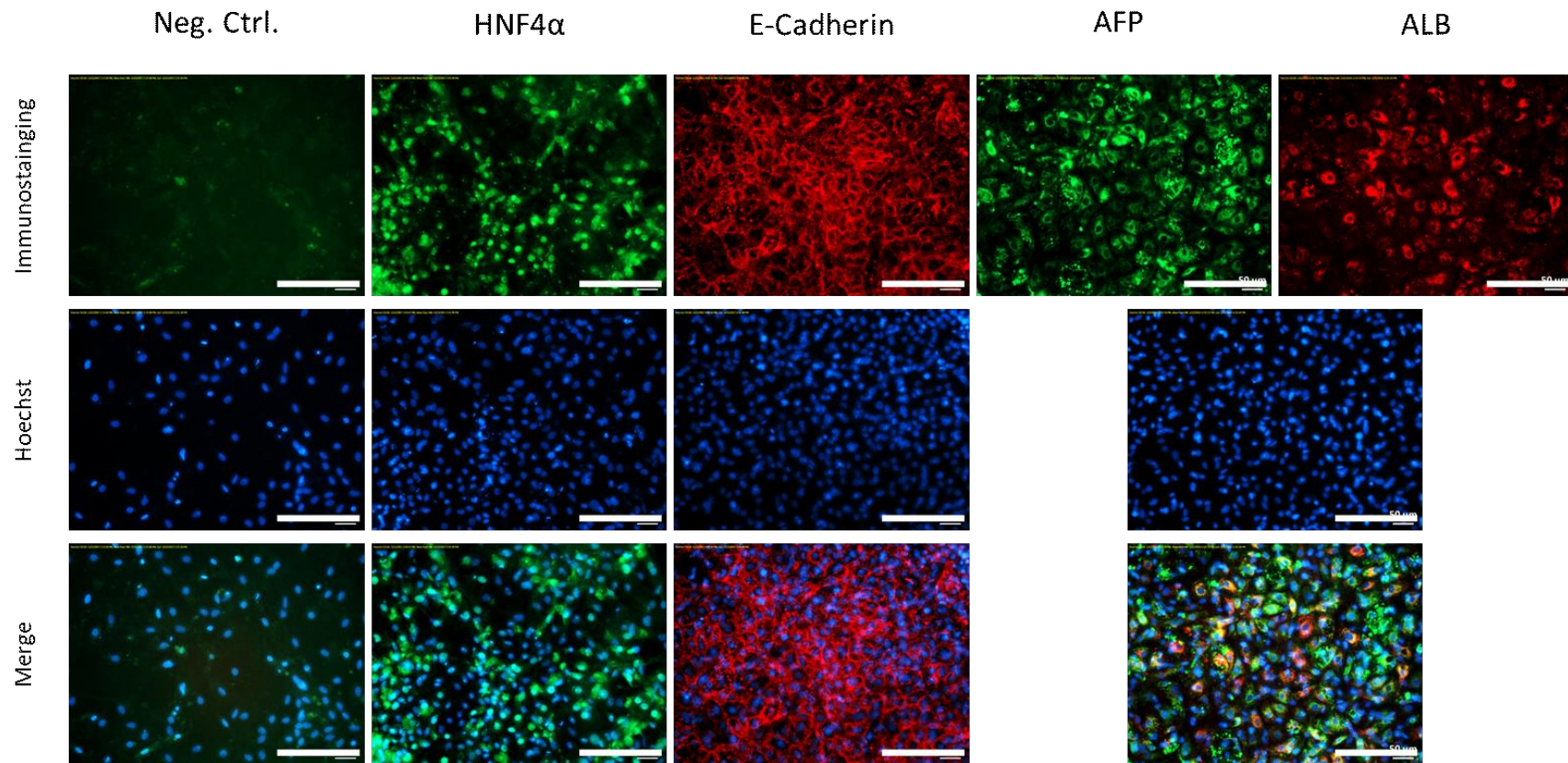


Fig. 19– Immunocytochemistry of UJiPS13 HLCs derived using LN/L15M. Cells were stained for HNF4α (rabbit α-HNF4α antibody 1:300, goat α-rbAF488 1:500), E-Cadherin (mouse α-E-Cadherin 1:300, α-mouse Cy3 1:500), AFP (rabbit α-AFP antibody 1:250, α-rb AF488 1:500) and ALB (mouse α-ALB 1:500, goat α-mouse Cy3 1:500). Nuclei were counterstained with Hoechst 33342 (1:5000). Derived HLCs were positive for the hepatocyte-associated transcription factor HNF4α indicating a clearly nuclear localization after producing overlay pictures with Hoechst 33342 counterstained nuclei. E-Cadherin staining showed strong membrane associated signaling surrounding one or two nuclei per stained structure. AFP and ALB were expressed in the cytoplasm. Cells that were positive for AFP only in rare occasions were also positive for ALB and vice versa. The negative control was faintly positive for autofluorescence. Large scale bar: 200 μm, small scale bar 50 μm.

Immunostaining of UJiPS13 differentiated on LN-mix / HepatoZYME

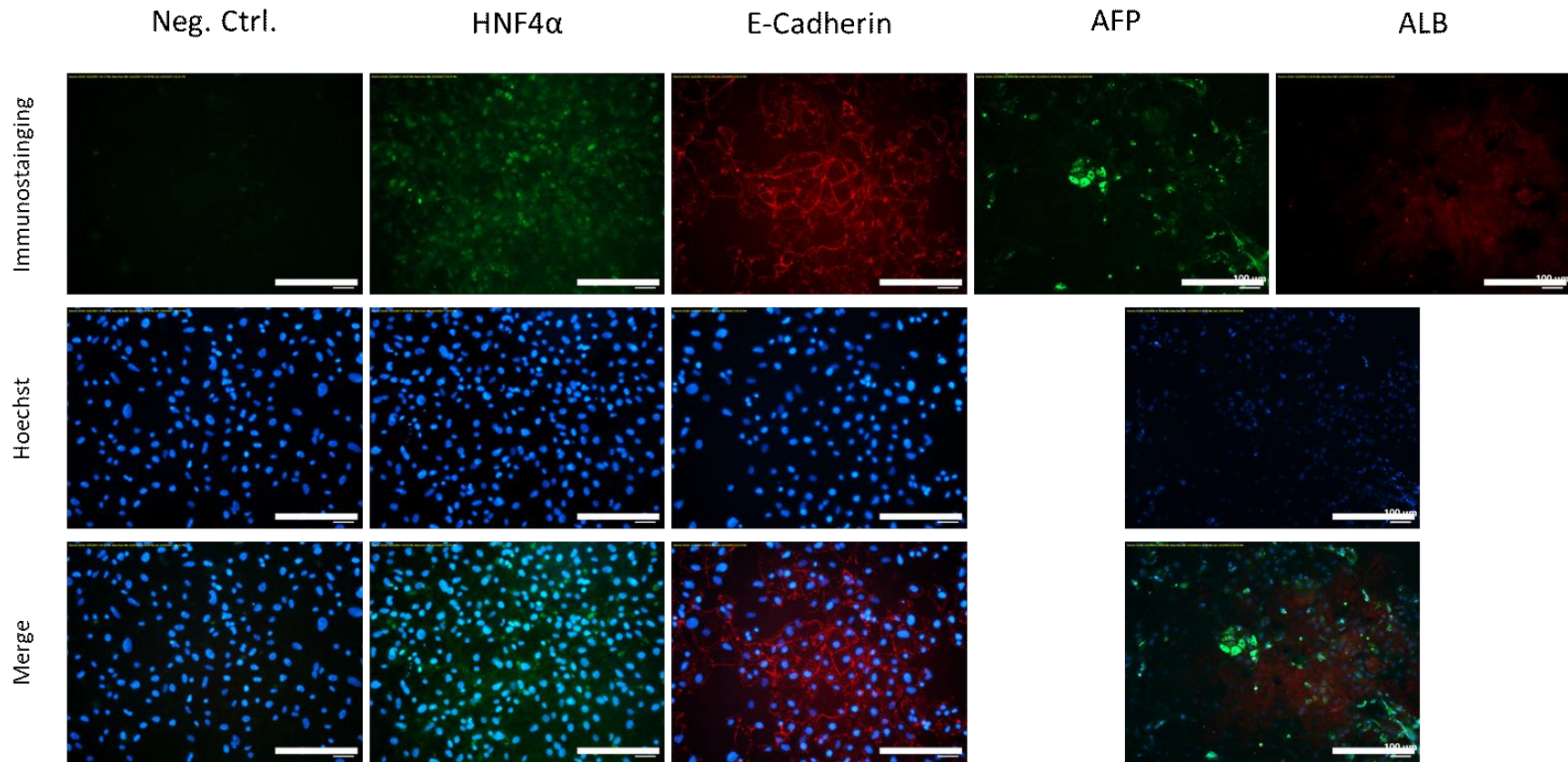


Fig. 20 – Immunocytochemistry of UJiPS13 HLCs derived using LN/HepatoZYME. Cells were stained for HNF4α (rabbit α-HNF4α antibody 1:300, goat α-rbAF488 1:500), E-Cadherin (mouse α-E-Cadherin 1:300, α-mouse Cy3 1:500), AFP and ALB. Nuclei were counterstained with Hoechst 33342 (1:5000). Scale bar: 50 μm. Derived HLCs were positive for the hepatocyte-associated transcription factor HNF4α indicating a clearly nuclear localization after producing overlay pictures with Hoechst 33342 counterstained nuclei. E-Cadherin staining showed dim membrane associated signaling surrounding one or two nuclei per stained structure. AFP was rarely expressed in the cytoplasm of derived HLCs, ALB expression could not be detected. The negative control was clearly negative for autofluorescence. Large scale bar: 200 μm, small scale bar 50 μm.

For semiquantitative evaluation of the hepatocyte-associated biomarkers HNF4 α , AFP, ALB and UGT1A1, flow cytometry was performed on HLCs derived from S12_13B and UJiPS13 using LN and HepatoZYME. Cells were fixated on the last day of differentiation. As the sample for UJiPS13 was lost during the staining procedure, only results for S12_13B are displayed.

Cells were co-stained for HNF4 α and ALB, respectively AFP and UGT1A1. Specificity of used antibodies for HNF4 α , AFP and ALB for nuclear respectively cytoplasmic structures, has been proven through immunocytochemical staining of cells of the same differentiation sample.

The population of HLCs was defined using forward (FS) and side scatter (SS) and set to exclude only small and almost ungranulated structures like cell debris (see Fig. 21). 64% of the parental cell population fell into the HLC gate and were analyzed for fluorescence signal intensity.

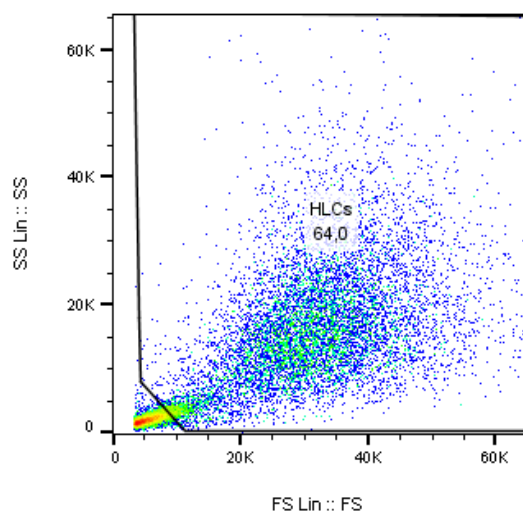


Fig. 21 – Gating of parental cell population of S12_13B derived hepatocyte-like cells for flow cytometry. Cells exhibiting small forward (FS) and side scatter (SS) values were excluded and considered cell debris. In total, 64% of the total population fell into the HLC gate and were analyzed for fluorescence signal intensity. HLCs – Hepatocyte-like cells

When compared to the technical negative control (unstained HLCs; gray in histogram), a clear shift in fluorescence signal intensity could be observed for HNF4 α . 80.2% of the analyzed cell population was positive for HNF4 α expression, 19.8% were counted negative. A shift in fluorescence intensity for albumin could only faintly be detected (2.36%), the majority of cells was negative for Albumin expression (97.7%). The dot plot diagram allows for the discrimination of negative (Q4: HNF4 α ⁻ ALB⁻), single positive (Q3: HNF4 α ⁺ ALB⁻; Q1: HNF4 α ⁻ ALB⁺) and double positive (Q2: HNF4 α ⁺ ALB⁺) cells. Here, only 0.02% of the gated population was single positive for ALB (Q2) and 78.1% single positive for HNF4 α . 2.08% of the cells, however, were positive for both markers indicating that cells which are positive for ALB, are also positive for HNF4 α (see Fig. 22A).

AFP again was abundantly expressed (89.1% positive cells) in the gated cell population. UGT1A1 could not be detected (99.8% negative, see Fig. 22B).

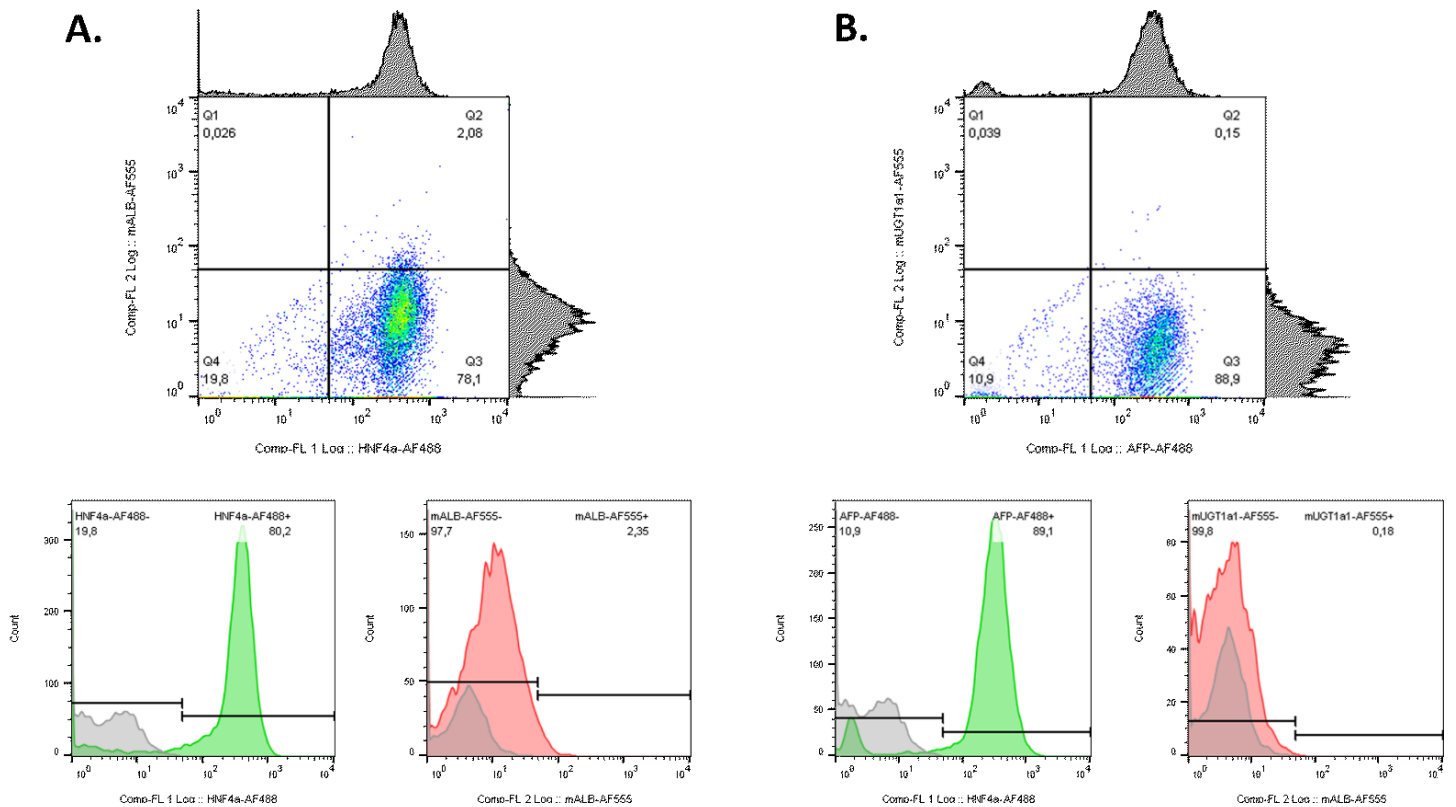


Fig. 22 – Dotplots and histograms for gated cell populations. **A.** HLCs stained for HNF4a (rabbit α -HNF4a antibody 1:300, goat α -rbAF488 1:500) and ALB (mouse α -ALB antibody 1:500, α -mouse Cy3 1:500). 80.2% of cells within the HLC gate are positive for HNF4a, whereas only 2.35% are positive for ALB. Around 2% of cells are positive for both markers. **B.** HLCs stained for AFP (rabbit α -AFP antibody 1:250, goat α -rbAF488 1:500) and UGT1a1 (mouse α -UGT1a1 1:200, α -mouse Cy3 1:500). Whereas 89.1% of cells within the HLC gate are positive for AFP, staining for UGT1A1 did not result in a shift in fluorescence intensity compared to the technical negative control (unstained HLCs). HLC – Hepatocyte-like cells, rb – rabbit, ALB – albumin, AFP – alpha fetoprotein

3.4 Biochemical assessment of derived hepatocyte-like cells

Derived HLCs were characterized employing a battery of biochemical assays assessing cellular functionality and metabolism.

3.4.1 Metabolic functionality of derived HLCs

To assess the basic capability to internalize and excrete molecules and proteins, derived HLCs were incubated in medium containing 1 mg/ml ICG for 30 min. Uptake and release was assessed after 30 min and 24 h by brightfield microscopy (see Fig. 23). Derived HLCs and HepG2 cells internalized indocyanine green within 30 min upon incubation resulting in a bright green signal and excreted the dye recognizably but not completely within 24h. No remarkable difference could be observed in ICG uptake and release between employed cell lines and conditions of hepatic differentiation. ICG uptake and release of derived HLCs was comparable to the biological positive control cell line HepG2.

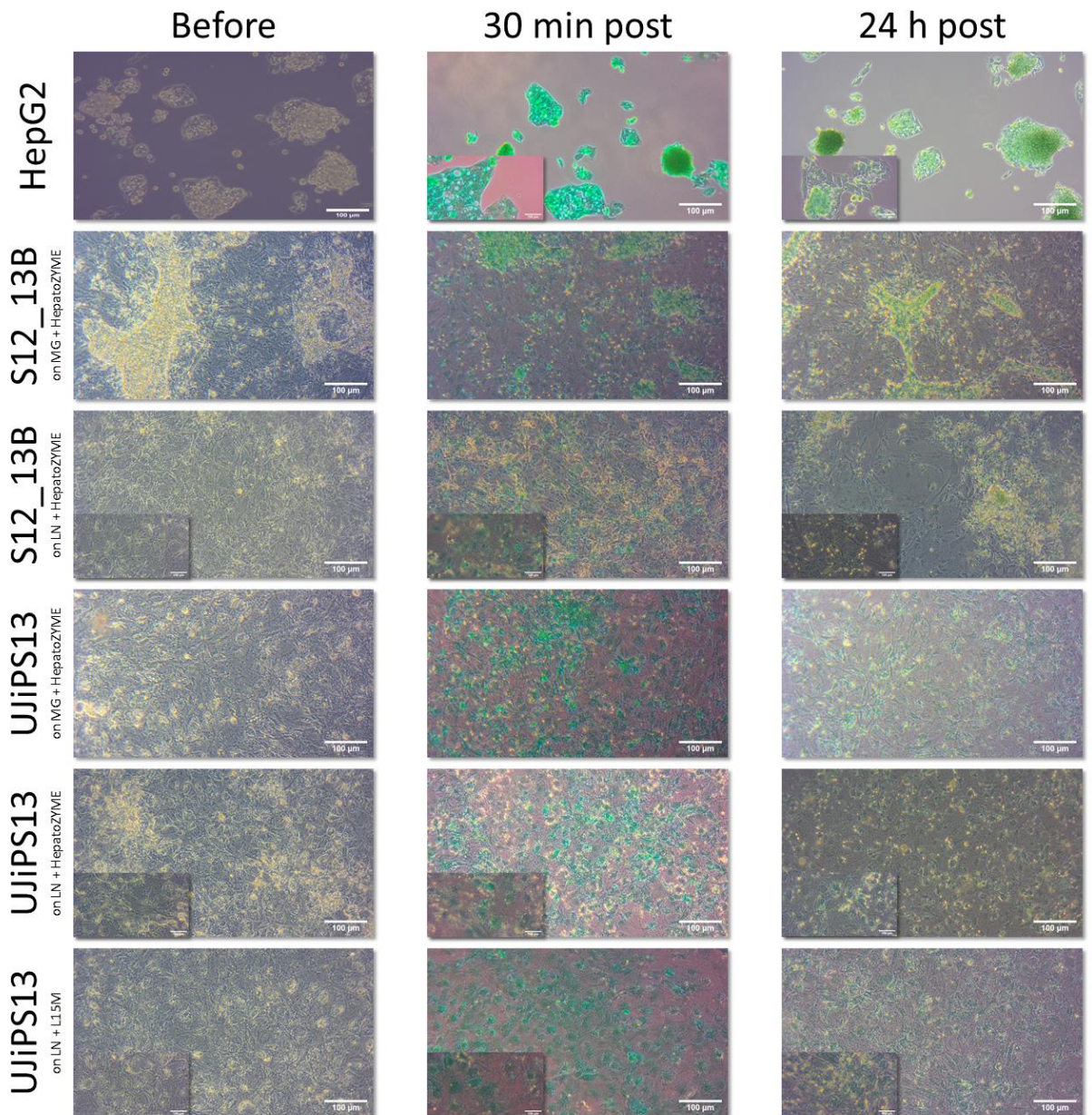


Fig. 23 – Indocyanin green (ICG) uptake and release by derived hepatocyte-like cells within 24h. Cells were incubated in medium containing 1 mg/ml ICG for 30 min. Uptake and release was assessed after 30 min and 24 h by brightfield microscopy. Derived HLCs and HepG2 cells internalized indocyanine green upon 30 min of incubation resulting in a bright green signal and excreted the dye recognizably but not completely within 24h. No remarkable difference could be observed in ICG uptake and release between employed cell lines and conditions of hepatic differentiation. Min – minutes, h – hours, HLCs – hepatocyte-like cells

The production of carbohydrate macromolecules like glycogen, a key feature of functional hepatocytes, was assessed by using the periodic acid Schiff reaction and counterstaining of nuclei with hematoxylin. The derived HLCs of every stained differentiation condition (S12_13B on LN/HepatoZYME, UjiPS13 on LN/HepatoZYME and LN/L15M) indicated a purple signal in the cells' cytoplasm that was comparable to the biological positive control HepG2 (see Fig. 24A-D).

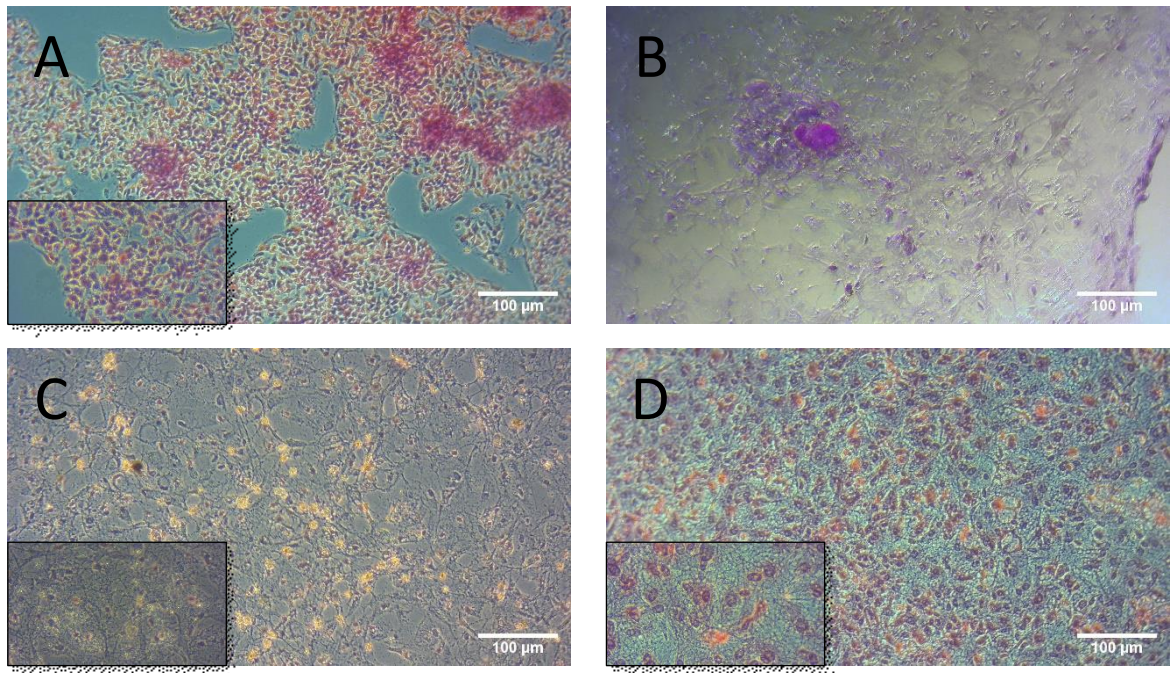


Fig. 24 – Glycogen storage detection by periodic acid Schiff reaction. Glycogen storage is indicated by a purple signal in the cytoplasm. Scale bar: 100 µm **A.** HepG2 cells. **B.** S12_13B on LN-mix + HepatoZYME **C.** UJiPS13 on LN-mix + HepatoZYME **D.** UJiPS13 on LN-mix + L15M. HLCs – Hepatocyte-like cells, LN – Laminin, L15M – Leibovitz 15 Maturation Medium, µm - micrometer

CYP3A4 activity of derived HLCs was determined by detection of luminescence signaling after incubation with a proluciferin (Luciferin-PFBE) for 3-4 h. A 1:1 mixture of medium containing the metabolized Luciferin with detection reagent resulted in measurable light signals that were quantified by a luminometer. Using Microsoft Excel, luminescence of the HLC samples was corrected for background signals by subtracting the mean luminescence signaling of the negative controls. After the first hepatic differentiation experiment, induction treatment with 10µM rifampicin for 24 h prior to activity measurement was introduced to increase the low metabolic activity of CYP3A4 and prove its inducibility by common CYP inducers.

The results of three separate CYP3A4 activity measurements (HepDif #1 - #3) are summarized in Fig. 25. Luminescence signaling was detectable for S12_13B and HepG2 but not UJiPS13 independent of the employed matrix-medium combination. For S12_13B, Matrigel + L15M based differentiation yielded in HLCs with lowest luminescence signaling with a mean of 35.67 RLU/ml. HLCs differentiated on LN + HepatoZYME exhibited higher luminescence signaling (157.33 RLU/ml) and showed a 72% increase of mean luminescence upon rifampicin mediated CYP3A4 induction (271.33 RLU/ml). The biological positive control HepG2 showed low mean luminescence signaling without (50.33 RLU/ml) but a 280% increase (193.33 RLU/ml) upon CYP3A4 induction.

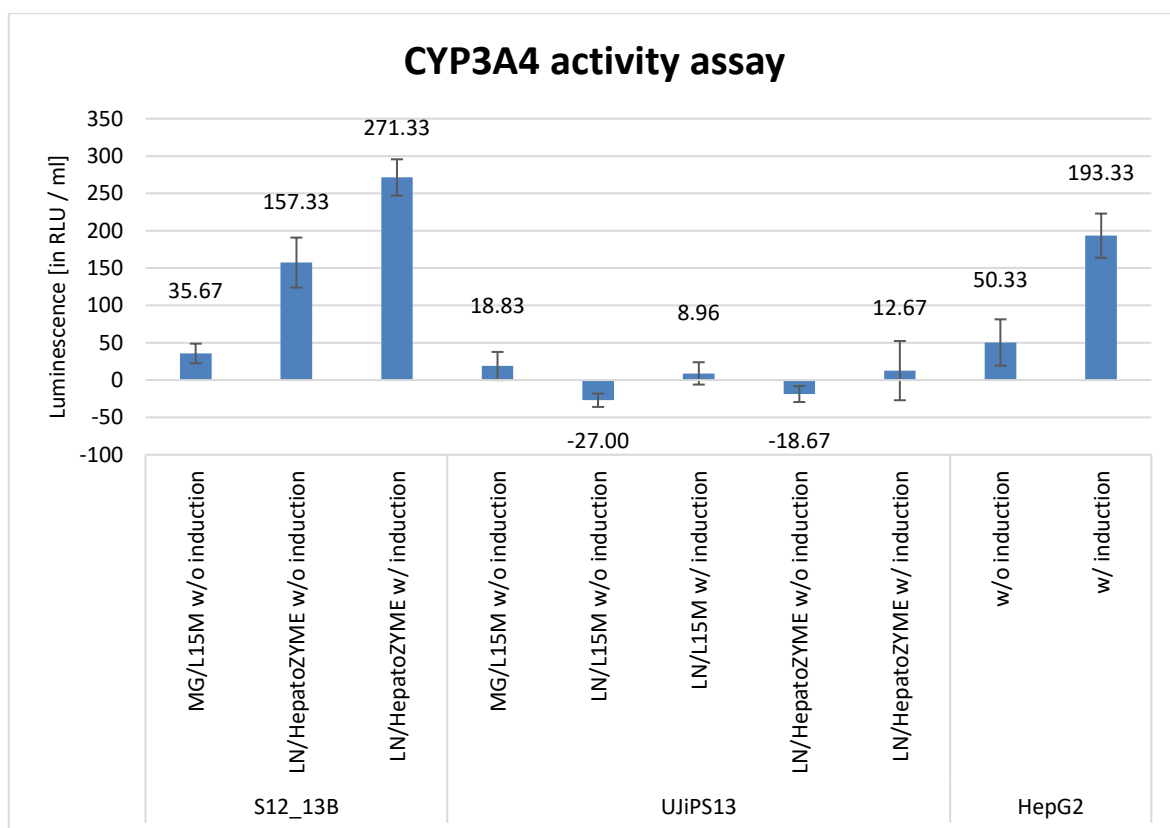


Fig. 25 – CYP3A4 activity assay of derived hepatocyte-like cells and HepG2 cells. Bar graphs indicate the mean luminescence measured (in RLU/ml) and corresponding standard deviations (SD). S12_13B derived HLCs exhibited luminescence signaling after background correction for all employed matrix-medium combinations. Inducibility of CYP3A4 after 24h of treatment with 10 μ M rifampicin could be shown on HLCs differentiated on LN/HepatoZYME. UJiPS13 derived HLCs did not show luminescence signaling after correction for background. HepG2 cells, again, did show luminescence signaling which could be increase by rifampicin-mediated CYP3A4 induction. HLC – Hepatocyte-like cells, ml – milliliter, h – hours, μ M – micromolar, LN – Laminin, MG – Matrigel, w/o – without, w/ - with

Another important feature of functional hepatocytes is the production and secretion of urea into the culture medium. To detect urea secretion, supernatant medium samples were taken at D4 (DE stage), D7 (HE stage) and the last day of differentiation (HLC stage) and incubated with a chromogenic reagent that forms colored complexes upon binding to urea. The resulting color intensity of the was measured spectrophotometrically at 520 nm and is directly proportional to the urea concentration of the sample. By utilizing a standard dilution row of known urea concentrations, the urea concentration within the samples was calculated and visualized as bar graph with Microsoft Excel (see Fig. 26). Urea could not be detected in DE or HE stages throughout differentiation of both cell lines independent of the employed cell culture matrix. At the last day of differentiation, 2.08 mg/dl urea was measured for S12_13B HLCs derived using LN/L15M. No urea was detectable in medium from HLCs derived using MG/L15M or LN/HepatoZYME.

For UJiPS13, highest yield of urea production was determined in HLCs derived with LN/L15M (3.56 mg/dl) followed by MG/L15M. No urea could be detected in medium from HLCs derived using LN/HepatoZYME.

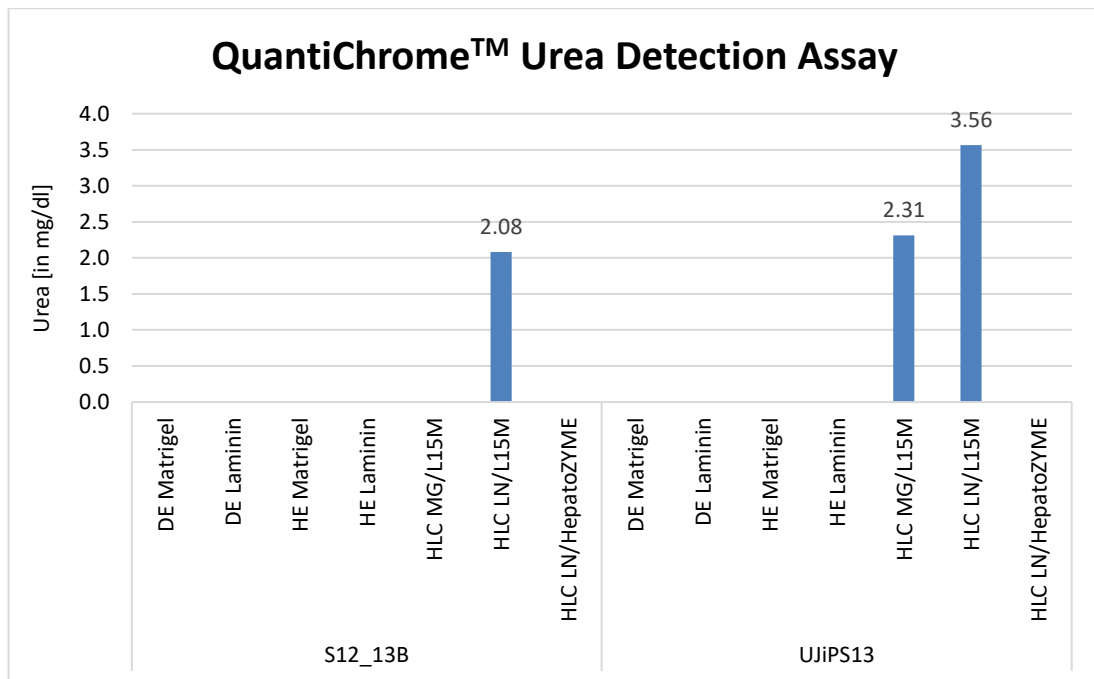


Fig. 26 – Concentration of urea (in mg/dl) in supernatant medium from three different time points (DE (D4), HE (D7), HLC (last day of differentiation)) throughout the hepatic differentiation process. Medium samples were incubated with a chromogenic reagent forming colored complex with urea. Final urea concentrations were calculated using a standard dilution curve and Microsoft Excel. For S12_13B, only the LN/L15M condition produced detectable urea concentrations (2.08 mg/dl). For UJiPS13, MG/L15M (2.31 mg/dl) and LN/L15M (3.56 mg/dl) mediated differentiation yielded in detectable urea secretion. DE – Definitive Endoderm, HE – Hepatic Endoderm, HLC – Hepatocyte-like cells, MG – Matrigel, LN – Laminin, L15M – Leibovitz 15 Maturation Medium, DE – definitive endoderm, HE – hepatic endoderm, mg – milligram, dl – deciliter,

Same supernatant media samples were used to detect albumin secretion during DE, HE and HLC stage. Appropriate amounts of Nunc MaxiSorb™ flat bottom 96-well plates were coated with α -human-ALB-antibody (A80-129A), blocked and incubated in technical triplicates with a standard dilution row of known albumin concentrations, fresh media samples and supernatant HLC media samples.

Surprisingly, albumin secretion could only be detected in the supernatant of medium at DE stage where ALB expression is expected to be lowest to absent. No albumin was found in media samples of HE or HLC, independent of employed matrix-medium combination or utilized cell line (see Fig. 27).

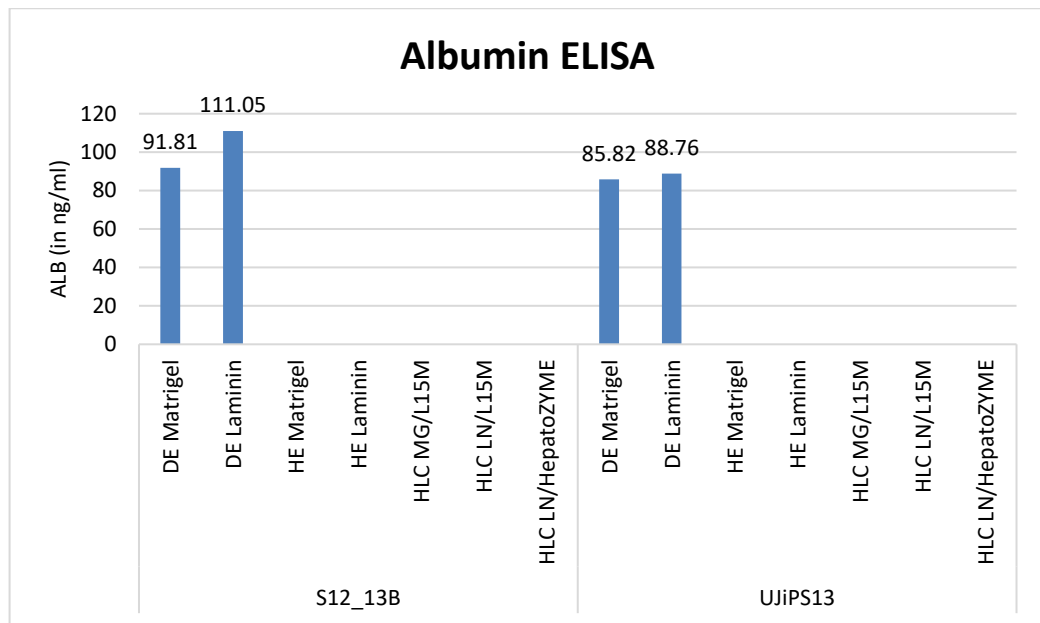


Fig. 27 - **Albumin secretion detected by enzyme-linked immunosorbent assay (ELISA)**. 96-well plates were coated with ALB-specific antibodies, blocked and incubated with media samples and a standard dilution row with known albumin concentrations. Final sample albumin concentrations were calculated using the standard dilution curve and Microsoft Excel. Unexpectedly, no albumin secretion could be detected in medium samples of HE and HLC stage, independent of the employed matrix-medium combination, but excessively in medium of DE stages for both cell lines differentiated on MG (S12_13B: 91.81 ng/ml; UJiPS13: 85.82 ng/ml) and LN (S12_13B: 111.05 ng/ml; UJiPS13: 88.76 ng/ml). ELISA – Enzyme linked immunosorbent assay, DE – Definitive Endoderm, HE – Hepatic Endoderm, HLC – Hepatocyte-like cells, MG – Matrigel, LN – Laminin, ALB – Albumin, ng – nanogram, ml – milliliter

3.5 Analysis of CYP2D6 expression on transcriptome and protein level

The presence of CYP2D6 in derived HLCs was determined on transcript level by RT-qPCR, and on protein level by immunocytochemistry and Western blot.

For RT-qPCR, RNA was isolated from derived HLCs on the last day of differentiation, quality controlled, transcribed into cDNA and finally analyzed. The fold change in gene expression, normalized to the house keeping gene *RLP37A* and relative to gene expression in human PSCs, was calculated using the $\Delta\Delta C_t$ method in Microsoft Excel and visualized as bar graph with logarithmic y-axis.

Compared to pluripotent stem cells, *CYP2D6* expression was upregulated 2.5 (LN/L15M) to 7.9 fold (MG/L15) in S12_13B derived HLCs and 3.8 (LN/HepatoZYME) to 10.1 fold (LN/L15M) in UJiPS13 derived HLCs. Adult and fetal liver cells exhibited highest expression levels of the enzyme with 6645 resp. 60 fold change. *CYP2D6* expression was increased 8.6 fold in HepG2 cells (see Fig. 28).

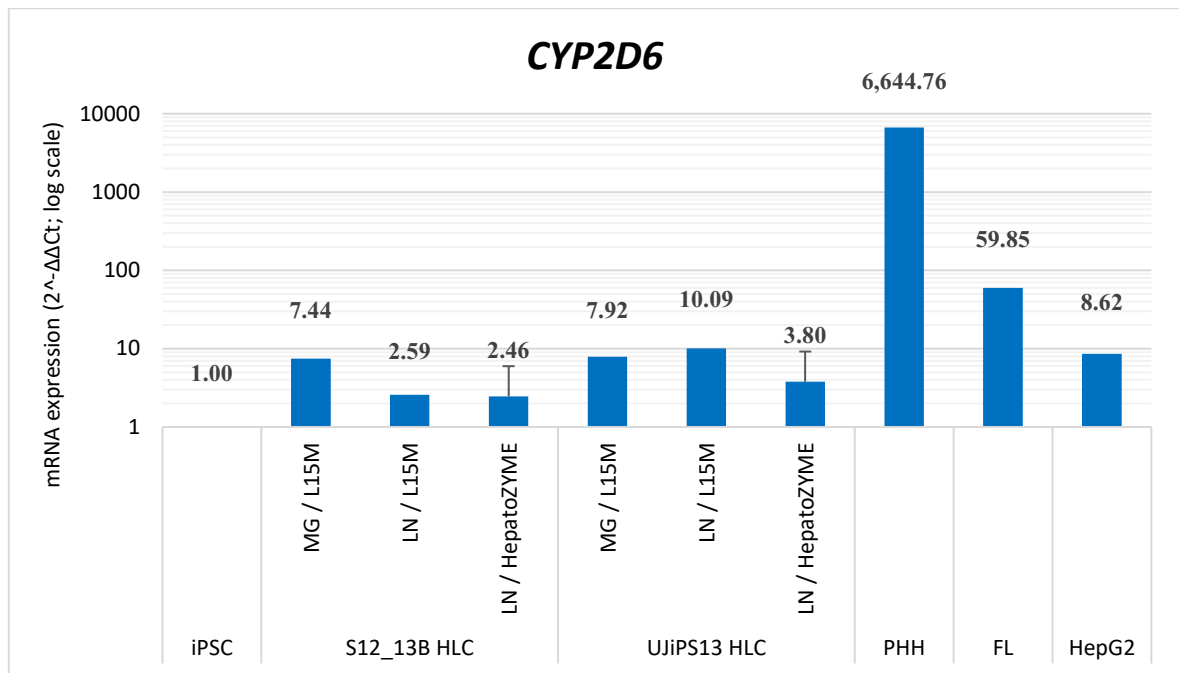


Fig. 28 – Expression of CYP2D6 transcripts in pluripotent stem cell derived HLCs at the end of the hepatic differentiation process and three biological positive controls (PHH, FL, HepG2). The fold change in gene expression, normalized to the house keeping gene RPL37a and relative to gene expression in human PSCs, was calculated using the $\Delta\Delta C_t$ method in Microsoft Excel and visualized as bar graph with logarithmic y-axis. MG – Matrigel, LN – Laminin, L15M – Leibovitz 15 Maturation Medium, PHH – Primary Human Hepatocytes, FL – Fetal Liver Cells, HLC – Hepatocyte-like cells

To determine CYP2D6 expression on a protein level, designated wells of derived HLCs and the biological positive control cell line HepG2 were fixated on the last day of differentiation. Cells were permeabilized and stained with CYP2D6-specific primary and AF488-conjugated secondary antibodies as described before and visualized using the fluorescence microscope. Nuclei were counterstained with Hoechst 33342.

Whereas the biological positive control indicated cytoplasmic localization of CYP2D6, staining of S12_13B derived HLCs using MG/L15M and LN/HepatoZYME and UJiPS13 derived HLCs using MG/L15M and LN/L15M resulted in membrane-associated fluorescence signaling. Overlays of immunostainings with counterstained nuclei indicated that stained structures enclosed one to two nuclei. UJiPS13 HLCs derived using LN/HepatoZYME did not show membrane associated but rather nuclear fluorescence signaling (see Fig. 29).

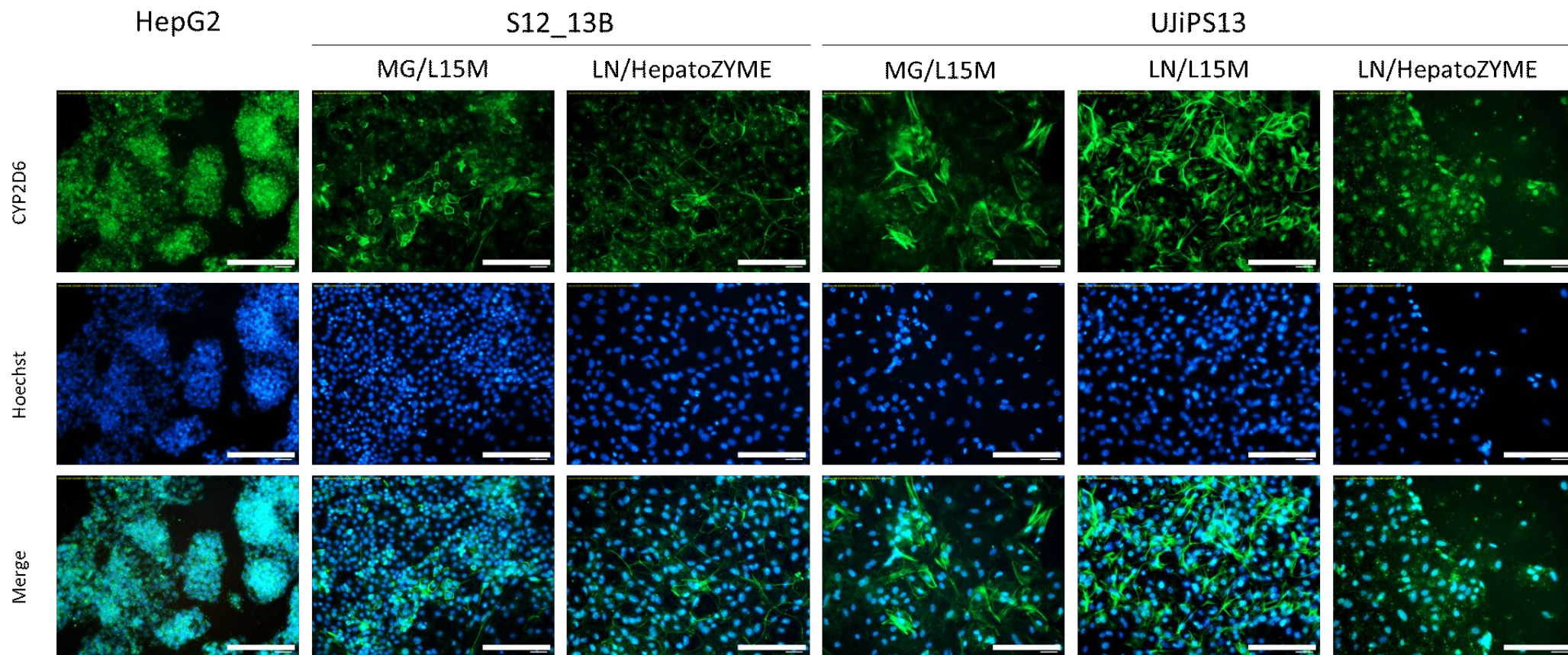


Fig. 29 – Immunocytochemical staining of derived hepatocyte-like cells and the biological positive control cell line HepG2. On the last day of hepatic differentiation, designated wells of derived HLCs and the biological positive control cell line HepG2 were fixated, permeabilized and stained with CYP2D6-specific primary and AF488-conjugated secondary antibodies. Nuclei were counterstained with Hoechst 33342. Whereas the biological positive control indicated cytoplasmic localization of CYP2D6, staining of S12_13B derived HLCs using MG/L15M and LN/HepatoZYME and UjiPS13 derived HLCs using MG/L15M and LN/L15M resulted in membrane-associated fluorescent signalling. UjiPS13 HLCs derived using LN/HepatoZYME did not show membrane associated but nuclear fluorescent signalling. Scale bar: 50 μ m. HLC – Hepatocyte-like cells, MG – Matrigel, LN – Laminin, L15M – Leibovitz 15 Maturation Medium, μ m - micrometer

Due to the unexpected membrane-associated signaling in immunocytochemistry, Western Blot analysis was utilized to confirm presence and appropriate molecular weight of CYP2D6 proteins in cell lysate of derived HLCs. β -Actin was used as loading control. Herefore, protein content of cell lysates was quantified by BCA assay, resolved on 10% SDS-PAGE, blotted onto a nitrocellulose membrane, stained with CYP2D6-/ β -Actin-specific antibodies and analyzed as described in the methods section (2.5.4.4. Membrane Transfer and Blotting).

Staining of the housekeeping protein and loading control β -Actin resulted in neat single bands at approximately 43 kDa for tested samples. Only band #10 (S12_13B HLC on MG/L15M) and #15 (S12_13B LN/HepatoZYME) exhibited a faint signal intensity. Western blot analysis for CYP2D6 revealed three separate bands in the region of its expected molecular weight (56 kDa) at approximately 65 kDa, 60 kDa and 56 kDa. Whereas HepG2 cells show a clear, strong band at 56 kDa and a second band at approximately 65 kDa, derived HLCs show a stronger signal at approximately 65 kDa, a weaker signal at approx. 60 kDa and faint to no visible signal at 56 kDa (see Fig. 30).

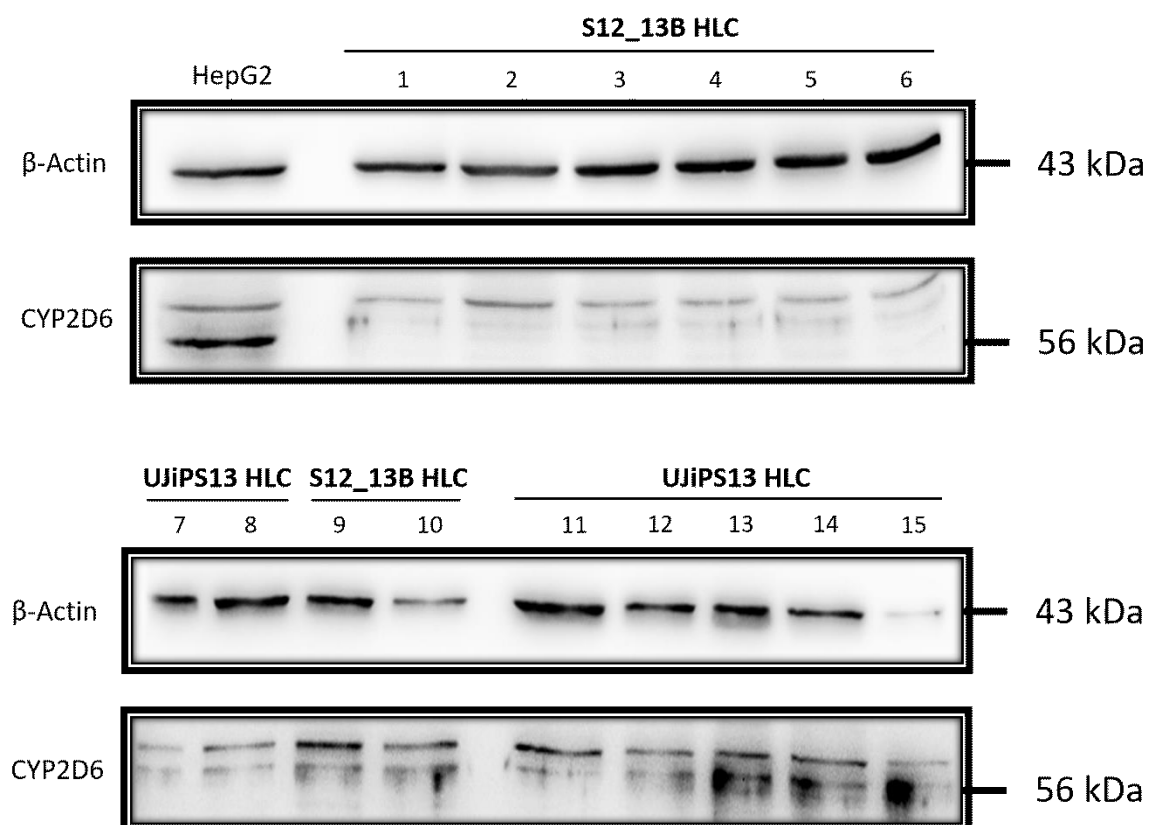


Fig. 30 – Photographs from nitrocellulose membranes of Western Blot analysis. 50 μ g of protein lysate from derived HLCs and the biological positive control HepG2 was resolved by 10% SDS-PAGE, blotted on nitrocellulose membranes and stained for CYP2D6 (rb, 1:800) resp. β -actin. UJiPS13 HLC: MG/L15M (#7-8), LN/L15M (#1), LN/HepatoZYME (#2-6); S12_13B HLC: MG/L15M (#9-10), LN/L15M (#13), LN/HepatoZYME (#11+12+14+15). HLC – Hepatocyte-like cells, MG – Matrigel, LN – Laminin, L15M – Leibovitz 15 Maturation Medium, rb – rabbit, kDa – kilo Dalton

Signal intensities of visualized bands from CYP2D6 were combined, quantified using Fusion FX and normalized to signal intensities of the loading control β -Actin. CYP2D6 / β -Actin ratios indicate the

highest expression of CYP2D6 in HepG2 cells (0.5391). Across all employed matrix-medium combinations, S12_13B derived HLCs indicate a higher expression compared to UJiPS13 derived HLCs on proteome level. However, due to varying sample availability from the different differentiation conditions, standard deviations could only be calculated from S12_13B LN/HepatoZYME and UJiPS13 LN/HepatoZYME (see Fig. 31).

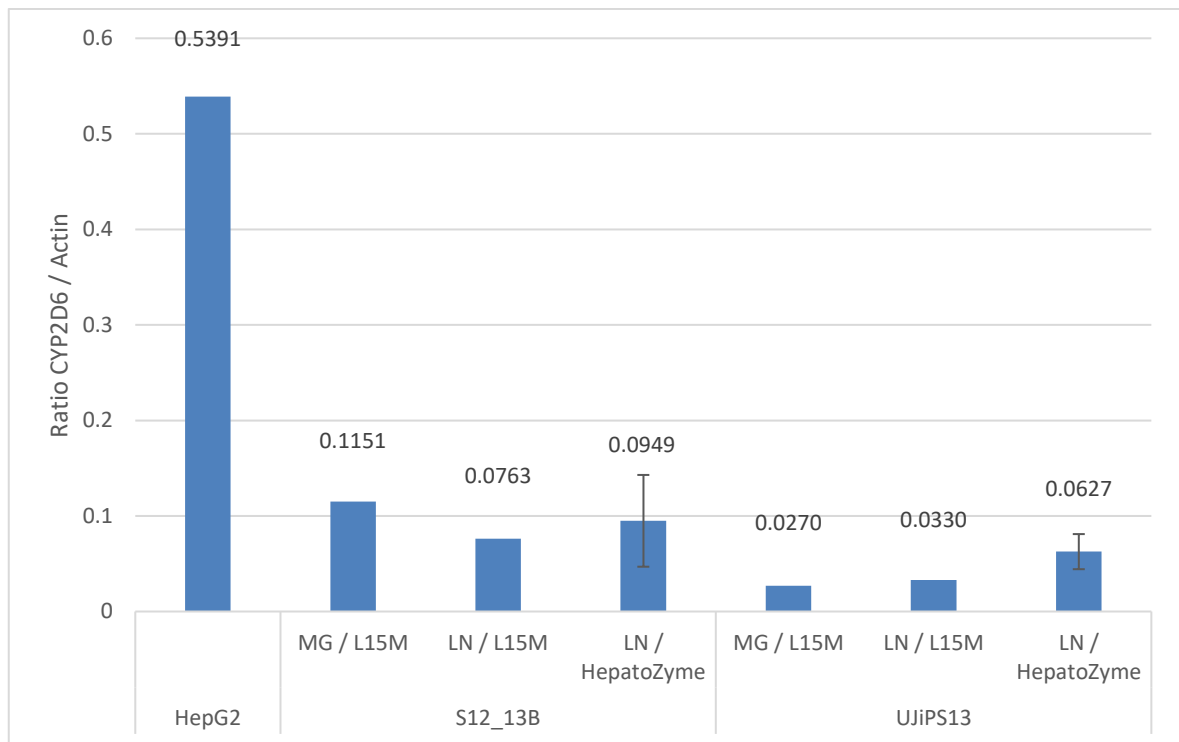


Fig. 31 – Ratios of CYP2D6/Actin expression of derived hepatocyte-like cells and HepG2 cells. 50 µg of protein lysate was resolved on 10% SDS-PAGE, blotted onto a nitrocellulose membrane, stained with CYP2D6-/β-Actin-specific antibodies. Resulting bands were visualized by Fusion FX and background corrected using the rolling ball technique. Mean signal intensities of 1 to 5 biological replicates were used to calculate expression ratios between CYP2D6 and the loading control β-actin. Where three or more replicates were available, standard deviations are displayed. Highest expression was visible in HepG2 cells. Independent from the employed matrix/medium combination S12_13B exhibited higher expression of CYP2D6 when compared to UJiPS13 derived HLCs. Statistical significance for differences in CYP2D6 expression between the differentiation conditions could not be obtained. HLC – Hepatocyte-like cells, SDS – sodium dodecyl sulphate, MG – Matrigel, LN – Laminin, L15M – Leibovitz 15 Maturation Medium, µg – microgram

To test for statistical significance of the observed difference between HLCs from S12_13B and UJiPS13 derived on LN/HepatoZYME, Mann-Whitney-U testing was applied. The Mann-Whitney-U test statistic (6) was greater than the critical value (0, for $n_1=5$, $n_2=3$). P-value was therefore greater than 0.05 and the difference seen between S12_13B and UJiPS13 HLCs derived on LN/HepatoZYME statistically not significant.

4 Discussion

4.1 Scope of this thesis in relation to current literature

Between 1950 and 2013, more than 450 pharmaceuticals had to be withdrawn from the market for the most common reasons being hepatotoxicity (18%), immune related reactions (17%) and cardiotoxicity (14%) (73). Minding that bringing a new drug candidate from bench to bedside and onto the market is a time and cost expensive procedure, spending an average of 12 years and US\$ 800 million to 12 billion (78), it is of tremendous economic and clinical importance to identify unsuitable new drug candidates as early during the drug development phase as possible.

The current strategy of drug discovery and development (DDD) involves the testing of new drug candidates for a validated drug target on safety and efficacy in *in-vitro* and *in-vivo* experiments. For *in-vitro* safety and efficacy testing, usually a high-throughput approach is utilized to screen a large library of compounds for target affinity and intrinsic activity. Identified lead compounds are tested in depth in *in-vivo* experiments typically lasting for several weeks to month before they may be applied to healthy human volunteers during a phase I clinical trial (163).

Despite major drawbacks such as limited availability and reproducibility of results as well as *in-vitro* metabolic instability, primary human hepatocytes are currently still the gold standard for whole cell-based *in-vitro* drug safety studies (164). Since the dawn of induced pluripotent stem cells, iPSC-derived hepatocyte like cells offer an alternative source for whole cell-based *in-vitro* assays. Human iPSC can be easily and reproducibly generated from various tissues and from individuals with different genetic backgrounds (105,117,153,154) and differentiated efficiently into cells with hepatocyte-like functionality (126–129,142), however, with a rather fetal than adult phenotype (143). To adequately address the question whether a new drug compound imposes a risk of hepatotoxic effects, drug metabolizing systems such as the enzyme superfamily Cytochrome P450 are of key importance. The highly polymorphic enzyme CYP2D6 alone is responsible for the metabolism of approximately 25% of currently applied pharmaceuticals including major drug classes such as β -blockers, opioids, antiarrhythmics and several anti-cancer drugs (42).

Induced pluripotent stem cell technology has been employed by one group before to generate PHH-derived HLCs accounting for various *CYP2D6* genotypes (84). Here, PHH of 12 donors were reprogrammed using non-integrating viral transfection (SeV), differentiated into HLCs and assessed for their individual donor specific drug metabolism capacity and responsiveness. In addition to being restricted to Sendai virus reprogrammed iPSC, Takayama et. al. did not employ defined materials for the hepatic differentiation process limiting their applicability in regulatory environments. In this work, I employed two iPSC lines derived in house from fibroblasts respectively urine cells carefully selected for their distinct *CYP2D6* genotypes and assessed their potential to differentiate into HLCs. Hepatic differentiation was performed using a semi (supplemented L15 Medium containing 8% FBS) and a fully defined hepatic differentiation medium (HepatoZYME™). The derived HLCs were

compared for their molecular and biochemical properties with special focus on the expression of CYP2D6.

4.2 Unharmonized CYP2D6 phenotype prediction may cause opposing dosage adjustment recommendations for similar CYP2D6 genotypes

Immediately prior to conducting the experimental part of this thesis, 4 µg of genomic DNA of the employed pluripotent stem cell lines was sent to CeGat GmbH, a DIN EN ISO 15189:2014 accredited diagnostics laboratory, for TaqMan™ PCR-based genotyping. This revealed a CYP2D6*1/*2 genotype correlating to an EM phenotype for S12_13B and a CYP2D6*4/*17 genotype correlating to an IM phenotype for UJiPS13 (see Table 8).

CYP2D6*1 represents the reference haplotype or wild type (WT) isoform of CYP2D6. First sequenced by Kimura et. al. in 1989, this allelic variant is associated with normal metabolic function and, therefore, constitutes to an extensive metabolizing (EM) phenotype (165). It has allele frequencies varying between 33-35.6 % in European, 36-40.4% in American Caucasians, 43.7% in Ghanaians and 28.8-34.7% in African American populations (166).

CYP2D6*2, formerly known as CYP2D6L (167), is characterized by carrying an intronic part of the CYP2D7 pseudogene in intron 1, and three single nucleotide polymorphisms (SNPs) – one in the 5' upstream regulatory region (-1584C>G) and two nonsynonymous changes (2850C>T; 4180G>C) leading to amino acid changes of the final protein (R296C (rs16947); S486T (rs1135840)) compared to the WT variant (168,169). Although showing higher expression than CYP2D6*1 in human liver tissue, *2 has a slightly reduced metabolic activity compared to *1. It, however, still contributes to an EM phenotype (59). CYP2D6*2 has allele frequencies of 22-32.4% in European and 25.2-33.7% in American Caucasians, 10.9% in Ghanaian and between 17.5-26.9% in African American populations (166).

CYP2D6*4 is the most common *null* allele in Caucasians with an allele frequency of 20-25% and contributing to 70-90% of all PMs. In other ethnicities, in contrast, CYP2D6*4 shows much lower allele frequencies of approximately 1% in Chinese (170) or 5-6% in various African and African American populations (71,171) explaining the low incidence of PMs in these populations (166). Defining for CYP2D6*4 is the SNP rs3892097 describing a 1846G>A resp. c.506-1G>A mutation of the first nucleotide of exon 4 that leads to an altered reading frame of the transcribed mRNA with a premature stop codon and an impaired protein synthesis (172,173).

CYP2D6*17 reflects a reduced functioning allelic variant of CYP2D6*2 carrying the previously described gene conversion in intron 1, the two nonsynonymous mutations 2850C>T (R296C) and 4180G>C (S486T) and an additional SNP, namely 1111C>T, resulting in the amino acid change T107I (rs28371706) (174,175). *17 is nearly absent in European Caucasians but has high frequencies

in African and Afro-American populations (59,175) such as 34% in Zimbabwean Shona population belonging to the Bantu (174) or 28% in Ghanaians (176).

Although substantial information about the genetic constitution and the corresponding physiological impact of individual CYP2D6 allele variants has been acquired until today, genotype to phenotype translation is not a trivial task. Currently available pharmacogenetic (PGx) testing and clinical practice guidelines are not harmonized and vary in their phenotype assignments. This yields in inconsistent therapeutic recommendations for physicians and confusion for affected patients. CeGat GmbH classified the phenotype affiliation according to the Clinical Pharmacogenetics Implementation Consortium (CPIC) and the Dutch Pharmacogenetics Working Group (DPWG) guidelines (see Table 8). Both consortiums are internationally renowned entities independently publishing international guidelines for pharmacogenetic impacts on currently approved pharmaceuticals.

Founded in 2009 as a shared project between the US-based PharmGKB and the Pharmacogenomics Research Network (PGRN), the rationale behind CPIC was to implement peer reviewed guidelines supporting the translation of laboratory testing results in the field of pharmacogenetics into actionable prescribing decisions for specific drugs (177). By now CPIC published more than 20 of these guidelines on dose adaptations for over 46 currently available pharmaceuticals including CYP2D6-metabolized major clinical drugs such as tramadol, oxycodone (178), tamoxifen (179), several SSRI (180) or ondansetron (181). DPWG, the European CPIC equivalent, was founded in 2005 by the Royal Dutch Association for the Advancement of Pharmacy. Primary goal of the DPWG was the development of pharmacogenetic-based dose adjustment recommendations for the Dutch healthcare system through systematic literature review and their immediate integration into the national computerized drug prescription system. The recommendations were implemented in October 2006 and allowed for an automated medication surveillance and an integrated approach to directly apply current knowledge about individual pharmacogenetic differences into clinical routine (182). Since its establishment until the present day, the CPWG conducted 90 risk assessments for gene-drug interactions resulting in 49 guidelines for therapeutics recommendations on aberrant pharmacological phenotypes (183). The DWPG guidelines are further the cornerstone of the Horizon 2020 funded clinical trial PREPARE led by Ubiquitous Pharmacogenomics (UPGx), a consortium with the major goal of implementing the DPWG guidelines as European pharmacogenetic standards for individual clinical prescription decisions (184,185).

Both consortiums, CPIC and DPWG, agree on using the ‘activity score’ (AS) introduced by Gaedigk et. al. (186) for genotype to phenotype translation. This system is based on the attribution of activity values ranging from 0 (no activity) to xN (multiplied activity) to specific allele variants of CYP2D6 (see Table 15).

Activity value	Most common allelic CYP2D6 variants
0	*3, *4, *4xN, *5, *6, *7, *16, *36, *40, *42, *56B
0.5	*9, *10, *17, *29, *41, *45, *46
1	*1, *2, *35, *43, *45xN
2	*1xN, *2xN, *35xN

Table 15 – Common CYP2D6 allele variants and their corresponding activity value

Activity values for both alleles of a single individual are added to obtain the activity score which is then used for phenotype attribution and dose adjustment recommendations. CPIC and DPWG, however, differ in genotype to phenotype translation by interpretation of the individual activity score (see Table 16). Both systems agree that an AS of 0 correlates with a PM phenotype. Whereas in CPIC guidelines IMs have an AS of 0.5, EMs of 1 – 2 and UMs of > 2, DPWG classifies AS of 0.5 – 1 as IMs, 1.5 – 2.5 as EMs and all AS > 2.5 as UMs. An activity score of 1 will be classified differently in both guidelines receiving an IM phenotype in DPWG guidelines (187) and a EM in CPIC guidelines (178). This leads to different dosage recommendation for the same individual depending on which guidelines are followed.

	PM	IM	EM	UM
CPIC	0	0.5	1-2	> 2
DPWG	0	0.5 – 1	1.5 – 2.5	> 2.5

Table 16 – Comparison of CPIC and DPWG genotype to phenotype attribution. In both systems an AS of 0 correlates with a PM phenotype. Whereas in CPIC guidelines IMs have an AS of 0.5, EMs of 1 – 2 and UMs of > 2, DPWG classify AS of 0.5 – 1 as IMs, AS of 1.5 – 2.5 as EMs and all AS > 2.5 as UMs. PM – poor metabolizer, IM – intermediate metabolizer, EM – extensive metabolizer, UM – ultrafast metabolizer, AS – activity score, CPIC – clinical pharmacogenetics implementation consortium, DPWG – Dutch pharmacogenetics working group

Exemplary, nortriptyline, a common tricyclic antidepressant, would be prescribed to the same patient with a 40% reduction of the starting dose when classified as IM according to the DPWG compared to the CPIC EM classification (188).

When designing a cell-based *in-vitro* testing system for the investigation of the impact of various CYP2D6 phenotypes on pharmacodynamics and pharmacokinetics of a drug respectively the patient's response, knowledge about the current genotype to phenotype translation is essential for an accurate interpretation of obtained results. Given the high occurrence of null alleles such as *3, *4 and *5 in African, American and European populations and the high occurrences of the *10 allele with reduced activity in Asian population, many patients may display an AS of 1 and will therefore be classified as either IM or EM (188). This has happened with several other tested cell lines during prework for this thesis (data not shown). Four cell lines of an industrial project partner of the ISRM received genotyping results with unclear phenotype affiliation (all *1/*4 or *2/*4; all activity score: 1). Until further harmonization of phenotype attribution between both consortiums occur, either clear IM (AS = 0.5), EM (AS = 1.5-2) and UM (AS > 2.5) phenotypes should be employed for the

development of an cell-based CYP2D6 testing system or one of the consortiums should be defined as the main target of the assay in development.

The cell lines used during course of this thesis, S12_13B (*1/*2, activity score: 2) and UJiPS13 (*4/*17, activity score 0.5), represent true EM (S12_13B) respectively IM (UJiPS13) phenotypes and may therefore be used to assess differences between EM and IM phenotypes. For future implementation of other cell lines and genotypes, regulatory discrepancies in genotype to phenotype translation must be kept in mind and properly accounted for.

4.3 Differentiation of hiPSC carrying different CYP2D6 genotype variants into HLCs

Hepatic differentiation of induced pluripotent stem cells into HLCs was performed employing a three-step protocol adapted from Wang et. al. (142) which mimics physiological hepatogenesis *in vitro*. In three independent differentiation experiments (HepDif#1 – HepDif#3), two iPS cell lines (S12_13B, UJiPS13) carrying distinct *CYP2D6* genotypes were differentiated using three different matrix – medium combinations (MG + L15M, LN + L15M, LN + HepatoZYME; see Table 14) and then assessed for their molecular and biochemical properties.

4.3.1 Definite Endoderm (DE) derivation

During the first step of differentiation, the undifferentiated pluripotent stem cells were directed towards definitive endoderm by changing the pluripotency supporting stem cell medium to DE Medium. The morphology of the cells in culture changed from tightly packed colonies of small, round cells with high nucleus to cytoplasm ratio and prominent nucleoli to larger cells capable of migrating out of the formerly tight colonies. These single cells exhibited higher cytoplasm to nucleus ratios and dendritic outgrowths. This change in cellular behavior and morphology could be explained by endothelial to mesenchymal transition (EMT), a process observed during gastrulation where epiblast cells start to round up and migrate into the primitive streak to form meso- or endodermal cells (see section 1.1.3.1. Embryonal Development (Organogenesis)). EMT is a process known to happen during definitive endoderm formation being, at least partly, regulated by Activin A-induced autocrine/paracrine TGF- β signaling (189).

At DE stage, hepatic differentiation of both pluripotent stem cell lines was assessed for the expression of DE stage marker SOX17 as well as HNF4 α , a key nuclear receptor during liver formation and adult liver homeostasis, AFP, expressed by visceral endoderm, and SOX2, a pluripotency and neural progenitor cells associated transcription factor. Derived DE cells should therefore be positive for SOX17 but largely negative for HNF4 α , whose expression is induced during hepatoblast formation (HE stage) (190), AFP and SOX2 (191). As expected, DE cells derived from both cell lines during

hepatic differentiation showed no fluorescence signaling for SOX2 in stage specific ICC staining indicating loss of pluripotency associated protein expression and derivation of a non-ectodermal cell type. Interestingly for this stage of hepatic differentiation, cells stained positive for HNF4 α but negative for SOX17.

For the positive outcome of the HNF4 α detection, unspecific staining of the antibody is an unlikely explanation as a generally sufficient blocking step with 10% NDS for 1h was integrated into the immunostaining method and the HNF4 α signaling was specific for the expected nuclear localization. The most likely reasons for the unexpected signaling are either spectral overlap from (over)excitation of the Hoechst33342 counterstain or a true specific staining of nuclear HNF4 α . Although exciting Hoechst33342 and AF488 at 488 nm using the same UV bulb, the employed fluorescence microscope has emission specific dichroic filters in place, making spectral overlap an unlikely reason for the staining signal. For HNF4 α itself, however, up to twelve isoforms (HNF4 α 1 – HNF4 α 12) have been described (192). The isoforms can be largely divided into two groups by the associated regulatory promotor regions P1 (e.g. HNF4 α 1 – α 3) or P2 (HNF4 α 7 – α 9) and are differentially expressed throughout various tissues and their development stages (193). During DE stage of hepatic differentiation of iPSC, P2 regulated expression of HNF4 α isoforms 7-9 containing the exon 1D (194) is upregulated whereas the isoforms containing exon 1A (HNF4 α 1 – α 3) associated with more mature hepatic gene expression are upregulated at HE stage. Exon 1D encodes an altered N-Terminal region of the translated protein from amino acid 1 to 38 (MRLSKTLVDMDMADYSAALDPAYTTLEFENVQVLTMGN \rightarrow MVSVNAPLGAPVESSY) (195), now containing a binding site for the promotor region of Lefty1. Lefty1 might play an important role during definite endoderm differentiation and is, among others, involved in upregulation of GATA4 and might further influence FOXA2 and SOX17 expression (196).

The actual epitope of the employed monoclonal antibody (Catalogue number: ab92378, Abcam) for HNF4 α is proprietary but lies within the first 100 amino acids of the protein (197). As 72% of their N-terminal region is homologous, this antibody might not be appropriate to distinguish between the various HNF4 α isoforms. A more suitable monoclonal antibody candidate represents the anti-HNF-4-alpha antibody K9218 (Catalogue number: ab41898, Abcam, or PP-K9218-00, R&D Systems) recognizing the HNF4 α -1A isoform sequence MADYSAALDPAYTTLEFENVQVLTMGNDTSPSEGTLNAPNSLGVSAL (aa 3-49). K9218 has already been successfully employed to distinguish between P1 and P2 isoforms in clinical samples of colorectal carcinomas (198) and AFP-positive lung cancer tissues (199).

Negativity for nuclear SOX17 at DE stage is unexpected as SOX17 is a key mediator of multipotency in definitive endoderm allowing further specification into hepatocytes or insulin-producing pancreatic β cells (200–202). Most likely reason for the absence of SOX17 in S12_13B derived DE in HepDif #2 is the usage of degraded AF647-tagged secondary antibody during the staining procedure. For this reason, during experiment HepDif#3 instead of a AF647- a Cy3-conjugated secondary antibody was employed. Again, SOX17 could not be detected. As the cells matured

appropriately throughout the differentiation process yielding in hepatocyte like cells with expected properties during both experiments, a technical issue of the immunostaining process seems the likeliest reason for non-detectability of SOX17. Other possible reasons include the decay of the employed primary antibody or decay of the protein itself for insufficient nuclear penetration of the employed fixative in this cell type.

4.3.2 Hepatic Endoderm (HE) derivation

Hepatic endoderm is then derived from DE stage by changing the cell culture medium to KO-DMEM medium supplemented with 20% KOSR, 1% NEAA, 1% DMSO, 1% P/S, 0.5% GlutaMAX and 0.1 mM 2-BME and culturing the derived DE cells in this medium for additional four days.

At HE stage, derived cells were checked for appropriate changes in morphology by brightfield microscopy and adequate differentiation by immunocytochemistry. The four days lasting culturing of definitive endodermal cells induced further morphological changes resulting in a typical, homogenous cell population with increasing numbers of binucleated cells. Due to detachment of derived cells during staining procedure, no utilizable staining could be obtained during HepDif #2 where cell line S12_13B was differentiated on a Laminin-mixture. During HepDif #3, UjIPS13 derived HE cells, again, started to detach from the cell culture ware, again, while performing the staining procedure. Although a sheet of cells was lost, sufficient numbers of UjIPS13 derived HE cells could be analyzed but only a fraction of HE cells indicated positive nuclear staining for HNF4 α and cytoplasmic staining for AFP. Both markers are early endodermal differentiation markers that are expected to be expressed at this stage. Derived cells, as expected, showed no signaling for SOX2 and SOX17. The employed procedure included a usually sufficient fixation step using a 20 min incubation with 4% PFA at RT on the seventh day of differentiation but analysis by ICC took place at the end of the differentiation process. To prevent cellular detachment during ICC staining in upcoming experiments, stage specific ICC should be performed on the day of fixation or within five days upon fixation.

4.3.3 HLC maturation

Derived HE cells may then be matured into hepatocyte-like cells by switching the cell culture medium to growth factor supplemented L15 maturation medium or growth factor supplemented, fully defined but proprietary HepatoZYME™ medium. On the last day of differentiation, derived HLCs were characterized by employing a battery of molecular and biochemical assays. Before initiating the characterization process, derived HLCs were assessed for their general morphology. HLCs adopted a polygonal flat shape characteristic of human hepatocytes with increasing numbers of binucleated cells. Comparing derived cells from S12_13B and UjIPS13, S12_13B HLCs indicated a recognizable increase of small lipid droplets in their cytoplasm. This is likely due to the source of

the fibroblast used as starting material for the episomal reprogramming process being a steatosis patient that underwent bariatric surgery (154). Induced pluripotent stem cells may retain an epigenetic memory from their parental cell line that influences lineage specific differentiation potential and characteristics of the derived cell line (203,204). As not only directly affected central organs display features of non-alcoholic liver disease (NAFLD) such as insulin resistance and impaired AKT/mTOR pathway signaling (155), fibroblasts obtained from patients with (low-grade) steatosis may harbor epigenetic imprinting that explains the observed increase in lipid droplet incorporation of S12_13B derived HLCs.

For all employed conditions and cell lines, a reduction in the pluripotency-associated biomarker OCT4 and an upregulation of hepatocyte-associated biomarker expression could be observed on transcriptome level. The derived cell types, however, indicated a rather fetal than mature hepatic phenotype. Compared to primary cell types (PHH and FL), ALB and CYP3A4 expression was lower in derived HLCs. AFP expression, however, was equal to fetal liver and the tumor cell line HepG2. Expression of HNF4 α was comparable in iPSC derived HLCs, PHH and FL cells.

Expression of hepatocyte associated genes was further assessed on protein level by immunocytochemistry for all differentiation runs and conditions and then confirmed by flow cytometry for S12_13B differentiated on LN mixture and HepatoZYME. Although all employed conditions yielded varying positivity for hepatocyte-associated biomarkers, for S12_13B, differentiation on LN111/521 mixture and HepatoZYME indicated comparable results for HNF4 α and E-Cadherin but stronger signaling for AFP and ALB expression when compared to differentiation on MG / L15M. Flow cytometric analysis supported the results for HNF4 α and AFP expression but indicated negativity for albumin and UGT1a expression.

Staining of HNF4 α and AFP resulted in appropriately distinguishable shifts in single median fluorescence intensity (MFI) signals of the stained sample against the unstained control. Cy3-tagged sample of UDP-glucuronosyltransferases (UGTs), an enzyme critically involved in glucuronidation of many endogenous (bilirubin, steroids) and exogenous (pharmaceuticals, environmental toxins) compounds, did not indicate a shift at all and is therefore considered expression negative. However, as the employed antibody for UGT1A1 has not been used for flow cytometry by this lab before and as the antibody is not optimized for this assay by the manufacturer, there are several points to consider before trusting the obtained results. These considerations include, among others, optimization of the fixation, permeabilization and staining procedures employing varying exposure times, incubation temperatures and buffer concentrations as well as finding optimal primary and secondary antibody concentrations. Unfortunately, the unstained control samples used for discrimination between expression positive and negative populations, yielded lower events during analysis than the stained samples making it difficult to set the appropriate position for the border between antigen-positive and -negative fluorescence intensity. For ALB expression, the stained samples indicate an increase in median fluorescence intensity which is not strong enough to cross border to what is counted as expression positive. Again, as flow cytometry is a complex technique with various variables that

need to be addressed to be able to properly trust obtained results and, secondly, is quite susceptible for subjective interpretation, further assay development is necessary to use flow cytometric analysis for HLC assessment.

For UJiPS13, strongest signaling for hepatocyte-associated gene expression was obtained by ICC when differentiated using LN111/521 and L15M medium. Employing LN111/521 and HepatoZYME which indicated to be a preferential option for hepatic differentiation of S12_13B, AFP expression was low and ALB expression could not be detected on protein level. This indicates that different pluripotent stem cell lines, although exhibiting equivalent morphology and expressing similar pluripotency markers, harbor intrinsic characteristics leading to varying efficiencies in directed differentiation capabilities. Observed differences may be explained by genetic imprinting of the primary tissue from which the iPSC lines were generated, the employed reprogramming technique, passage number (or more accurate: total amount of cell doublings) as well as the donor-specific genetic constitution. The sample for flow cytometric analysis of this HepDif experiment was sadly lost during the staining procedure. Flow cytometric data for UJiPS13 could therefore not be retrieved. Next to the expression of hepatocyte-associated biomarkers, the biochemical functionality of derived HLCs was assessed. Internalization and excretion of macromolecules was addressed by using the ICG uptake/release assay. Within 30 min upon application of indocyanine green to the cell culture medium, all derived cells independent of the employed differentiation condition exhibited green fluorescence, which was substantially, albeit not completely, lost within 24 hours. This indicates that derived HLCs are viable and metabolically active cells. PAS staining then illustrated derived cells' capability of producing macromolecules such as glycogen, a key molecule mainly produced by the liver for short- and intermediate-term energy storage. Urea production was assessed spectrophotometrically at 520 nm upon incubation with a chromogenic reagent that forms complexes with present urea molecules. For S12_13B-derived HLCs, urea could only be detected when differentiated on LN-mix and L15M medium whereas UJiPS13-derived HLCs were capable to secrete urea when differentiated on MG / L15M medium and LN / L15M. Despite the promising results from the ICC staining, S12_13B differentiated on LN / HepatoZYME surprisingly did not show measurable urea production. Measurable amounts of secreted albumin molecules could surprisingly only be detected in DE stage media where it is supposed to be absent. This finding was observed again after repeating the albumin ELISA a second time by a different operator on a different day indicating that the result is reproducible. As neither iPSC nor DE are usually capable of producing or even secreting albumin into the culture medium, accidental contamination of DE medium seems the likeliest reason for these unsuspected results. Activin A is usually dissolved in PBS (-/-) and a final concentration of 0.2% bovine serum albumin (BSA) acting as a stabilizing carrier protein. An accidental usage of HSA instead BSA could cause a specific binding reaction to present human albumin that has not been produced by the early differentiation cell cultures. As albumin ELISAs are time and cost intensive, media of several different experiments were combined onto one plate. The employed fresh DE, HE and HLC media samples used as negative control were

not the specific lot employed for the experiments but belonged to another experiment assessed simultaneously. As similar results have not appeared during other experiments performed using the batch of Activin A aliquots, a final explanation for the high ELISA signaling values in DE stage culture media remains unclear.

Biotransformation, another major feature of hepatocytes, was representatively assessed by a CYP3A4 activity assay. CYP3A4 expression was induced by adding 10 μ M of the antibiotic rifampicin to the cell culture medium 24 hours before assessment. After adding the pro-luciferin Luciferin-PFBE to the stimulated cells, Luciferin Detection Reagent induced luminescent signaling which could be measured employing a luminometer. S12_13B indicated highest enzyme activity when differentiated on LN with HepatoZYME as medium of choice. As expected, CYP3A4 activity was increased, in total by 72% compared to the untreated cells. Although CYP3A4 expression could be detected on transcriptome level by RT-qPCR, unexpectedly, no luminescence signaling was observed for UJiPS13 derived HLCs. Not unlike CYP2D6, also CYP3A4 exhibits great inter-individual differences in enzyme expression and activity (205,206). With more than 397 exonic variants of the CYP3A4 gene to be known, people can be divided into three groups of metabolizers (poor, normal or rapid metabolizers) (44). The reduced mRNA levels in RT-qPCR and not detectable CYP3A4 activity in the luminescence assay may therefore be explained by interindividual genetic variability. Reduced activity is much more common in Asian and African populations than European Caucasians (207) but whether this is an appropriate explanation for the encountered observations remains unclear and further experimental clarification is needed.

Overall, it can be stated that the derived cells from both cell lines after completing the hepatic differentiation protocol exhibit features of, rather fetal than adult, hepatocytes including expression of hepatocyte associated biomarkers on transcriptome and proteome level as well as biochemical properties such as production, uptake and release of macromolecules, capability of biotransformation, and urea production and secretion at varying degrees.

4.4 Differences in CYP2D6 expression of derived HLCs

HLCs derived from both pluripotent stem cell lines and various differentiation conditions were finally analyzed for the expression of CYP2D6. Two to three confluent wells of a 6-well plate were harvested at the last day of differentiation for RNA isolation. Isolated RNA was quality controlled, transcribed into cDNA and used for CYP2D6-specific RT-qPCR. One well of a 12-well plate was fixed with 4% PFA at the last day of differentiation, permeabilized and incubated with a CYP2D6-specific primary and subsequently with an AF488-conjugated secondary antibody. Nuclei were counterstained with DAPI and fluorescence signaling finally visualized using a fluorescence microscope. Another two to three confluent wells of a 6-well plate were used for isolation of the total

protein content of derived HLCs. Protein concentration was determined by BCA and 50 µg / sample used for Western Blot analysis.

4.4.1 Higher mRNA expression of CYP2D6 in HLCs derived from UJiPS13 compared to HLCs derived from S12_13B

On transcriptome level, *CYP2D6* expression varied between S12_13B and UJiPS13 and the employed differentiation conditions. S12_13B when differentiated on MG and L15M indicated a higher expression of *CYP2D6* (7.4-fold increase) than cells differentiated using LN-mix matrices with L15M or HepatoZYME (2.6- resp. 2.5-fold increase). For UJiPS13, differentiation on LN/L15M indicated highest *CYP2D6* expression (10.1-fold increase) followed by MG/L15M (7.9-fold increase) and LN/HepatoZYME (3.8-fold increase). Upregulation of *CYP2D6* expression in derived HLCs was in general, however, low. The particularly higher mRNA expression observed in UJiPS13 when compared to S12_13B derived HLCs are rather unexpected as various studies indicated a high correlation coefficient between *CYP2D6* transcript levels and enzyme activity (60,83,168) and the genetic constitution of this cell line (*CYP2D6**4/*17) is associated with decreased enzyme activity. Whereas Rodriguez-Antona et al. already reported liver samples exhibiting high mRNA levels with low enzyme activities (83), Temesvari et al. excluded the *CYP2D6**4 and other non-functional variants from their correlation model of mRNA level and dextromethorphan O-demethylase activity thereby increasing the correlation coefficient (r) from unstated lower values to 0.9130 (60). High mRNA expression combined with low enzyme activity, therefore, seems to be a known feature of PM-phenotype associated genetic variants of *CYP2D6*. Although this feature might be an appropriate reason for the observed higher mRNA transcript levels of UJiPS13-derived HLCs compared to S12_13B derived HLCs, it does not explain the up to five times lower expression of transcripts in HLCs derived of S12_13B. Even though sample sizes for all differentiation conditions are small (between 1-3 replicates per differentiation condition) and more repetitions are indicated to obtain statistical significance, the known heritage of S12_13B from a patient prone to the production of low-grade steatosis might offer an appropriate explanation for the experimental observations. Steatosis and NAFLD are associated with reduced *CYP2D6* mRNA and activity levels in hepatic microsomes (208) and S12_13B HLCs indicated an increased amount of lipid droplets incorporation into the cytoplasm of derived cells.

Independent from cell line and differentiation condition, derived HLCs exhibited lower *CYP2D6* expression on transcriptome level than the human primary cell lines (PHH and FL) and a more comparable one to the human carcinoma cell line HepG2. This indicates the need of further assay development to derive a functionally more mature hepatocyte-like phenotype.

4.4.2 Immunocytochemical staining of CYP2D6 resulted in unexpected, non-specific signaling

To confirm expression of CYP2D6 on protein level, immunostainings (ICC) were performed and resulted in extracellular resp. membrane-bound fluorescence signaling. Highlighted structures included one to two counterstained nucleus indicating staining of cell membranes of individual cells growing in tissue-like clusters. This is a rather unexpected result as CYP2D6 is known to be localized on the cytoplasmic side of the membrane of the endoplasmic reticulum and not at the cellular membrane. As a blocking step with 10% normal goat resp. donkey serum is included into the staining procedure and other contemporaneously produced intracellular staining did not indicate signaling by off-target localizations, the employed antibody for CYP2D6 detection was taken into consideration. The CYP2D6-specific antibody (Cat. No.: PA5-39598, ThermoFisher Scientific) is a polyclonal rabbit IgG antibody suspension with human CYP2D6 specificity but with unstated molecular antigen structures. According to the material data sheet (MDS) of the supplier, this product has been successfully employed for paraffin-embedded immunohistochemical staining of tissue slices and Western Blot analysis. It, however, has not been employed for immunocytochemical staining at the ISRM before. As information is sparse regarding its utility for ICC of PFA-fixed cells, it resembles the most likely reason for the unexpected signaling. Polyclonal antibodies are heterozygous mixtures of diverse monoclonal antibodies and derived from a hosts' immune response including antibodies from multiple plasma cells. In contrast to homogenous monoclonal antibody solutions, polyclonal antibody suspensions may react with different epitopes of the same antigen thereby increasing the likelihood of detecting the antigen of choice independent of sample preparation induced antigen masking but at cost of an increasing chance of non-specific binding reactions (209). As this antibody has not been optimized for ICC at the ISRM, usability of this product might be obtained by optimizing the staining procedure through, for example, optimization of primary and secondary antibody concentrations by antibody titration experiments, or by switching to a new antibody product with proven usability. A proper antibody candidate for immunofluorescence staining of CYP2D6 might be the monoclonal antibody clone JM44-23 which recognizes a stated epitope from amino acid position 300 to the C-terminus of human CYP2D6 (Catalogue Number: MA5-32735, ThermoFisher Scientific).

4.4.3 CYP2D6-specific Western Blot analysis of HLC derived whole cell lysates revealed two additional bands of higher molecular weight and reflected the predicted CYP2D6 phenotypes

As performed ICC staining did not achieve expected results, Western Blot analysis was performed to confirm CYP2D6 expression on protein level. Staining of neat single bands of β -actin, the loading control, at height of 43 kDa indicated appropriated protein expression, lysate preparation and blotting on nitrocellulose membrane blots after 10% SDS-PAGE. For CYP2D6, Western Blots analysis revealed three separate bands visible with various intensities at approximately 56, 60 and 65 kDa. Interestingly, in samples from HepG2 cells the band at the expected size of 56 kDa indicated strongest signaling whereas for derived HLCs from all lines and conditions showed strongest bands at approx. 65 kDa.

Detection of multiple bands can have multiple reasons ranging from technical issues of the Western Blot procedure to biological variations of the protein under investigation.

A typical technical reason for seeing multiple bands on a Western Blot is protein degradation. Here, the employed antibody binds to protein fragments of various sizes migrating further through the SDS matrix, the smaller the degraded protein fragment becomes. If the protein fragment still contains the specific epitope of the antibody, various bands become visible on the final blot. Degradation, however, would result in bands reflecting protein (fragments) of smaller sizes than the expected full-size protein. As the additional bands lie above the expected size of CYP2D6 (56 kDa) at 60-65 kDa, protein degradation is an unlikely reason for the observed results.

Another technical reason for obtaining multiple bands during Western Blot analysis is non-specific binding of the employed antibody. Non-specific binding is defined as every binding interaction between the employed antibody and any other structure than the specific target, the antibody was raised against, resulting in off target signaling. Non-specific binding may be caused by, amongst others, binding reactions of the antibody to the nitrocellulose membrane, antibody trapping by FcR receptors expressed on the surface of various cell types, homologous epitopes on other proteins than the protein that should be detected, or usage of inappropriate primary or secondary antibody concentrations (both too high or too low) for the amount of protein loaded onto the gel. During the Western Blot experiments of this thesis, non-specific binding to the nitrocellulose membrane was addressed by including a blocking step with 5% milk powder in TBS-T at RT for two hours. This concentration of blocking reagent and membrane exposure time should be sufficient to prevent non-specific binding reactions to the surface of the nitrocellulose membrane. Capture of antibodies by FcR comparable to other immunoassays such as flow cytometry or immunocytochemistry does not represent a common reason for non-specific binding in Western Blots if the protein lysate is separated by SDS-PAGE before blotting. During SDS-PAGE, a reducing agent, here β -mercaptoethanol, is added to the loading buffer to break down disulfide bonds that are necessary for proper protein folding. Detergents such as SDS then catalyze the unfolding of proteins by applying negative charges

to the amino acid side groups. The now linearized polypeptide chains can finally be separated purely by charge through applying an electric field to the probes. Negatively charged proteins run through a polymer of polyacrylamide towards the positive electrode (anode). As Fc-binding functions according to the lock-key principle, linearization of the FcR prevents interception of the applied CYP2D6 specific, and any other, antibodies during SDS-PAGE based Western Blots. Hanukoglu et al., however, described the occurrence of non-specific binding events for Cytochrome P450 ssc (today: CYP11A1) at 70-90 kDa during Western Blots resulting most likely from the addition of β -mercaptoethanol to the loading buffer (210). Further experiments are indicated to investigate whether utilization of alternative reducing agents such as 5-10 μ M dithiothreitol might result in the disappearance of the unexpected bands.

The employed antibody product could as well be a technical reason for the occurrence of unexpected bands as it is the same antibody product used for immunocytochemical staining of CYP2D6 (Cat. No.: PA5-39598, ThermoFisher Scientific). Being a polyclonal antibody product derived from clones of several plasma cells and, therefore, targeting several CYP2D6 associated epitopes, non-specific binding reactions to homologous amino acid sequences present in different molecules such as other CYP enzymes might, again, explain the occurrence of the additional bands. PA5-49598 has further not been used at the ISRM to detect CYP2D6 by Western Blot analysis before. The dilution of 1:800 used for the performed experiments lies within the suppliers' recommendation of a dilution between 1:500 to 1:1000 but the experimental layout for this recommendation is not specified in more detail than using an extract from 293 cells. It is unclear whether this antibody was optimized for detection of CYP2D6 in whole cell lysates, microsomal preparations, or recombinant protein products. Additional experiments are indicated to determine optimal protein preparation, blocking procedures, protein separation conditions and primary and secondary antibody concentrations for robust and appropriate CYP2D6 detection by Western Blot analysis.

Leaving the possibility of technical reason for the occurrence of the unexpected banding aside, the observed additional bands might also be valid signals with biological explanations as posttranslational modifications can alter the molecular weight of a protein under investigation. PTMs are defined as (non-)covalent changes introduced to a polypeptide after the translation process and may include non-covalent incorporation of co-factors (e.g. heme), association of subunits of polypeptides to form oligomeric proteins, cleavage of signal peptides, formation of disulfide bonds or covalent modifications of amino acid side chains (e.g. phosphorylation, glycosylation, methylation, ubiquitination) (211). Although having been considered to not undergo any posttranslational modifications for a long time and data on PTMs for CYP2D6 is sparse, He et al. identified 19 potential phosphorylation (10 Ser, 7 Thr, 2 Tyr residues), one possible glycosylation (Asn398) and one possible acetylation (Gly2) site using computational biology (43). In 2008, Redlich et al. identified for the first time that Ser135 is phosphorylated *in vivo* by mass spectrometry of titanium dioxide enriched phosphopeptides derived from microsomal fractions of surgical human liver samples (212). Sangar et al. postulated in 2009 that PKA-mediated phosphorylation of Ser135,

and to lesser extent Ser148 and Ser217, is critically involved in driving the bimodal targeting of CYP2D6 to endoplasmic reticulum and mitochondria. According to this study, the CYP2D6 polypeptide contains a 22 amino acid region functioning as membrane anchor for the ER membrane at the N-terminus which is followed by an adjacent 13 amino acid lasting, positively charged mitochondrial targeting signal (213). Being translated by membrane-free ribosomes in the cytosol, the hydrophobic NH₂-terminus of the CYP2D6 polypeptides mediates a translational hold signal once it emerges from the ribosome. It binds to signal recognition particles (SRPs) present in the cytosol. Translation is resumed once a complex is formed consisting of SRP, nascent polypeptide and the ER membrane bound SRP receptor. The SRP is released, the emerging CYP2D6 polypeptide translocated into the ER membrane and the remaining protein finally translated at the cytosolic side of the ER membrane. PKA-mediated phosphorylation of nascent CYP2D6 polypeptide chains at Ser135, and putatively Ser138 and Ser217, reduced SRP binding affinity towards and led to the translation of soluble CYP2D6 proteins into the cytosol. These cytosolic CYP2D6 are prime candidates for mitochondrial translocation mediated by heat shock proteins (Hsp) such as Hsp 70 and Hsp 90. The biological role of a present PKC consensus site within the CYP2D6 polypeptide at Tyr138 still remains to be determined (214). The three visible bands of performed Western Blots might therefore resemble different stages of the CYP2D6 protein from translation until reaching its final destinations in ER membrane or the mitochondrial inner membrane space or matrix. As CYP2D6, in contrast to for example CYP1A1, does not undergo endoproteolytic cleavage for mitochondrial translocation, the increased molecular weight observed may be explained by multiple phosphorylation at above mentioned PTM sites and/or not fully disrupted tertiary or quaternary protein structures.

Finally and although not statistically significant, observed higher expression of CYP2D6 protein in HLCs derived from S12_13B compared to HLCs derived from UJiPS13 independent of employed differentiation conditions reflects the expected result for the distinct geno- and phenotype of the employed parental cell line. S12_13B carrying the WT and an allele associated with normal metabolization capacity should indicate a higher expression profile on protein level than hepatic cells carrying a null allele associated with disruption of protein expression (*4) and a protein variant associated with reduced enzyme activity. To be able to obtain statistical significance more repetitions of performed experiment are indicated but this was beyond the scope of this thesis.

4.5 Comparison of employed matrix-media combinations for hepatic differentiation

To be able to compare the three employed matrix-media combinations (MG + L15M, LN-mix + L15M, LN-mix + HepatoZYME), for each cell line and differentiation condition a point system was applied to the respective results. If a matrix-medium combination supported derivation of HLCs displaying typical morphology, this combination received one point. For RT-qPCR, 0 points were annotated to conditions that indicated lowest increase or decrease in the direction of the gold standard PHH depending on the investigated biomarker. For ICC, not detectable staining results were annotated with 0 points, detectable staining with low abundance with 1 point and detectable staining with high abundance with 2 points. Capability of internalizing and secreting indocyanine green resulted in 1 point, detectable production of macromolecules such as glycogen again 1 point. CYP3A4 activity was rewarded with 2 points for highest detectable RLU measures, 1 point for the second best condition and 0 points to the condition with lowest or no detectable luminescence. For urea secretion, each mg/dl that could be detected in the medium, one point was assigned (0 – 0.99 mg/dl: 1 point, 1-1.99 mg/dl: 2 points, 2-2.99 mg/dl: 3 points, 3-3.99 mg/dl: 4). Due to the unexpected and biologically not explainable results, the ALB-specific ELISA was excluded from the comparison. CYP2D6-specific Western Blot was, again, included yielding in 2 points for conditions indicating highest detectable CYP2D6 yields, followed by one point for the second best condition and zero points for the condition indicated the lowest yield. All points per condition were added for each cell line and the sum of both cell line added thereafter (see Table 17).

Whereas all matrix and media combinations were capable of supporting typical HLC morphology at the end of hepatic differentiation, S12_13B derived HLCs showed most comparable *OCT4* mRNA expression levels to PHH when differentiated using LN/L15M and LN/HepatoZYME. As both conditions showed comparable expression patterns to PHH, both conditions received two points. For *AFP* expression, HLCs differentiated using MG / L15M indicated lowest expression in both cell lines. Low expression is assigned with two points when *ALB* can be detected as a low *AFP* to *ALB* ratio is associated with a more mature hepatocyte phenotype, and lower expression of this biomarker is desired in derived HLCs. *CYP3A4* transcripts are highest in HLCs differentiated on LN/L15M for both cell lines, followed by LN/HepatoZYME. MG/L15M indicated lowest *CYP3A4* expression on transcriptome level. However, compared to primary cells overall *CYP3A4* expression was low. *HNF4α* expression was high in all derived HLCs independent from cell line and differentiation conditions. Highest transcript detection was seen in HLCs derived on LN/L15M (UJiPS13) resp. LN/HepatoZYME (S12_13B).

In immunostainings, LN/L15M based hepatic differentiation of UJiPS13 indicated high expression for all biomarkers except CYP2D6 where no specific signaling could be detected. Whereas HNF4α and E-Cadherin were also visible on LN/HepatoZYME mediated differentiation, AFP expression was low and ALB could not be detected. S12_13B, in contrast, showed highest expression for hepatic

biomarkers in HLCs derived using LN/HepatoZYME. As ALB staining was not as abundant and bright compared to UJiPS13 HLCs differentiated using LN/L15M, here only one point was assigned. Sadly, due to loss of wells during the differentiation process, no immunostainings could be obtained for S12_13B derived HLCs differentiated using LN/L15M.

All cells were capable of internalizing and releasing indocyanine green, hence one point for each condition. PAS staining was only performed for samples differentiated on LN/L15M and LN/HepatoZYME. CYP3A4 activity was highest for S12_13B differentiated on LN/HepatoZYME followed by MG/L15M. Overall, no CYP3A4 activity could be measured for UJiPS13 derived HLCs independent of the employed differentiation condition.

Urea secretion into spent cell culture medium was detectable at highest concentrations in UJiPS13 derived HLCs using LN/HepatoZYME followed by MG/L15M. For S12_13B derived HLCs, urea secretion could only be detected when differentiated on LN/L15M. LN/HepatoZYME did not show to support urea secretion across both cell lines.

As CYP2D6-specific immunocytochemical staining indicated non-specific binding reactions, Western Blot analysis was performed. LN/HepatoZYME indicated highest yields of CYP2D6 polypeptides in UJiPS13 followed by LN/L15M. For S12_13B derived HLCs, CYP2D6 production was induced most when differentiated on MG/L15M followed by LN/HepatoZYME.

Overall, the present results indicate that the combination of LN111/LN521 and L15M best support hepatic differentiation of iPSC with a total sum of 36 points followed by LN/HepatoZYME (32 points) and MG/L15M (28 points) (see Table 17). Separated for the individual cell lines S12_13B and UJiPS13, however, LN/HepatoZYME reached the highest score for S12_13B derived HLCs (18 points) followed by MG/L15M (16 points) and LN/L15M (13 points). This is easily explained by the fact that the samples of S12_13B derived HLCs dedicated for ICC lifted off during the differentiation process leaving a total score of 10 points for ICC and up to 2 points for CYP3A4 activity vacant. Adding a mean score of 5.8 reached by all cell lines and conditions for immunocytochemical staining, LN/L15M would further consolidate its pole position of best supporting hepatic differentiation of pluripotent stem cells into HLCs. However, as several assays were performed with a limited amount of replicates further repetitions of performed experiments are indicated to obtain statistical significance.

Assay	Differentiation condition (S12_13B UJiPS13)		
	MG / L15M	LN / L15M	LN / HepatoZYME
Morphology	1 1	1 1	1 1
qRT-PCR	<i>OCT4</i>	0 0	2 0
	<i>AFP</i>	2 2	0 0
	<i>ALB</i>	1 0	2 1
	<i>CYP2D6</i>	2 1	1 2
	<i>CYP3A4</i>	1 0	2 2
	<i>HNF4α</i>	0 0	1 2
ICC	<i>AFP</i>	1 1	/ 2
	<i>ALB</i>	0 1	/ 2
	<i>E-Cad.</i>	2 0	/ 2
	<i>HNF4α</i>	2 2	/ 2
	<i>CYP2D6</i>	0 0	/ 0
ICG uptake/release	1 1	1 1	1 1
PAS staining	/ /	1 1	1 1
CYP3A4 activity	1 0	/ 0	2 0
Urea secretion	0 3	3 4	0 0
Western Blot (CYP2D6 production)	2 0	0 1	1 2
Sum per cell line	16 12	13 23	18 14
Sum in total	28	36	32

Table 17 – Comparison of employed matrix-media combinations for hepatic differentiation of induced pluripotent stem cells. Points were given for supporting proper morphology in derived HLCs (one point), degree of upregulation of hepatocyte- resp. downregulation of pluripotency-associated mRNA expression (two points for up-/downregulation nearest to PHH, one point for second nearest, 0 for third nearest). For ICC, not detectable staining results were annotated with 0 points, detectable staining with low abundance with 1 point and detectable staining with high abundance with 2 points. Capability of internalizing and secreting indocyanine green resulted in 1 point, detectable production of macromolecules such as glycogen again 1 point. CYP3A4 activity was rewarded with 2 points for highest detectable RLU measures, 1 point for the second best condition and 0 points to the condition with lowest or no detectable luminescence. For urea secretion, each mg/dl that could be detected in the medium, one point was assigned (0 – 0.99 mg/dl: 1 point, 1-1.99 mg/dl: 2 points, 2-2.99 mg/dl: 3 points, 3-3.99 mg/dl: 4). CYP2D6-specific Western Blot was assigned with 2 points for conditions indicating highest detectable CYP2D6 yields, followed by one point for the second best condition and zero points for the condition indicated the lowest yield. MG – Matrigel, LN – Laminin, qRT-PCR – quantitative real time polymerase chain reaction, AFP – alpha fetoprotein, ALB – albumin, ICC – immunocytochemistry, ICG – indocyanine green, PAS – periodic acid Schiff

4.6 Strengths, limitations and outlook of performed study

During the execution of the experiments of this study, the review of obtained results and the writing process of this thesis, several strength and limitations of this study became apparent which shall be discussed in this chapter. Further, analysis of the strength and limitations shall lay the foundation for an outlook and recommendations for further experiments that may support the development of a cell-based assay for CYP2D6-specific toxicity studies.

A major strength of this thesis is the usage of two carefully selected induced pluripotent stem cell lines. S12_13B, derived from human dermal fibroblasts of a low-grade steatosis patient, and UJiPS13, derived from urine cells of a 51 year old African male, were reprogrammed at the laboratories of the ISRM using non-integrating episomal vectors (117) harboring *OCT4*, *SOX2*, *NANOG*, *KLF4*, *c-MYC* and *LIN28*. Using non-integrative reprogramming based on episomal vectors, as employed during reprogramming of both cell lines, is preferential to integrative methods (i.e. retro-/lentivirus) as integration is associated with consecutive expression of reprogramming factors in hiPSC and derivatives, disruption of metabolically relevant genes, acquisition and accumulation of SNP and CNVs, dysregulation of genomic imprinting and karyotypic abnormalities (215). All of these may critically alter metabolic pathways and cellular behavior thereby negatively influence comparability of in PSC-derived cells and tissues to primary cells and tissues.

Both cell lines were reprogrammed and characterized by an established panel of molecular and biochemical assays by scientist having up to 13 years of experience in handling and assessing this relatively new and, at times, difficult to handle cell type. This combination of characterization tools and experience assures the production of state-of-the-art, fully reprogrammed induced pluripotent stem cell lines (153,154).

Another strength of this thesis is the employment of several completely defined media and matrices to support cell culture in pluripotent state (LN-521, StemMACS iPS Brew) or hepatic differentiation (LN111/-521 mixture, DE medium, HE medium, HepatoZYME). Usage of completely defined materials reduces the impact of batch-to-batch variations on differentiation efficiency and molecular and biochemical features of the derived cell type and increases comparability between experiments and validity of data.

Scientists of the ISRM, further, have distinct experience in endodermal and hepatic differentiation of pluripotent stem cell lines and characterization of derived hepatocyte-like cells (132,150,216). Being adapted from a protocol published by Wang et. al. (142), S12_13B and UJiPS13 were differentiated employing a hepatic differentiation protocol that has proven to support proper derivation of HLCs multiple times and across several laboratories before. Most assays for characterizing derived HLCs have also already been in place prior of starting the experiments of this thesis including hepatocyte specific RT-qPCR, ICC, ICG and PAS staining, detection of secreted urea and ALB in cell culture medium, CYP3A4 activity measurement and Western Blot analysis. Assessment of CYP2D6 could therefore be populated into a validated panel of existing assays.

A major limitation of this study is the usage of three different differentiation conditions (MG + L15M, LN-mix + L15M, LN-mix + HepatoZYME) with only a limited number of repetitions per cell line and differentiation condition. Whereas MG + L15M has only been used once during the first differentiation run (HepDif#1), LN-mix and L15M resp. LN-mix + HepatoZYME have been used twice in the second and third differentiation (HepDif#2 and #3). To obtain statistical significance, further repetitions employing identical differentiation conditions and both cell lines are necessary. As several wells per differentiation were lost to apoptosis and lifting off of cells, some assays such as RT-qPCR or Western Blot analysis could not be performed in triplicates for all conditions and cell lines as anticipated. Where triplicates for an experiment could be obtained, standard deviations were calculated and visualized with error bars in the diagrammatic representation of the results. Together with the rather fetal phenotype of derived HLC, this loss of cells throughout hepatic differentiation indicates the need of further process development work regarding the employed protocol.

One easily implementable improvement of the employed differentiation protocol is the depletion of aminoglycoside antibiotics such as streptomycin from every cell culture and differentiation medium. Aminoglycosides are clinically known for their severe oto- and nephrotoxic side effects mainly caused by inducing apoptosis through intracellular ROS production. Streptomycin and other aminoglycosides bind to intracellular Fe^{III} ions generating the redox reactive Fe^{II}-aminoglycoside complexes within the cytosol. These complexes bind to phosphoinositide inducing the release of the as electron donor acting arachidonic acid into the cytoplasm and catalyze the formation of reactive oxygen species (ROS) from molecular oxygen. Increasing levels of ROS trigger caspase-dependent and -independent apoptosis mechanisms (217). Although having no impact on cellular viability, proliferation capacity and expression of pluripotency markers in pluripotent stem cells, presence of aminoglycoside has indicated a significant negative impact on cell viability during neuronal and hepatic differentiation (218). As aminoglycosides interact with chaperon proteins such as HSP73 and calreticulin, which are important for proper protein folding and quality control of proteins within the ER (217,218), further impact of aminoglycosides on a broad range biochemical processes throughout hepatic differentiation may not be ruled out. Despite a higher chance of loosing experiments to contamination, addition of antibiotics such as 100 µg/ml penicillin-streptomycin should be completely excluded from differentiation protocols.

Although many assays for the molecular and biochemical assessment of derived HLCs have been implemented and are in routine usage, several methods could be improved. For ICG uptake and release assay, fluorescence signaling could be quantified and the number of fluorescence-positive cells counted using the computer program imageJ. As cells at HLC stage, however, are mostly not growing as single layers, it has proven difficult to focus on one specific layer where a representative amount of cells could be assessed contemporaneously. Further method development allowing a quantifiable discrimination of fluorescence positive and negative cells is strongly indicated and would significantly improve the validity of this method.

Regarding the CYP3A4 activity assay, method validity could be drastically improved by assessing the amount of viable cells within the employed well before starting measurement of the activity. Although a fixed number of cells are plated in each well at the beginning of a differentiation experiment, above mentioned recognizable incidence of apoptosis might interfere with signal intensity and result in underestimation of CYP3A4 activity of derived HLCs. Easily performable cell count and viability assays such as the CellTiter-Glo® 2.0 assay (Cat. No.: G9241, Promega) measure ATP levels per well under investigation by Luciferase-catalyzed production of oxyluciferin from luciferin in the presence of Mg^{2+} and molecular oxygen. The resulting luminescence (in RLU) is linear to the amount of cells within a cell culture well. Detection of the amount of viable cells within a cell culture well right before measuring CYP3A4 activity allows for the normalization of obtained activity levels and improves the validity of this method as well as comparability of data between different experimental conditions.

As flow cytometric analysis has not been used for the assessment of HLCs before the experiments conducted during this thesis, this method may need several rounds of method development. Cells for flow cytometry were singularized using TrypLE Select at 37°C/5% CO₂ for 5 min, counted using a Neubauer chamber, fixated with 2% PFA for 15 min, permeabilized with 0.5% Triton-X-100 in PBS (+/+) for 20 min and stained using primary and secondary antibodies and described in the Materials and Methods section (see 2.5.2. Flow cytometry). Using this fixation, permeabilization and staining conditions, employed primary and secondary antibody concentration should be optimized by an antibody titration experiment comparing several decreasing antibody concentrations to find a concentration with optimal staining indices ($[MFI \text{ pos.} - MFI \text{ neg.}]/(2x \text{ SD})$) for this experimental layout. Too high or too low antibody concentration will result in non-specific binding reactions or false negative results of the conducted experiments. Although antibody specificity of the primary and secondary antibodies, except UGT1A, has been addressed by using the same antibodies and antibody concentrations in ICC experiments conducted before flow cytometry, implementation of proper technical negative controls is important to account for false positive results. Using above mentioned staining panel, the proper technical negative control to address non-specific binding of the secondary antibody reflects a “no primary antibody” control where a sample of 2×10^5 cells is stained only with secondary antibodies. However, even with an extensively optimized flow cytometry assay, it must be kept in mind that analysis of flow cytometric data is highly subjective and must be reviewed carefully. Obtained flow cytometric data from HNF4 α -AF488 and ALB-PE double stained samples of S12_13B derived HLCs was assumed negative for ALB expression with only 2.35% of cell falling into the positive gate (see Fig. 22). However, a clear shift in median fluorescence intensity is visible in ALB-PE stained samples which is eventually not strong enough to fall into set positive gate. Discrimination between expression positive and negative populations is made on the unstained sample peaks in the histogram plots. Initially, the gate for expression positive cells was set at the right end of the individual peaks including 99.8% and 99.9% of the unstained cells into the negative gate resulting in 80.2% HNF α resp. 2.35% ALB expression positive cells upon

staining. 2.08% of the sample were double positive for HNF4 α and ALB expression. Slightly shifting the gates to still acceptable 99.1% (AF488) resp. 98% (PE) negative populations for the unstained samples increased the amount of positive cells in the HNF α -AF488 stained samples to 95.7% and ALB-PE to 30.5% expression positive cells. A shift in 0.7% resp. 1.9% of unstained samples into the positive gate was accompanied by a 15.5% resp. 28.15% increase in expression positive cells for HNF4 α resp. ALB (see Fig. 32).

As ALB expression of this sample has already been detected by ICC (see Fig. 17), expression negativity employing the initial gating strategy may be overruled upon reanalysis. The fact that flow cytometry has not been used at the ISRM to detect expression of hepatic differentiation markers, the initially negative results are more likely to be a technical artifact than true negativity. Low shifts in median fluorescence intensity may result from suboptimal staining conditions such as too low primary or secondary antibody concentrations or too short primary or secondary antibody incubation times. This example of the variability of flow cytometric data analysis indicates its intrinsic subjectivity and its need for careful review of data interpretation.

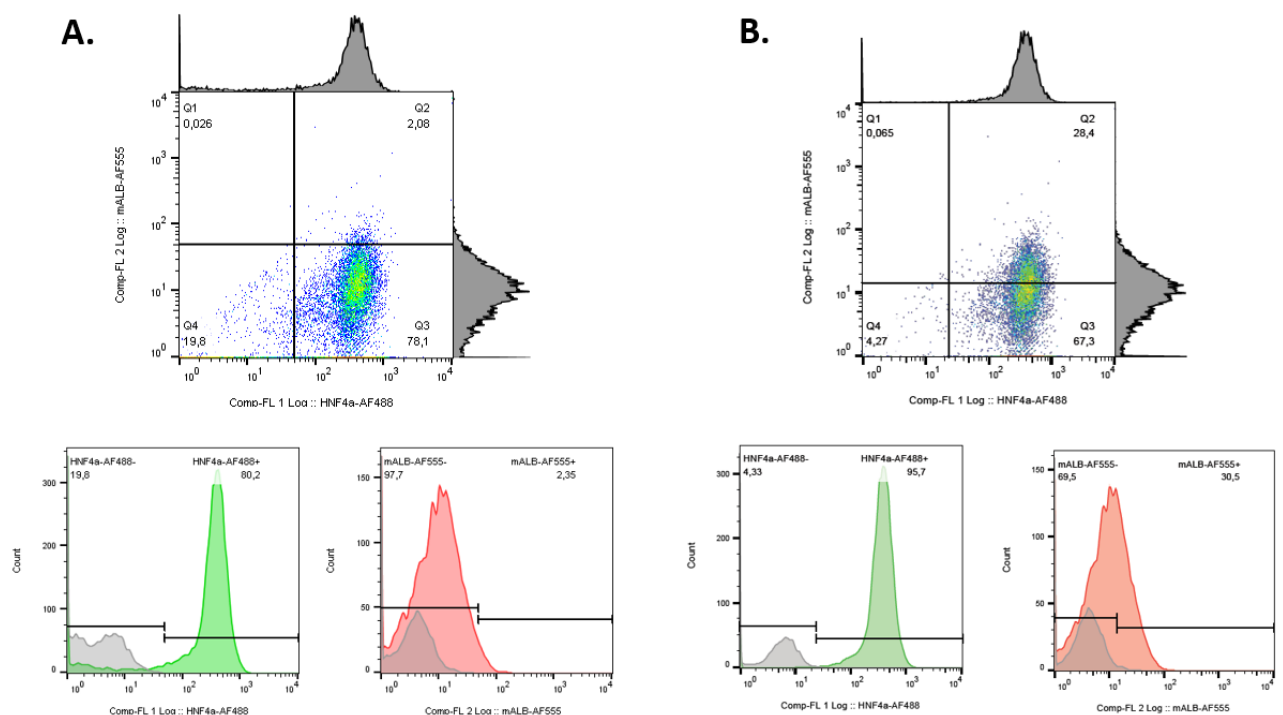


Fig. 32 – Comparison of different gating strategies for flow cytometric data from S12_13B double stained for HNF4 α and ALB. **A.** Gating strategy used for data displayed in results section (see Fig. 22). Gating was set to include all cells but cellular debris as well as 99.8% of the unstained peak into the negative population for AF488, and 99.9% of the unstained peak into the negative population for PE. Upon staining of cells with HNF4 α - and ALB-specific primary and AF488-/PE-labelled secondary antibodies, 80.2% of the cells were positive for HNF4 α and 2.35% positive for ALB. Compensation was applied using single stained samples of the same sample preparation. **B.** Alternative gating strategy. Experimental conditions and compensation remained unaltered. Gating was set to include only the expected HLC population as well as 99.1% of the unstained peak into the negative population for AF488, and 98% of the unstained peak into the negative population for PE. Upon staining of cells with HNF4 α - and ALB-specific primary and AF488-/PE-labelled secondary antibodies, 95.7% of the cells were positive for HNF4 α and 30.5% positive for ALB. Compensation was applied using single stained samples of the same sample preparation. AFP – alpha fetoprotein, ALB – albumin, HLC – Hepatocyte-like cells, FS – front scatter, SS – side scatter

One major limitation of CYP2D6-specific analysis of derived HLCs was the employment of the polyclonal primary antibody PA5-39598 for immunocytochemistry and Western Blot analysis. As almost no information is available about any molecular target structures and antigen specificity, it is unclear whether this antibody suspension is utilizable for immunocytochemistry or whole cell protein preparation based Western Blot analysis. Cross reactivity of single clones within this antibody suspension with more preserved epitopes shared with other enzymes of the CYP2 superfamily might interfere with CYP2D6 specific detection during aforementioned assays and decrease validity of data. In future experiments regarding the expression of CYP2D6, a monoclonal antibody with known and specified epitopes as well as proven versatility for ICC and Western Blot analysis should be employed. Nevertheless, Western Blot analysis performed employing PA5-39598 reflected expected reduction in CYP2D6 expression on protein level from UJiPS13 based on the cell lines' IM associated phenotype.

The performed experiments throughout this study brought insights into the expression of CYP2D6 in pluripotent stem cell derived hepatocyte-like cells carrying different genotype variants associated with normal and reduced enzyme activities in human hepatocytes. In order to get a more accurate model of human *in-vivo* liver tissue, future differentiation experiments should be executed in order to obtain an *in-vitro* model more comparable to human liver histology. Currently employed two dimensional differentiation of pluripotent stem cells into tissue specific derivatives mostly neglects the three dimensional nature of organogenesis *in vivo*. The human liver does not form in single layer sheets consisting of a single cell type but depends on orientation specific signaling and decreasing resp. increasing paracrine signaling concentrations from adjacent heart, lung, pancreas and other tissues. Co-culture of pluripotent stem cells or PSC-derived lineage specific multipotent progenitor cells such as hepatoblast with Ito-, stellate, Kupffer and/or endothelial cells in a three dimensional scaffold more accurately reflecting the liver's physiological lobule system should be the ultimate goal of hepatic *in-vitro* models. This might also lead to the derivation of a more mature PSC derived hepatic cell type.

Beyond the scope of this project, however, very important for developing a CYP2D6 specific cell based assay is the measurement of CYP2D6 activity in derived HLCs. One possibility to assess CYP2D6 activity *in vitro* is to assess the metabolism of the estrogen receptor inhibitor prodrug tamoxifen into its active metabolite endoxifen. Tamoxifen is metabolized via two pathways, 4-hydroxytamoxifen and N-desmethyltamoxifen to its predominant active metabolite endoxifen. Approximately 92% of tamoxifen is metabolized by CYP3A4 and CYP3A5 to N-desmethyltamoxifen and then finally hydroxylated by CYP2D6 to endoxifen. One possibility to measure CYP2D6 activity could be to assess the capacity of HLCs derived from different CYP2D6 variants to metabolize tamoxifen to endoxifen. Therefore, at the last day of hepatic differentiation, a 12-well of derived HLCs could be incubated with a specific amount of tamoxifen. Endoxifen production might then be determined by high-performance liquid chromatography (HPLC) as described by Jin et al. (219). However, roughly 7% of tamoxifen is metabolized to 4-

hydroxytamoxifen which can be converted to endoxifen as well but by CYP3A4. For CYP3A4 being involved in metabolite levels in supernatant as well, detection of endoxifen concentrations will always be erroneous and not completely representative for CYP2D6 activity.

Alternatively, two commercial kits (Catalogue Number: K703-200, Biovision resp. V8891, Promega) are available to assess CYP2D6 activity not from cell based assays but from microsomal fractions or HLC lysate by generation of fluorescence resp. luminescence upon metabolization of CYP2D6 specific substrates. This testing system might offer an easy to use assay for the detection of CYP2D6 activity from whole cell protein lysates, however, as the CYP2D6 specific non-fluorescent substrate is proprietary, it is not clear whether other CYP enzymes present in HLCs might interfere with the metabolization of this molecule and therefore generation of fluorescence throughout the testing procedure. Irrespective of the employed method for the measurement of CYP2D6 activity, possible interference of other CYP enzymes must be kept in mind and accounted for.

5 Conclusion

To adequately address hepatotoxicity of existing pharmaceuticals as well as new drug candidates in early drug development, a cost effective, readily available cell-based testing system exhibiting low batch-to-batch variation and accounting for individual pharmacogenomic properties would imply a major advantage to the current gold standard of patient-pooled primary human hepatocytes (PHH). Primary goal of this thesis was to initiate and support the development of a cell-based drug toxicity testing kit for pharmaceuticals metabolized by CYP2D6, one of the major drug metabolizing enzymes of the human body. To achieve this, five objectives were addressed in the scope of this thesis.

First, two induced pluripotent stem cell lines were selected based on their distinct CYP2D6 genotype variant. S12_13B (CYP2D6*1/*2) and UJiPS13 (CYP*4/*17) are ideal candidates for the development of a CYP2D6-specific cell-based assay as both cell lines represent true EM- resp. IM-associated genotypes.

Secondly, both cell lines were differentiated into hepatocyte-like cells employing three matrix-medium combinations to compare the ISRM's standard hepatic differentiation system with regulatory more suitable completely xenofree materials. At the end of the differentiation conditions, derived HLCs showed typical morphology of HLCs derived at the ISRM. S12_13B, derived from fibroblasts of a patient suffering from low-grade steatosis, showed a recognizable amount of small lipid droplets within their cytoplasm at HLCs stage.

Thirdly, hepatocyte-like cells from all iPSC lines and differentiation conditions exhibited downregulation of the pluripotency associated biomarker OCT4 as well as an increase in hepatocyte-associated gene expression on transcriptome and protein level. The high AFP to ALB ratio and low biotransformation capacity indicated a rather fetal than mature phenotype of derived HLCs, a common phenomenon employing current differentiation protocols. Despite their rather fetal phenotype, these cells indicated typical metabolic functionality of human hepatocytes such as uptake and release of macromolecules, glycogen storage, induction of biotransformation capacity by typical inducers such as rifampicin for CYP3A4 and urea secretion.

Special focus was laid on investigation of expression of the important drug metabolizing enzyme CYP2D6. CYP2D6 was upregulated upon differentiation but further method development and more repetitions of the experiments needs to be performed to obtain statistical significance.

Comparing employed matrix and medium combinations indicated that hepatic differentiation was best supported by employing the LN111/LN521 mixture (3:1) in combination with L15M medium. The completely defined matrix/medium combination LN-mix/HepatoZYME did not support induction of CYP3A4 activity nor urea secretion during the experiments performed throughout the course of this thesis. Further development of the differentiation method is indicated to obtain a more mature hepatocyte-like phenotype and increase induction efficiency of typical metabolic functionality.

This exciting work provides insight into the expression pattern of the important phase I biotransformation enzyme CYP2D6 and lays the foundation for the development of a CYP2D6 specific cell-based toxicity testing system derived from induced pluripotent stem cells. Using iPSC technology, limitations of the current gold standard PHH such as batch-to-batch variability and neglecting individual pharmacogenomic impact on new drug candidates may be overcome.

6 References

1. Karlstadt RG, Hogan DL, Foxx-Orenstein A. Normal Physiology of the Gastrointestinal Tract and Gender Differences. In: Principles of Gender-Specific Medicine. 1st ed. San Diego: Academic Press; 2004. p. 377–96.
2. Kirch J, May CA, Lorke D, Winkelmann A, Schwab W, Herrmann G, et al. Hepatobiliäres System und Pancreas. In: Taschenlehrbuch Anatomie. 1st ed. Thieme; 2011. p. 388–410.
3. Abdel-Misih SRZ, Bloomston M, Bismuth H. Liver Anatomy. Surg Clin North Am. 2010;90(4):643–53.
4. Eipel C, Abshagen K, Vollmar B. Regulation of hepatic blood flow: the hepatic arterial buffer response revisited. World J Gastroenterol. 2010 Dec 28;16(48):6046–57.
5. Lodge PA. Liver. In: Gray's anatomy: the anatomical basis of clinical practice. 41st ed. London: Elsevier; 2016. p. 1160–72.
6. Couinaud C. Le foie: études anatomiques et chirurgicales. Masson. 1957;
7. Lüllmann-Rauch R. Anhangsdrüsen des Verdauungssystems. In: Taschenlehrbuch Histologie. 4th ed. Stuttgart: Thieme; 2012. p. 413–28.
8. Adams DH, Eksteen B. Aberrant homing of mucosal T cells and extra-intestinal manifestations of inflammatory bowel disease. Nat Rev Immunol. 2006 Mar;6(3):244–51.
9. Saxena R, Theise ND, Crawford JM. Microanatomy of the human liver - Exploring the hidden interfaces. Hepatology. 1999;30(6):1339–46.
10. Francis K, Henry GJ. XXIX. The anatomy and physiology of the liver. Philos Trans R Soc London. 1833 Jan 1;123:711–70.
11. Mall FP. A study of the structural unit of the liver. Am J Anat. 1906 Jul 25;5(3):227–308.
12. Rappaport AM, Borowy ZJ, Loughheed WM, Lotto WN. Subdivision of hexagonal liver lobules into a structural and functional unit; role in hepatic physiology and pathology. Anat Rec. 1954 May;119(1):11–33.
13. Fu X, Sluka JP, Clendenon SG, Dunn KW, Wang Z, Klaunig JE, et al. Modeling of xenobiotic transport and metabolism in virtual hepatic lobule models. PLoS One. 2018 Sep 1;13(9):e0198060.
14. Sadler TW. Einführung - Kurze Geschichte der Embryologie. In: Taschenlehrbuch Embryologie. 12th ed. Stuttgart: Thieme; 2014. p. 14–6.
15. Sadler TW. 1. Woche - von der Ovulation bis zur Implantation. In: Taschenlehrbuch Embryologie. 12th ed. Stuttgart: Thieme; 2014. p. 58–78.
16. Genbacev OD, Prakobphol A, Foulk RA, Krtolica AR, Ilic D, Singer MS, et al. Trophoblast L-Selectin – Mediated Adhesion at the Maternal-Fetal Interface. Science (80-). 2003;299(JANUARY):405–8.
17. Sadler TW. Zweischichtige Keimscheibe (2. Woche). In: Taschenlehrbuch Embryologie. 12th ed. Stuttgart: Thieme; 2014. p. 79–90.
18. Sadler TW. Dreiblättrige Keimscheibe (3. Woche). In: Taschenlehrbuch Embryologie. 12th ed. Stuttgart: Thieme; 2014. p. 91–104.

19. Arnold SJ, Robertson EJ. Making a commitment: cell lineage allocation and axis patterning in the early mouse embryo. 2009;10(FEBRUARY):91–103.
20. Shen MM. Nodal signaling : developmental roles and regulation. *Development*. 2007;1034:1023–34.
21. Zorn AM, Wells JM. Molecular Basis of Vertebrate Endoderm Development. *Int Rev Cytol*. 2007 Jan 1;259:49–111.
22. Sadler TW. Embryonalperiode (3.-8. Woche). In: *Taschenlehrbuch Embryologie*. 12th ed. Stuttgart: Thieme; 2014. p. 105–36.
23. Sadler TW. Leber- und Gallenblase. In: *Taschenlehrbuch Embryologie*. 12th ed. Stuttgart: Thieme; 2014. p. 312–5.
24. Gouon-Evans V, Boussemaert L, Gadue P, Nierhoff D, Koehler CI, Kubo A, et al. BMP-4 is required for hepatic specification of mouse embryonic stem cell–derived definitive endoderm. *Nat Biotechnol*. 2006;24(11):1402–11.
25. Zorn AM. Liver Development [Internet]. *Stembook*. Harvard Stem Cell Institute; 2008 [cited 2020 Mar 22]. Available from: <https://www.stembook.org/node/512#R137%0D>
26. Giancotti A, Monti M, Nevi L, Safarikia S, D’Ambrosio V, Brunelli R, et al. Functions and the Emerging Role of the Foetal Liver into Regenerative Medicine. *Cells*. 2019 Aug 16;8(8):914.
27. Kamiya A, Kinoshita T, Miyajima A. Oncostatin M and hepatocyte growth factor induce hepatic maturation via distinct signaling pathways. *FEBS Lett*. 2001;492(1–2):90–4.
28. Taga T. gp130 and the interleukin-6 family of cytokines. *Annu Rev Immunol*. 1997;15:797–819.
29. Imamura M, Kojima T, Lan M, Son S, Murata M, Osanai M, et al. Oncostatin M induces upregulation of claudin-2 in rodent hepatocytes coinciding with changes in morphology and function of tight junctions. *Exp Cell Res*. 2007;313(9):1951–62.
30. Michalopoulos GK, Bowen WC, Mule K, Luo J. HGF-, EGF-, and dexamethasone-induced gene expression patterns during formation of tissue in hepatic organoid cultures. *Gene Expr*. 2003;11(2):55–75.
31. Aumüller G, Aust G, Doll A, Engele J, Kirsch J, Mense S, et al. Entwicklung des hepatobiliären Systems. In: *Anatomie (Duale Reihe)*. 2nd ed. Thieme; 2010. p. 668–9.
32. Lauth W. Overview. In: *Hepatic Circulation: Physiology and Pathophysiology*. San Rafael (CA): Morgan & Claypool Life Sciences; 2009.
33. Rassow J, Hauser K, Netzker R, Deutzmann R. Biochemie der Leber. In: *Biochemie (Duale Reihe)*. 3rd ed. Thieme; 2012. p. 745–9.
34. Julien E, El Omar R, Taviani M. Origin of the hematopoietic system in the human embryo. *FEBS Lett*. 2016;590(22):3987–4001.
35. Kost J, Goldbard R. Natural and Modified Polysaccharides. In: *Handbook of Biodegradable Polymers*. 1998. p. 275.
36. Food and Agricultural Organization of the United Nations. Chapter 3: Calculation of the Energy Content of Foods - Energy Conversion Factors. In: *Food energy - methods of analysis and conversion factors*. Rome; 2003.

37. Engelgau MM, Narayan KM, Herman WH. Screening for type 2 diabetes. *Diabetes Care*. 2000 Oct 1;23(10):1563–80.
38. Rassow J, Hauser K, Netzker R, Deutzmann R. Der Harnstoffzyklus. In: *Biochemie (Duale Reihe)*. 3rd ed. Stuttgart: Thieme; 2012. p. 139–43.
39. Batshaw ML. Hyperammonemia. *Curr Probl Pediatr*. 1984 Nov 1;14(11):6–69.
40. Merlot AM, Kalinowski DS, Richardson DR. Unraveling the mysteries of serum albumin—more than just a serum protein. Vol. 5, *Frontiers in Physiology*. 2014. p. 299.
41. Rassow J, Hauser K, Netzker R, Deutzmann R. Die Proteine des Blutserums. In: *Biochemie (Duale Reihe)*. 3rd ed. Stuttgart: Thieme; 2012. p. 744.
42. Nishimura M, Yaguti H, Yoshitsugu H, Naito S, Satoh T. Tissue distribution of mRNA expression of human cytochrome P450 isoforms assessed by high-sensitivity real-time reverse transcription PCR. *Yakugaku Zasshi*. 2003;123(5):369–75.
43. He ZX, Chen XW, Zhou ZW, Zhou SF. Impact of physiological, pathological and environmental factors on the expression and activity of human cytochrome P450 2D6 and implications in precision medicine. *Drug Metab Rev*. 2015;47(4):470–519.
44. Zanger UM, Schwab M. Cytochrome P450 enzymes in drug metabolism: Regulation of gene expression, enzyme activities, and impact of genetic variation. *Pharmacol Ther*. 2013;138(1):103–41.
45. Seviour DK, Pelkonen O, Ahokas JT. Hepatocytes: The powerhouse of biotransformation. *Int J Biochem Cell Biol*. 2012;44(2):257–61.
46. Rassow J, Hauser K, Netzker R, Deutzmann R. Entgiftung. In: *Biochemie (Duale Reihe)*. 3rd ed. Stuttgart: Thieme; 2012. p. 718–24.
47. Nebert DW, Wikvall K, Miller WL. Human cytochromes P450 in health and disease. *Philos Trans R Soc B Biol Sci*. 2013;368(1612):1–21.
48. Zhou S. Members of the CYP Superfamily: Family, subfamily, Clan, and Motif. In: *Cytochrome P450 2D6 (Structure, Function, Regulation and Polymorphism)*. 1st ed. CRC Press (Taylor & Francis Group); 2016. p. 3–15.
49. Gonzalez JF, Gelboin VH. Human cytochromes P450: evolution and cDNA-directed expression. *Environ Health Perspect*. 1992;98:81–5.
50. Omura Tsuneo, Sato R. The Carbon Monoxide-binding Pigment of Liver Microsomes. *J Biol Chem*. 1964;239(7):2370–8.
51. Gopisankar MG. CYP2D6 pharmacogenomics. *Egypt J Med Hum Genet*. 2017;18:309–13.
52. Shimada T, Yamazaki H, Mimura M, Inui Y, Guengerich FP. Interindividual variations in human liver cytochrome P-450 enzymes involved in the oxidation of drugs, carcinogens and toxic chemicals: studies with liver microsomes of 30 Japanese and 30 Caucasians. *J Pharmacol Exp Ther*. 1994;270(1):414–23.
53. Ahn T, Yun C-H. Molecular Mechanisms Regulating the Mitochondrial Targeting of Microsomal Cytochrome P450 Enzymes. *Curr Drug Metab*. 2011;11(10):830–8.
54. Kawashima A, Satta Y. Substrate-Dependent Evolution of Cytochrome P450: Rapid Turnover of the Detoxification-Type and Conservation of the Biosynthesis-Type. *PLoS One*. 2014 Jun 30;9(6):e100059.

55. Lynch T, Price A. The effect of cytochrome P450 metabolism on drug response, interactions, and adverse effects. *Am Fam Physician*. 2007;76(3):391–6.
56. Ingelman-Sundberg I. Genetic polymorphisms of cytochrome P 450 evolutionary aspects and functional diversity. *Pharmacogenomics J*. 2005;(5):6–13.
57. Daly AK, Brockmoller J, Broly F, Eichelbaum M, Evans WE, Gonzalez FJ, et al. Nomenclature for human CYP2D6 alleles. *Pharmacogenet Genomics*. 1996;6(3):193–201.
58. Ingelman-Sundberg M, Daly AK, Oscarson M, Nebert DW. Human cytochrome P450 (CYP) genes: recommendations for the nomenclature of alleles. *Pharmacogenet Genomics*. 2000;10(1):91–3.
59. Zanger UM, Raimundo S, Eichelbaum M. Cytochrome P450 2D6: Overview and update on pharmacology, genetics, biochemistry. *Naunyn Schmiedebergs Arch Pharmacol*. 2004;369(1):23–37.
60. Temesvári M, Kóbori L, Paulik J, Sárvány E, Belic A, Monostory K. Estimation of drug-metabolizing capacity by cytochrome P450 genotyping and expression. *J Pharmacol Exp Ther*. 2012;341(1):294–305.
61. Bebia Z, Buch SC, Wilson JW, Frye RF, Romkes M, Cecchetti A, et al. Bioequivalence revisited: influence of age and sex on CYP enzymes. *Clin Pharmacol Ther*. 2004;76(6):618–27.
62. Mahgoub A, Dring L., Idle J., Lancaster R, Smith R. Polymorphic hydroxylation of debrisoquine in man. *Lancet*. 1977;310(8038):584–6.
63. Zhou SF. Regulation of human CYP2D6. In: *Cytochrome P450 2D6 (Structure, Function, Regulation and Polymorphism)*. CRC Press (Taylor & Francis Group); 2016. p. 315–39.
64. Johnson TN, Tucker GT, Rostami-Hodjegan A. Development of CYP2D6 and CYP3A4 in the First Year of Life. *Clin Pharmacol Ther*. 2008;83(5):670–1.
65. Stevens JC, Marsh SA, Zaya MJ, Regina KJ, Divakaran K, Le M, et al. Developmental changes in human liver CYP2D6 expression. *Drug Metab Dispos*. 2008;36(8):1587–93.
66. Matsunaga N, Inoue M, Kusunose N, Kakimoto K, Hamamura K, Hanada Y, et al. Time-Dependent Interaction between Differentiated Embryo Chondrocyte-2 and CCAAT/Enhancer-Binding Protein α Underlies the Circadian Expression of CYP2D6 in Serum-Shocked HepG2 Cells. *Mol Pharmacol*. 2012;81(5):739 LP – 747.
67. Pan X, Ning M, Jeong H. Transcriptional regulation of CYP2D6 expression. *Drug Metab Dispos*. 2017;45(1):42–8.
68. Zeng L, Chen Y, Wang Y, Yu L-R, Knox B, Chen J, et al. MicroRNA hsa-miR-370-3p suppresses the expression and induction of CYP2D6 by facilitating mRNA degradation. *Biochem Pharmacol*. 2017;140:139–49.
69. Rowland P, Blaney FE, Smyth MG, Jones JJ, Leydon VR, Oxbrow AK, et al. Crystal structure of human cytochrome P450 2D6. *J Biol Chem*. 2006;281(11):7614–22.
70. Gaedigk A, Sangkuhl K, Whirl-Carrillo M, Klein T, Steven Leeder J. Prediction of CYP2D6 phenotype from genotype across world populations. *Genet Med*. 2017;19(1):69–76.
71. Zhou SF. Polymorphism of human cytochrome P450 2D6 and its clinical significance: Part II. *Clin Pharmacokinet*. 2009;48(12):761–804.

72. Takimoto T, Kijima T, Otani Y, Nonen S, Namba Y, Mori M, et al. Polymorphisms of CYP2D6 Gene and Gefitinib-Induced Hepatotoxicity. *Clin Lung Cancer*. 2013;14(5):502–7.
73. Onakpoya IJ, Heneghan CJ, Aronson JK. Post-marketing withdrawal of 462 medicinal products because of adverse drug reactions: A systematic review of the world literature. *BMC Med*. 2016;14(1):1–11.
74. Liu W, Deng Y, Liu Y, Gong W, Deng W. Stem cell models for drug discovery and toxicology studies. *J Biochem Mol Toxicol*. 2013;27(1):17–27.
75. Kumar N, Sharma U, Singh C, Singh B. Thalidomide: Chemistry, Therapeutic Potential and Oxidative Stress Induced Teratogenicity. *Curr Top Med Chem*. 2012;12(13):1436–55.
76. Ponce RA. Safety assessment of immunomodulatory biologics: The promise and challenges of regulatory T-cell modulation. *J Immunotoxicol*. 2011;8(4):389–97.
77. Suntharalingam G, Perry MR, Ward S, Brett SJ, Castello-Cortes A, Brunner MD, et al. Cytokine Storm in a Phase 1 Trial of the Anti-CD28 Monoclonal Antibody TGN1412. *New Engl J*. 2006;355(10):1018–2028.
78. Orloff J, Douglas F, Pinheiro J, Levinson S, Branson M, Chaturvedi P, et al. The future of drug development: Advancing clinical trial design. *Nat Rev Drug Discov*. 2009;8(12):949–57.
79. Gerets HHJ, Tilmant K, Gerin B, Chanteux H, Depelchin BO, Dhalluin S, et al. Characterization of primary human hepatocytes, HepG2 cells, and HepaRG cells at the mRNA level and CYP activity in response to inducers and their predictivity for the detection of human hepatotoxins. *Cell Biol Toxicol*. 2012;28(2):69–87.
80. Zhang D, Luo G, Ding X, Lu C. Preclinical experimental models of drug metabolism and disposition in drug discovery and development. *Acta Pharm Sin B*. 2012;2(6):549–61.
81. Corbett JL, Duncan SA. iPSC-Derived Hepatocytes as a Platform for Disease Modeling and Drug Discovery. *Front Med*. 2019;6(November):1–12.
82. Castell J V., Jover R, Martnez-Jimnez CP, Gmez-Lechn MJ. Hepatocyte cell lines: their use, scope and limitations in drug metabolism studies. *Expert Opin Drug Metab Toxicol*. 2006;2(2):183–212.
83. Rodríguez-Antona C, Donato MT, Boobis A, Edwards RJ, Watts PS, Castell J V., et al. Cytochrome P450 expression in human hepatocytes and hepatoma cell lines: Molecular mechanisms that determine lower expression in cultured cells. *Xenobiotica*. 2002;32(6):505–20.
84. Takayama K, Morisaki Y, Kuno S, Nagamoto Y, Harada K, Furukawa N, et al. Prediction of interindividual differences in hepatic functions and drug sensitivity by using human iPSC-derived hepatocytes. *Proc Natl Acad Sci U S A*. 2014;111(47):16772–7.
85. Grskovic M, Javaherian A, Strulovici B, Daley GQ. Induced pluripotent stem cells — opportunities for disease modelling and drug discovery. *Nat Rev Drug Discov*. 2011;10:915.
86. Meseguer-Ripolles J, Khetani SR, Blanco JG, Iredale M, Hay DC. Pluripotent Stem Cell-Derived Human Tissue: Platforms to Evaluate Drug Metabolism and Safety. *AAPS J*. 2017;20(1):20.
87. Liu G, David BT, Trawczynski M, Fessler RG. Advances in Pluripotent Stem Cells: History, Mechanisms, Technologies, and Applications. *Stem Cell Rev Reports*. 2020;16(1):3–32.

88. Christopherson GT, Nesti LJ. Stem cell applications in military medicine. *Stem Cell Res Ther.* 2011;2(40):1–10.
89. Martin GR. Isolation of a pluripotent cell line from early mouse embryos cultured in medium conditioned by teratocarcinoma stem cells. *Proc Natl Acad Sci U S A.* 1981;78(12):7634–8.
90. Thomson JA, Itskovitz-Eldor J, Shapiro SS, Waknitz MA, Swiergiel JJ, Marshall VS, et al. Embryonic Stem Cell Lines Derived from Human Blastocysts. *Science (80-).* 1998;282(5391):1145–7.
91. Eguizabal C, Aran B, Chuva de Sousa Lopes SM, Geens M, Heindryckx B, Panula S, et al. Two decades of embryonic stem cells: a historical overview. *Hum Reprod Open.* 2019;2019(1):1–17.
92. McLaren A. Ethical and social considerations of stem cell research. *Nature.* 2001;414(6859):129–31.
93. Baldwin T. Morality and human embryo research. Introduction to the Talking Point on morality and human embryo research. *EMBO Rep.* 2009;10(4):299–300.
94. Wert G de, Mummery C. Human embryonic stem cells: research, ethics and policy. *Hum Reprod.* 2003;18(4):672–82.
95. Murry CE, Keller G. Differentiation of Embryonic Stem Cells to Clinically Relevant Populations: Lessons from Embryonic Development. *Cell.* 2008;132(4):661–80.
96. Zhang S-C, Wernig M, Duncan ID, Brüstle O, Thomson JA. In vitro differentiation of transplantable neural precursors from human embryonic stem cells. *Nat Biotechnol.* 2001;19(12):1129–33.
97. Assady S, Maor G, Amit M, Itskovitz-Eldor J, Skorecki KL, Tzukerman M. Insulin Production by Human Embryonic Stem Cells. *Diabetes.* 2001;50(8):1691–7.
98. Kehat I, Kenyagin-Karsenti D, Snir M, Segev H, Amit M, Gepstein A, et al. Human embryonic stem cells can differentiate into myocytes with structural and functional properties of cardiomyocytes. *J Clin Invest.* 2001;108(3):407–14.
99. Hübner K, Fuhrmann G, Christenson LK, Kehler J, Reinbold R, De La Fuente R, et al. Derivation of Oocytes from Mouse Embryonic Stem Cells. *Science (80-).* 2003;300(5623):1251–6.
100. Takahashi K, Yamanaka S. Induction of Pluripotent Stem Cells from Mouse Embryonic and Adult Fibroblast Cultures by Defined Factors. *Cell.* 2006;126(4):663–76.
101. Takahashi K, Tanabe K, Ohnuki M, Narita M, Ichisaka T, Tomoda K, et al. Induction of Pluripotent Stem Cells from Adult Human Fibroblasts by Defined Factors. *Cell.* 2007;131(5):861–72.
102. Yu J, Vodyanik MA, Smuga-Otto K, Antosiewicz-Bourget J, Frane JL, Tian S, et al. Induced Pluripotent Stem Cell Lines Derived from Human Somatic Cells. *Science (80-).* 2007;318(5858):1917–20.
103. The Nobel Assembly at Karolinska Institutet. The Nobel Prize in Physiology or Medicine 2012 (Press Release) [Internet]. 2012 [cited 2019 Jun 25]. Available from: <https://www.nobelprize.org/prizes/medicine/2012/press-release/>

104. Roßbach M, Hadenfeld M, Brüstle O. Industrial Applications of Stem Cells. In: *Translational Stem Cell Research*. Humana Press, Totowa, NJ; 2011. p. 91–102.
105. Okita K, Yamakawa T, Matsumura Y, Sato Y, Amano N, Watanabe A, et al. An efficient nonviral method to generate integration-free human-induced pluripotent stem cells from cord blood and peripheral blood cells. *Stem Cells*. 2013;31(3):458–66.
106. Fusaki N, Ban H, Nishiyama A, Saeki K, Hasegawa M. Efficient induction of transgene-free human pluripotent stem cells using a vector based on Sendai virus, an RNA virus that does not integrate into the host genome. *Proc Japan Acad Ser B*. 2009;85(8):348–62.
107. Warren L, Manos PD, Ahfeldt T, Loh Y-H, Li H, Lau F, et al. Highly Efficient Reprogramming to Pluripotency and Directed Differentiation of Human Cells with Synthetic Modified mRNA. *Cell Stem Cell*. 2010;7(5):618–30.
108. Kim D, Kim C-H, Moon J-I, Chung Y-G, Chang M-Y, Han B-S, et al. Generation of human induced pluripotent stem cells by direct delivery of reprogramming proteins. *Cell Stem Cell*. 2009;4(6):472–6.
109. Chen G, Gulbranson DR, Hou Z, Bolin JM, Ruotti V, Probasco MD, et al. Chemically defined conditions for human iPSC derivation and culture. *Nat Methods*. 2011;8(5):424–9.
110. Rodin S, Antonsson L, Niaudet C, Simonson OE, Salmela E, Hansson EM, et al. Clonal culturing of human embryonic stem cells on laminin-521/E-cadherin matrix in defined and xeno-free environment. *Nat Commun*. 2014;5(3195):1–13.
111. Beers J, Gulbranson DR, George N, Siniscalchi LI, Jones J, Thomson JA, et al. Passaging and colony expansion of human pluripotent stem cells by enzyme-free dissociation in chemically defined culture conditions. *Nat Protoc*. 2012;7(11):2029–40.
112. Yasuda S, Ikeda T, Shahsavarani H, Yoshida N, Nayer B, Hino M, et al. Chemically defined and growth-factor-free culture system for the expansion and derivation of human pluripotent stem cells. *Nat Biomed Eng*. 2018;2(3):173–82.
113. Soares FAC, Chandra A, Thomas RJ, Pedersen RA, Vallier L, Williams DJ. Investigating the feasibility of scale up and automation of human induced pluripotent stem cells cultured in aggregates in feeder free conditions. *J Biotechnol*. 2014;173(1):53–8.
114. Shafa M, Sjonnesen K, Yamashita A, Liu S, Michalak M, Kallos MS, et al. Expansion and long-term maintenance of induced pluripotent stem cells in stirred suspension bioreactors. *J Tissue Eng Regen Med*. 2012;6(6):462–72.
115. Schlaeger TM, Daheron L, Brickler TR, Entwisle S, Chan K, Cianci A, et al. A comparison of non-integrating reprogramming methods. *Nat Biotechnol*. 2015;33(1):58–63.
116. Soufi A. Mechanisms for enhancing cellular reprogramming. *Curr Opin Genet Dev*. 2014;25(1):101–9.
117. Yu J, Chau KF, Vodyanik MA, Jiang J, Jiang Y. Efficient Feeder-Free Episomal Reprogramming with Small Molecules. *PLoS One*. 2011;6(3):1–10.
118. Eschenhagen T, Mummery C, Knollmann BC. Modelling sarcomeric cardiomyopathies in the dish: from human heart samples to iPSC cardiomyocytes. *Cardiovasc Res*. 2015;105(4):424–38.
119. Beevers JE, Caffrey TM, Wade-Martins R. Induced pluripotent stem cell (iPSC)-derived dopaminergic models of Parkinson's disease. *Biochem Soc Trans*. 2013;41(6):1503–8.

120. Hofrichter M, Nimtz L, Tigges J, Kabiri Y, Schröter F, Royer-Pokora B, et al. Comparative performance analysis of human iPSC-derived and primary neural progenitor cells (NPC) grown as neurospheres in vitro. *Stem Cell Res.* 2017;25:72–82.
121. Lu J, Einhorn S, Venkatarangan L, Miller M, Mann DA, Watkins PB, et al. Morphological and Functional Characterization and Assessment of iPSC-Derived Hepatocytes for In Vitro Toxicity Testing. *Toxicol Sci.* 2015;147(1):39–54.
122. Baghbaderani BA, Tian X, Neo BH, Burkall A, Dimezzo T, Sierra G, et al. CGMP-manufactured human induced pluripotent stem cells are available for pre-clinical and clinical applications. *Stem Cell Reports.* 2015;5(4):647–59.
123. Martin U. Therapeutic Application of Pluripotent Stem Cells: Challenges and Risks. *Front Med.* 2017;4(229):1–8.
124. Mandai M, Watanabe A, Kurimoto Y, Hiram Y, Morinaga C, Daimon T, et al. Autologous Induced Stem-Cell-Derived Retinal Cells for Macular Degeneration. *N Engl J Med.* 2017;376(11):1038–46.
125. Rambhatla L, Chiu CP, Kundu P, Peng Y, Carpenter MK. Generation of hepatocyte-like cells from human embryonic stem cells. *Cell Transplant.* 2003;12(1):1–11.
126. Schwartz RE, Linehan JL, Painschab MS, Hu WS, Verfaillie CM, Kaufman DS. Defined conditions for development of functional hepatic cells from human embryonic stem cells. *Stem Cells Dev.* 2005;14(6):643–55.
127. Hay DC, Zhao D, Ross A, Mandalam R, Lebkowski J, Cui W. Direct differentiation of human embryonic stem cells to hepatocyte-like cells exhibiting functional activities. *Cloning Stem Cells.* 2007;9(1):51–62.
128. Agarwal S, Holton KL, Lanza R. Efficient Differentiation of Functional Hepatocytes from Human Embryonic Stem Cells. *Stem Cells.* 2008;26(5):1117–27.
129. Touboul T, Hannan NRF, Corbineau S, Martinez A, Martinet C, Branchereau S, et al. Generation of functional hepatocytes from human embryonic stem cells under chemically defined conditions that recapitulate liver development. *Hepatology.* 2010;51(5):1754–65.
130. Sullivan GJ, Hay DC, Park IH, Fletcher J, Hannoun Z, Payne CM, et al. Generation of functional human hepatic endoderm from human induced pluripotent stem cells. *Hepatology.* 2010;51(1):329–35.
131. Song Z, Cai J, Liu Y, Zhao D, Yong J, Duo S, et al. Efficient generation of hepatocyte-like cells from human induced pluripotent stem cells. *Cell Res.* 2009;19(11):1233–42.
132. Jozefczuk J, Prigione A, Chavez L, Adjaye J. Comparative analysis of human embryonic stem cell and induced pluripotent stem cell-derived hepatocyte-like cells reveals current drawbacks and possible strategies for improved differentiation. *Stem Cells Dev.* 2011;20(7):1259–75.
133. D'Amour KA, Agulnick AD, Eliazer S, Kelly OG, Kroon E, Baetge EE. Efficient differentiation of human embryonic stem cells to definitive endoderm. *Nat Biotechnol.* 2005;23(12):1534–41.
134. Aykul S, Martinez-Hackert E. Transforming growth factor- β family ligands can function as antagonists by competing for type II receptor binding. *J Biol Chem.* 2016;291(20):10792–804.

135. Teo KAK, Valdez IA, Dirice E, Kulkarni RN. Comparable Generation of Activin-Induced Definitive Endoderm via Additive Wnt or BMP Signaling in Absence of Serum. *Stem Cell Reports*. 2014;3(1):5–14.
136. Sineva GS, Pospelov VA. Inhibition of GSK3beta enhances both adhesive and signalling activities of beta-catenin in mouse embryonic stem cells. *Biol cell*. 2010;102(10):549–60.
137. Siller R, Greenhough S, Naumovska E, Sullivan GJ. Small-molecule-driven hepatocyte differentiation of human pluripotent stem cells. *Stem Cell Reports*. 2015;4(5):939–52.
138. Verheijen M, Lienhard M, Schrooders Y, Clayton O, Nudischer R, Boerno S, et al. DMSO induces drastic changes in human cellular processes and epigenetic landscape in vitro. *Sci Rep*. 2019;9(1):1–12.
139. Hay DC, Zhao D, Fletcher J, Hewitt ZA, McLean D, Urruticoechea-Uriguen A, et al. Efficient Differentiation of Hepatocytes from Human Embryonic Stem Cells Exhibiting Markers Recapitulating Liver Development In Vivo. *Stem Cells*. 2008;26(4):894–902.
140. Magner NL, Jung Y, Wu J, Nolta JA, Zern MA, Zhou P. Insulin and IGFs enhance hepatocyte differentiation from human embryonic stem cells via the PI3K/AKT Pathway. *Stem Cells*. 2013;31(10):2095–103.
141. Han S. Generation of Functional Hepatic Cells from Pluripotent Stem Cells. *J Stem Cell Res Ther*. 2012;1(S10):1–7.
142. Wang Y, Alhaque S, Cameron K, Meseguer-Ripolles J, Lucendo-Villarin B, Rashidi H, et al. Defined and scalable generation of hepatocyte-like cells from human pluripotent stem cells. *J Vis Exp*. 2017;2017(121):1–8.
143. Baxter M, Withey S, Harrison S, Segeritz CP, Zhang F, Atkinson-Dell R, et al. Phenotypic and functional analyses show stem cell-derived hepatocyte-like cells better mimic fetal rather than adult hepatocytes. *J Hepatol*. 2015;62(3):581–9.
144. Zeilinger K, Freyer N, Damm G, Seehofer D, Knöspel F. Cell sources for in vitro human liver cell culture models. *Exp Biol Med*. 2016;241(15):1684–98.
145. Shlomai A, Schwartz RE, Ramanan V, Bhatta A, De Jong YP, Bhatia SN, et al. Modeling host interactions with hepatitis B virus using primary and induced pluripotent stem cell-derived hepatocellular systems. *Proc Natl Acad Sci U S A*. 2014;111(33):12193–8.
146. Schwartz RE, Trehan K, Andrus L, Sheahan TP, Ploss A, Duncan SA, et al. Modeling hepatitis C virus infection using human induced pluripotent stem cells. *Proc Natl Acad Sci U S A*. 2012;109(7):2544–8.
147. Ng S, Schwartz RE, March S, Galstian A, Gural N, Shan J, et al. Human iPSC-derived hepatocyte-like cells support plasmodium liver-stage infection in vitro. *Stem Cell Reports*. 2015;4(3):348–59.
148. Zhang S, Chen S, Li W, Guo X, Zhao P, Xu J, et al. Rescue of ATP7B function in hepatocyte-like cells from Wilson's disease induced pluripotent stem cells using gene therapy or the chaperone drug curcumin. *Hum Mol Genet*. 2011;20(16):3176–87.
149. Rashid ST, Corbineau S, Hannan N, Marciniak SJ, Miranda E, Alexander G, et al. Modeling inherited metabolic disorders of the liver using human induced pluripotent stem cells. *J Clin Invest*. 2010;120(9):3127–36.
150. Graffmann N, Ring S, Kawala MA, Wruck W, Ncube A, Trompeter HI, et al. Modeling

- Nonalcoholic Fatty Liver Disease with Human Pluripotent Stem Cell-Derived Immature Hepatocyte-Like Cells Reveals Activation of PLIN2 and Confirms Regulatory Functions of Peroxisome Proliferator-Activated Receptor Alpha. *Stem Cells Dev.* 2016;25(15):1119–33.
151. Colatsky T, Fermini B, Gintant G, Pierson JB, Sager P, Sekino Y, et al. The Comprehensive in Vitro Proarrhythmia Assay (CiPA) initiative — Update on progress. *J Pharmacol Toxicol Methods.* 2016;81:15–20.
 152. Fermini B, Coyne KP, Coyne ST. Challenges in designing and executing clinical trials in a dish studies. *J Pharmacol Toxicol Methods.* 2018;94(September):73–82.
 153. Bohndorf M, Ncube A, Spitzhorn L-S, Enczmann J, Wruck W, Adjaye J. Derivation and characterization of integration-free iPSC line ISRM-UM51 derived from SIX2-positive renal cells isolated from urine of an African male expressing the CYP2D6 *4/*17 variant which confers intermediate drug metabolizing activity. *Stem Cell Res.* 2017;25:18–21.
 154. Kawala MA, Bohndorf M, Graffmann N, Wruck W, Zatloukal K, Adjaye J. Characterization of dermal fibroblast-derived iPSCs from a patient with low grade steatosis. *Stem Cell Res.* 2016;17(3):568–71.
 155. Wruck W, Kashofer K, Rehman S, Daskalaki A, Berg D, Gralka E, et al. Multi-omic profiles of human non-alcoholic fatty liver disease tissue highlight heterogenic phenotypes. *Sci Data.* 2015;2:1–10.
 156. Aden DP, Fogel A, Plotkin S, Damjanov I, Knowles BB. Controlled synthesis of HBsAg in a differentiated human liver carcinoma-derived cell line. *Nature.* 1979;282(5739):615–6.
 157. Ghule PN, Medina R, Lengner CJ, Mandeville M, Qiao M, Dominski Z, et al. Reprogramming the pluripotent cell cycle: restoration of an abbreviated G1 phase in human induced pluripotent stem (iPS) cells. *J Cell Physiol.* 2011;226(5):1149–56.
 158. Livak KJ, Schmittgen TD. Analysis of relative gene expression data using real-time quantitative PCR and the 2- $\Delta\Delta$ CT method. *Methods.* 2001;25(4):402–8.
 159. Schindelin J, Arganda-Carreras I, Frise E, Kaynig V, Longair M, Pietzsch T, et al. Fiji: An open-source platform for biological-image analysis. *Nat Methods.* 2012;9(7):676–82.
 160. Ho C-M, Dhawan A, Hughes RD, Lehec SC, Puppi J, Philippeos C, et al. Use of indocyanine green for functional assessment of human hepatocytes for transplantation. *Asian J Surg.* 2012;35(1):9–15.
 161. Huang L, Vore M. Multidrug resistance p-glycoprotein 2 is essential for the biliary excretion of indocyanine green. *Drug Metab Dispos.* 2001;29(5):634–7.
 162. Ochei J, Kolhatkar A. Staining Reactions of Carbohydrates. In: *Medical Laboratory Science - Theory and Practice.* 10th ed. New Dehli: Tata McGraw-Hill Publishing Company Limited; 2000. p. 451–8.
 163. Brodniewicz T, Gryniewicz G. Preclinical drug development. Vol. 67, *Acta Poloniae Pharmaceutica - Drug Research.* 2010. p. 578–85.
 164. Gu X, Albrecht W, Edlund K, Kappenberg F, Rahnenführer J, Leist M, et al. Relevance of the incubation period in cytotoxicity testing with primary human hepatocytes. *Arch Toxicol.* 2018;92(12):3505–15.
 165. Kimura S, Umeno M, Skodaj RC, Meyert UA, Gonzalez FJ. The Human Debrisoquine 4-Hydroxylase (CYP2D) Locus: Sequence and Identification of the Polymorphic CYP2D6 Gene,

- a Related Gene, and a Pseudogene. *Am J Hum Genet.* 1989;45:889–904.
166. Bradford LDA. CYP2D6 allele frequency in European Caucasians, Asians, Africans and their descendants. *Pharmacogenomics.* 2002;3(2):229–43.
 167. Johansson I, Lundqvist E, Bertilsson L, Dahl M-L, Sjöqvist F, Ingelman-Sundberg M. Inherited amplification of an active gene in the cytochrome P450 CYP2D locus as a cause of ultrarapid metabolism of debrisoquine. *Proc Natl Acad Sci USA.* 1993;90:11825–9.
 168. Zanger UM, Fischer J, Raimundo S, Stüven T, Evert BO, Schwab M, et al. Comprehensive analysis of the genetic factors determining expression and function of hepatic CYP2D6. *Pharmacogenetics.* 2001;11(7):573–85.
 169. Raimundo S, Toscano C, Klein K, Fischer J, Griese E-U, Eichelbaum M, et al. A novel intronic mutation, 2988G>A, with high predictivity for impaired function of cytochrome P450 2D6 in white subjects. *Clin Pharmacol Ther.* 2004;76(2):128–38.
 170. Wang S-L, Huang J-D, Lai M-D, Liu B-H, Lai M-L. Molecular basis of genetic variation in debrisoquin hydroxylation in Chinese subjects: Polymorphism in RFLP and DNA sequence of CYP2D6. *Clin Pharmacol Ther.* 1993;53(4):410–8.
 171. Leathart JB, London SJ, Steward A, Adams JD, Idle JR, Daly AK. CYP2D6 phenotype-genotype relationships in African-Americans and Caucasians in Los Angeles. *Pharmacogenetics.* 1998;8(6):529–41.
 172. Gough AC, Miles JS, Spurr NK, Moss JE, Gaedigk A, Eichelbaum M, et al. Identification of the primary gene defect at the cytochrome P450 CYP2D locus. *Nature.* 1990;347(6295):773–6.
 173. Hanioka N, Kimura S, Meyert UA, Gonzalez FJ. The Human CYP2D Locus Associated with a Common Genetic Defect in Drug Oxidation: A G1934-A Base Change in Intron 3 of a Mutant CYP2D6 Allele Results in an Aberrant 3' Splice Recognition Site. *Am J Hum Genet.* 1990;47:994–1001.
 174. Masimirembwa C, Persson I, Bertilsson L, Hasler J, Ingelman-Sundberg M. A novel mutant variant of the CYP2D6 gene (CYP2D617) common in a black African population: association with diminished debrisoquine hydroxylase activity. *Br J Clin Pharmacol.* 1996;42(6):713–9.
 175. Oscarson M, Hidestrand M, Johansson I, Ingelman-Sundberg M. A combination of mutations in the CYP2D6*17 (CYP2D6Z) allele causes alterations in enzyme function. *Mol Pharmacol.* 1997;52(6):1034–40.
 176. Griese EU, Asante-Poku S, Ofori-Adjei D, Mikus G, Eichelbaum M. Analysis of the CYP2D6 gene mutations and their consequences for enzyme function in a West African population. *Pharmacogenetics.* 1999;9(6):715–723.
 177. Relling M V, Klein TE. CPIC: Clinical Pharmacogenetics Implementation Consortium of the Pharmacogenomics Research Network. *Clin Pharmacol Ther.* 2011;89(3):464–7.
 178. Crews K, Gaedigk A, Dunnenberger H, Leeder J, Klein T, Caudle K, et al. Clinical Pharmacogenetics Implementation Consortium Guidelines for Cytochrome P450 2D6 Genotype and Codeine Therapy: 2014 Update. *Clin Pharmacol Ther.* 2014;95(4):376–82.
 179. Goetz MP, Sangkuhl K, Guchelaar H-J, Schwab M, Province M, Whirl-Carrillo M, et al. Clinical Pharmacogenetics Implementation Consortium (CPIC) Guideline for CYP2D6 and Tamoxifen Therapy. *Clin Pharmacol Ther.* 2018;103(5):770–7.

180. Hicks J, Bishop J, Sangkuhl K, Müller D, Ji Y, Leckband S, et al. Clinical Pharmacogenetics Implementation Consortium (CPIC) Guideline for CYP2D6 and CYP2C19 Genotypes and Dosing of Selective Serotonin Reuptake Inhibitors. *Clin Pharmacol Ther.* 2015;98(2):127–34.
181. Bell G, Caudle K, Whirl-Carrillo M, Gordon R, Hikino K, Prows C, et al. Clinical Pharmacogenetics Implementation Consortium (CPIC) guideline for CYP2D6 genotype and use of ondansetron and tropisetron. *Clin Pharmacol Ther.* 2017;102(2):213–8.
182. Swen J, Wilting I, Goede A de, Grandia L, Mulder H, Touw D, et al. Pharmacogenetics: From Bench to Byte. *Clin Pharmacol Ther.* 2008;83(5):781–7.
183. Lunenburg CATC, van der Wouden CH, Nijenhuis M, Crommentuijn-van Rhenen MH, de Boer-Veger NJ, Buunk AM, et al. Dutch Pharmacogenetics Working Group (DPWG) guideline for the gene–drug interaction of DPYD and fluoropyrimidines. *Eur J Hum Genet.* 2020;28(4):508–17.
184. Cecchin E, Roncato R, Guchelaar HJ, Toffoli G, Consortium P. Ubiquitous Pharmacogenomics (U-PGx): The Time for Implementation is Now. An Horizon2020 Program to Drive Pharmacogenomics into Clinical Practice. *Curr Pharm Biotechnol.* 2017;18:204–9.
185. van der Wouden C, Cambon-Thomsen A, Cecchin E, Cheung K, Dávila-Fajardo C, Deneer V, et al. Implementing Pharmacogenomics in Europe: Design and Implementation Strategy of the Ubiquitous Pharmacogenomics Consortium. *Clin Pharmacol Ther.* 2017;101(3):341–58.
186. Gaedigk A, Simon S, Pearce R, Bradford L, Kennedy M, Leeder J. The CYP2D6 Activity Score: Translating Genotype Information into a Qualitative Measure of Phenotype. *Clin Pharmacol Ther.* 2008;83(2):234–42.
187. van Schaik RHN, Grandia L, de Goede A, Bet PM, Beekers O, Guchelaar H, et al. Nederlandse consensus: CYP2D6 genotype “1-0” ingedeeld als intermediaire metaboliseerder. *Ned Tijdschr voor Klin Chemie en Lab.* 2008;33(1):52–3.
188. Bank P, Caudle K, Swen J, Gammal R, Whirl-Carrillo M, Klein T, et al. Comparison of the Guidelines of the Clinical Pharmacogenetics Implementation Consortium and the Dutch Pharmacogenetics Working Group. *Clin Pharmacol Ther.* 2018;103(4):599–618.
189. Li Q, Hutchins AP, Chen Y, Li S, Shan Y, Liao B, et al. A sequential EMT-MET mechanism drives the differentiation of human embryonic stem cells towards hepatocytes. *Nat Commun.* 2017;8(15166):1–12.
190. Delaforest A, Di Furio F, Jing R, Ludwig-Kubinski A, Twaroski K, Urick A, et al. HNF4A regulates the formation of hepatic progenitor cells from human iPSC-derived endoderm by facilitating efficient recruitment of RNA pol II. *Genes (Basel).* 2019;10(21):1–17.
191. Zhang S. Sox2, a key factor in the regulation of pluripotency and neural differentiation. *World J Stem Cells.* 2014;6(3):305.
192. Huang J, Levitsky LL, Rhoads DB. Novel P2 promoter-derived HNF4 α isoforms with different N-terminus generated by alternate exon insertion. *Exp Cell Res.* 2009;315(7):1200–11.
193. Ko HL, Zhuo Z, Chee E, Correspondence R. HNF4a Combinatorial Isoform Heterodimers Activate Distinct Gene Targets that Differ from Their Corresponding Homodimers. *Cell Rep.* 2019;26:2549–57.
194. Torres-Padilla ME, Fougère-Deschatrette C, Weiss MC. Expression of HNF4 α isoforms in

- mouse liver development is regulated by sequential promoter usage and constitutive 3' end splicing. *Mech Dev.* 2001;109(2):183–93.
195. HNF4A - Hepatocyte nuclear factor 4-alpha - Homo sapiens (Human) - HNF4A gene & protein [Internet]. [cited 2020 Apr 13]. Available from: <https://www.uniprot.org/uniprot/P41235>
 196. Hanawa M, Takayama K, Sakurai F, Tachibana M, Mizuguchi H. Hepatocyte Nuclear Factor 4 Alpha Promotes Definitive Endoderm Differentiation from Human Induced Pluripotent Stem Cells. *Stem Cell Rev Reports.* 2017;13(4):542–51.
 197. Recombinant Anti-HNF-4-alpha antibody [EPR3648] (ab92378) [Internet]. [cited 2020 Apr 13]. Available from: <https://www.abcam.com/hnf-4-alpha-antibody-epr3648-ab92378.html?productWallTab=Abreviews>
 198. Chellappa K, Jankova L, Schnabl JM, Pan S, Brelivet Y, Fung CL-S, et al. Src tyrosine kinase phosphorylation of nuclear receptor HNF4 α correlates with isoform-specific loss of HNF4 α in human colon cancer. *PNAS.* 2012;109(7):2302–7.
 199. Kishimoto T, Yano T, Hiroshima K, Inayama Y, Kawachi K, Nakatani Y. A case of α -fetoprotein-producing pulmonary carcinoma with restricted expression of hepatocyte nuclear factor-4 α in hepatoid foci: a case report with studies of previous cases. *Hum Pathol.* 2008;39:1115–20.
 200. Semb H. Expandable Endodermal Progenitors: New Tools to Explore Endoderm and Its Derivatives. *Cell Stem Cell.* 2008;3(4):355–6.
 201. Viotti M, Nowotschin S, Hadjantonakis AK. SOX17 links gut endoderm morphogenesis and germ layer segregation. *Nat Cell Biol.* 2014;16(12):1146–56.
 202. Patterson ES, Addis RC, Shablott MJ, Gearhart JD. SOX17 directly activates Zfp202 transcription during in vitro endoderm differentiation. *Physiol Genomics.* 2008;34(3):277–84.
 203. Bar-Nur O, Russ HA, Efrat S, Benvenisty N. Epigenetic memory and preferential lineage-specific differentiation in induced pluripotent stem cells derived from human pancreatic islet beta cells. *Cell Stem Cell.* 2011;9(1):17–23.
 204. Kim K, Doi A, Wen B, Ng K, Zhao R, Cahan P, et al. Epigenetic memory in induced pluripotent stem cells performed CHARM and guided analysis of methylation HHS Public Access. *Nature.* 2010;467(7313):285–90.
 205. Hirota T, Ieiri I, Takane H, Maegawa S, Hosokawa M, Kobayashi K, et al. Allelic expression imbalance of the human CYP3A4 gene and individual phenotypic status. *Hum Mol Genet.* 2004;13(23):2959–69.
 206. Miyazaki M, Nakamura K, Fujita Y, Guengerich FP, Horiuchi R, Yamamoto K. Defective Activity of Recombinant Cytochromes P450 3A4.2 and 3A4.16 in Oxidation of Midazolam, Nifedipine, and Testosterone. *Drug Metab Dispos.* 2008;36(11):2287–91.
 207. Guttman Y, Nudel A, Kerem Z. Polymorphism in Cytochrome P450 3A4 Is Ethnicity Related. *Front Genet.* 2019;10(224):1–6.
 208. Fisher CD, Lickteig AJ, Augustine LM, Ranger-Moore J, Jackson JP, Ferguson SS, et al. Hepatic cytochrome P450 enzyme alterations in humans with progressive stages of nonalcoholic fatty liver disease. *Drug Metab Dispos.* 2009;37(10):2087–94.

209. Stills HF. Polyclonal Antibody Production. In: *The Laboratory Rabbit, Guinea Pig, Hamster, and other Rodents*. Boston: Academic Press; 2012. p. 259–74.
210. Hanukoglu I. Elimination of non-specific binding in Western blots from non-reducing gels. *J Biochem Biophys Methods*. 1990;21(1):65–8.
211. Kia-Ki H, Martinage A. Post-translational chemical modification(s) of proteins. *Int J Biochem*. 1992;24(1):19–28.
212. Redlich G, Zanger UM, Riedmaier S, Bache N, Giessing ABM, Eisenacher M, et al. Distinction between human cytochrome P450 (CYP) isoforms and identification of new phosphorylation sites by mass spectrometry. *J Proteome Res*. 2008;7(11):4678–88.
213. Sangar MC, Anandatheerthavarada HK, Tang W, Prabu SK, Martin M V., Dostalek M, et al. Human liver mitochondrial cytochrome P450 2D6 - Individual variations and implications in drug metabolism. *FEBS J*. 2009;276(13):3440–53.
214. Avadhani NG, Sangar MC, Bansal S, Bajpai P. Bimodal targeting of cytochrome P450s to endoplasmic reticulum and mitochondria: The concept of chimeric signals. *FEBS J*. 2011;278(22):4218–29.
215. Kang X, Yu Q, Huang Y, Song B, Chen Y, Gao X, et al. Effects of Integrating and Non-Integrating Reprogramming Methods on Copy Number Variation and Genomic Stability of Human Induced Pluripotent Stem Cells. *PLoS One*. 2015;10(7):1–12.
216. Graffmann N, Ncube A, Wruck W, Adjaye J. Cell fate decisions of human iPSC-derived bipotential hepatoblasts depend on cell density. *PLoS One*. 2018;13(7):1–20.
217. Karasawa T, Steyger PS. Intracellular mechanisms of aminoglycoside-induced cytotoxicity. *Integr Biol*. 2011;3(9):879–86.
218. Varghese DS, Parween S, Ardah MT, Emerald BS, Ansari SA. Effects of Aminoglycoside Antibiotics on Human Embryonic Stem Cell Viability during Differentiation In Vitro. *Stem Cells Int*. 2017;2017(2451927):1–18.
219. Jin Y, Desta Z, Stearns V, Ward B, Ho H, Lee K-H, et al. CYP2D6 Genotype, Antidepressant Use, and Tamoxifen Metabolism During Adjuvant Breast Cancer Treatment. *J Natl Cancer Inst*. 2005 Jan 5;97(1):30–9.

7 Appendix

7.1 Appendix 1

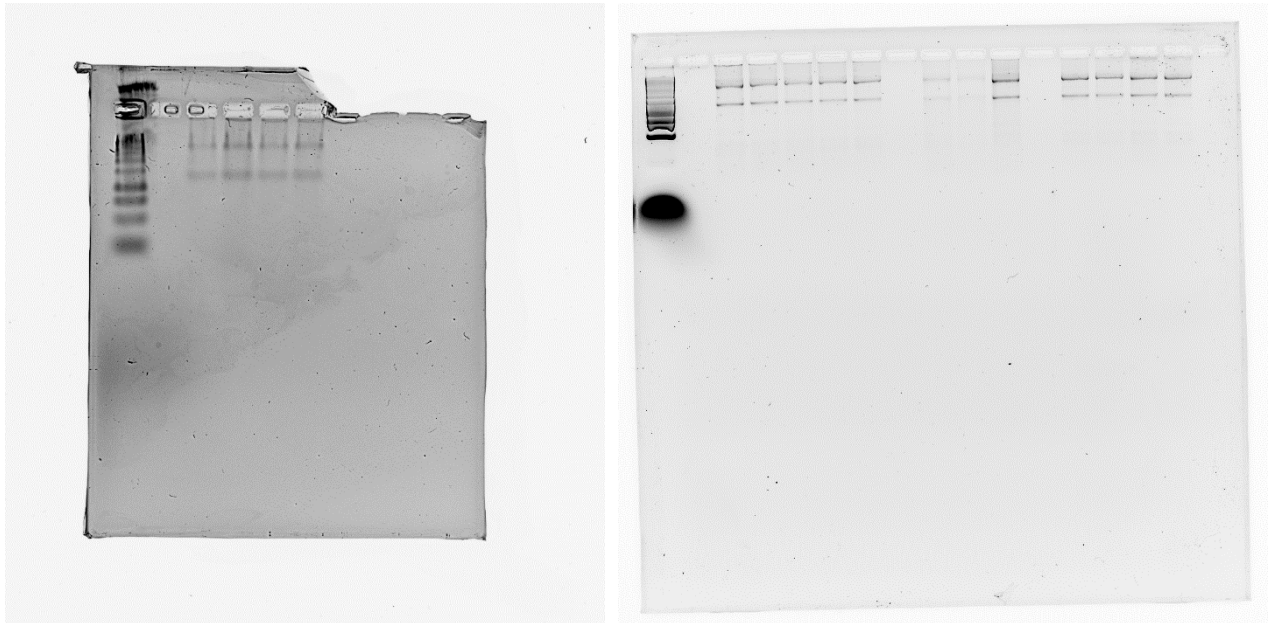


Fig. 33 - Complete depiction of gels produced for assessment of RNA quality upon RNA isolation at the last day of hepatic differentiation. **Left:** Picture of gel produced for the assessment of RNA samples isolated from S12_13B during HepDif#2. **Right:** Picture of gel produced for the assessment of RNA samples isolated from UJiPS13 during HepDif#3

7.2 Appendix 2

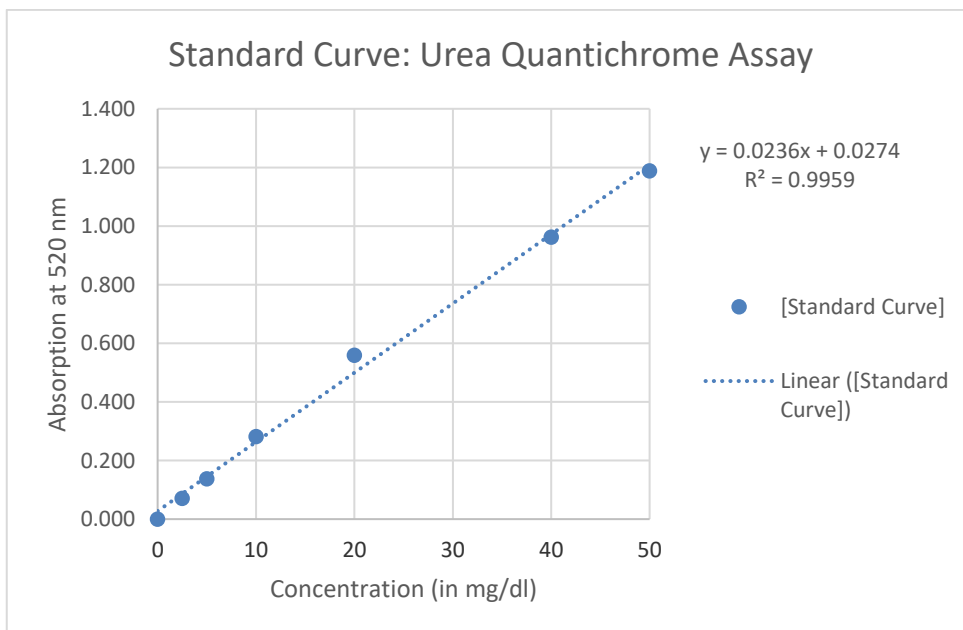


Fig. 34 – Standard curve of the Urea Quantichrome Assay. Prepared in duplicate, the absorption of standard row samples was used to determine the mean value and subtracted by the mean absorption of the blank. Results were plotted and the slope function employed to calculate the concentration of urea in differentiation samples.

8 Acknowledgements

I am utterly thankful to my supervisor **Prof. Dr. James A. Adjaye**.

Not only for giving me the opportunity to complete my medical degree thesis at your institute in a field of research I truly love. Helping me finding my feed within the local pluripotent stem cell industry in 2013 has been a major cornerstone to being able to seeing my study through to fruition. Your guidance and your open ear throughout the last years have been most valuable, I honestly cannot thank you enough.

Many thanks also to **Prof. Dr. Patrick Küry** for being willing to be my Co-Supervisor and offering me guidance throughout the practical and writing phase of this thesis.

During the course of this thesis **Dr. rer. nat. Nina Graffmann** and her passion for science, encouragement and guidance has been an invaluable source of motivation and knowledge. It was an absolute pleasure working with you.

Further, I would like to thank all members of the **Institute for Stem Cell Research and Regenerative Medicine (ISRM)**, especially Martina, Lukas, Soraia, Silke, Audrey, Lisa, Jörg, Wasco and Rita, for the entertaining and humorous hours at the lab, office or mensa.

Thank you so much **Viviana Haas**. You cheered up my long days and short nights while writing this thesis. You supported me, listened to my thoughts and fears and put them into the right perspectives. This thesis belongs to both of us! I love you!

Last but not least: Words can't describe how lucky I am to have a family like mine. You, **Mirosław Bielec** and **Heike Wenten-Bielec**, supported me as long as I can remember. You believed in me when nobody did, you offered me shelter, motivation or my personal space when I needed it. Although you mostly did not understand what I am doing during my thesis, you surely did know what I need when I needed it. You both are simply the best parents I could imagine. All I reached so far, would not have closely been possible without you. **Björn Bielec**, you do not just look like me, your support, your humor and your scientific brilliance really helped me throughout the writing and revision process of this thesis. Thank you for always being there, when I needed you!